Progress in Materials Science 58 (2013) 1388–1442

Contents lists available at SciVerse ScienceDirect

Progress in Materials Science

journal homepage: www.elsevier.com/locate/pmatsci

Review on the science and technology of water desalination by capacitive deionization

S. Porada [a,b], R. Zhao [a,c], A. van der Wal [c], V. Presser [d,e,*], P.M. Biesheuvel [a,c,*]

[a] Wetsus, Centre of Excellence for Sustainable Water Technology, Agora 1, 8934 CJ Leeuwarden, The Netherlands
[b] Department of Polymers and Carbon Materials, Faculty of Chemistry, Wroclaw University of Technology, Wybrzeze Wyspianskiego 27, 50-370 Wroclaw, Poland
[c] Department of Environmental Technology, Wageningen University, Bornse Weilanden 9, 6708 WG Wageningen, The Netherlands
[d] INM – Leibniz- Institute for New Materials INM gGmbH, Energy Materials Group, 66123 Saarbrücken, Germany
[e] Department of Materials Science and Engineering, Saarland University, 66123 Saarbrücken, Germany

ARTICLE INFO

Article history:
Received 7 December 2012
Accepted 1 March 2013
Available online 4 April 2013

ABSTRACT

Porous carbon electrodes have significant potential for energy-efficient water desalination using a promising technology called Capacitive Deionization (CDI). In CDI, salt ions are removed from brackish water upon applying an electrical voltage difference between two porous electrodes, in which the ions will be temporarily immobilized. These electrodes are made of porous carbons optimized for salt storage capacity and ion and electron transport. We review the science and technology of CDI and describe the range of possible electrode materials and the various approaches to the testing of materials and devices. We summarize the range of options for CDI-designs and possible operational modes, and describe the various theoretical–conceptual approaches to understand the phenomenon of CDI.

Contents

* Corresponding authors. Addresses: INM – Leibniz- Institute for New Materials INM gGmbH, Energy Materials Group, 66123 Saarbrücken, Germany (V. Presser), Wetsus, Centre of Excellence for Sustainable Water Technology, Agora 1, 8934 CJ Leeuwarden, The Netherlands (P.M. Biesheuvel).
E-mail addresses: volker.presser@inm-gmbh.de (V. Presser), maarten.biesheuvel@wetsus.nl (P.M. Biesheuvel).

0079-6425
http://dx.doi.org/10.1016/j.pmatsci.2013.03.005

1. Introduction

The availability of affordable clean water is one of the key technological, social, and economical challenges of the 21st century. Clean water, acknowledged as a basic human right by the United Nations [1], is still unavailable to one out of seven people worldwide. To complicate matters, increasing groundwater extraction around the globe results in progressive salt water ingress in wells and aquifers. As a consequence, there is a large interest in the development of economically attractive desalination technologies. Over the years, a number of desalination methods have been developed among which distillation, reverse osmosis, and electrodialysis are the most commonly known and widespread technologies [2]. A common goal for current research is to make these technologies more energy efficient and cost effective, both for the deionization of seawater and for brackish water.

Considering that there is more brackish water than freshwater in the world, it is clear that it is particularly attractive to utilize the large brackish water resources for human consumption and residential use, agriculture, and industry.

Capacitive Deionization (CDI) has emerged over the years as a robust, energy efficient, and cost effective technology for desalination of water with a low or moderate salt content [2]. The energy efficiency of CDI for water with a salt concentration below approximately 10 g/L is due to the fact that the salt ions, which are the minority compound in the water, are removed from the mixture. Instead, other methods extract the majority phase, the water, from the salt solution. Furthermore, energy release during electrode regeneration (ion release, or electrode discharge) can be utilized to charge a neighboring cell operating in the ion electrosorption step, and in this way energy recovery is possible. As we will explain later in detail, a CDI cycle consists of two steps, the first being an ion electrosorption, or charging, step to purify the water, where ions are immobilized in porous carbon electrode pairs. In the following step, ions are released, that is, are desorbed from the electrodes, and thus the electrodes are regenerated. The basic mechanism underlying capacitive deionization is schematically shown in Fig. 1.

With the majority of research on porous carbon electrodes over the past decades dedicated to capacitive energy storage devices, capacitive deionization had been somewhat overlooked. Though the application of porous carbon electrodes for water desalination had been documented since the 1960s when it was called "electrochemical demineralization" or "electrosorb process for desalting water" [3–7], only recently the academic interest in this technology increased exponentially, and companies have begun marketing commercial CDI technologies.

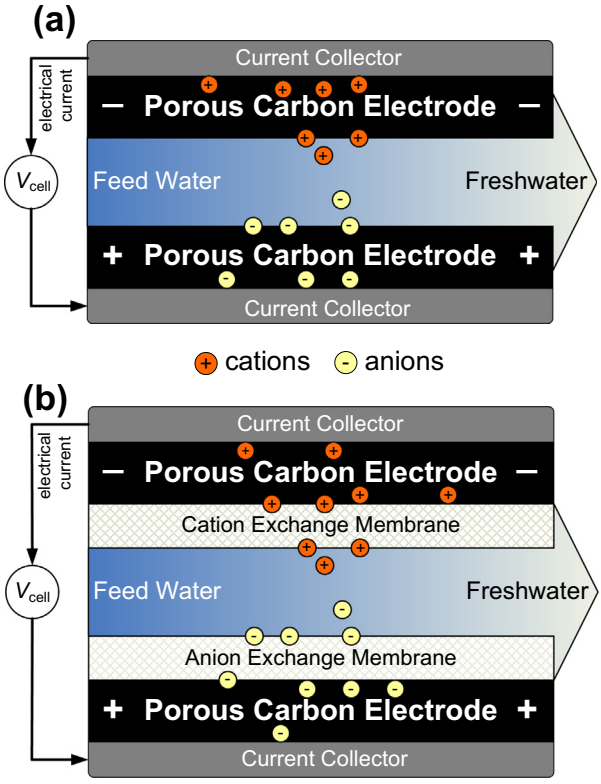

Fig. 1. Schematic design of a cell for (Membrane) Capacitive Deionization, (M)CDI. Upon applying a voltage difference between two porous carbon electrodes, ions are attracted into the electrode, cations into the negative electrode (cathode, on top), anions into the positive electrode (anode, bottom). As a result, desalinated water is produced. (A) CDI; (B) MCDI, where in front of the cathode a cation-exchange membrane is placed, while an anion-exchange membrane is placed in front of the anode.

CDI uses pairs of oppositely placed porous carbon electrodes which store ions upon applying an electrical voltage difference, see Fig. 1. Such electrodes can be assembled in stacks of multiple pairs. The ions are harvested from the water flowing through a "spacer channel" in between the two electrodes and are immobilized in the pores inside the carbon material. This process is based on the formation of electrical double layers (EDLs) inside the intraparticle pores. EDL formation is the cornerstone of capacitive energy storage and also the mechanism by which salt ions are immobilized and selectively extracted from saline water. After some time, all of the accessible intraparticle pore volume is saturated with electrosorbed ions and the storage capacity of the device is reached. In order to regenerate the carbon electrodes, the ions are released from the electrode by reducing or even reversing the cell voltage. In this way, a small stream enriched in ions is produced and the electrodes regain their initial ion uptake capacity. Ideally, without the presence of chemical reactions, this process is purely physical in nature and potentially enables CDI devices to have a long service life and low maintenance.

Compared to the classical work of the 20th century, various modifications and new technologies are nowadays considered for CDI, such as the inclusion of ion-exchange thin membrane barriers in front of the electrodes, see Fig. 1b [8–12], and optimized operational modes such as stop-flow operation during ion release [13], salt release at reversed voltage [12], constant-current operation [14], energy recovery from the desalination/release cycle [15,16], flow-through electrodes where the water is directed head-on through the electrodes [17,18], and flow electrodes based on carbon suspensions [19].

On the materials side, new materials and design strategies for novel and improved electrodes continue to emerge. Fundamentally, even the very basic question of the "best" material remains unanswered. Naturally, the choice of electrode material largely depends on required performance (desalting capacity, final salt concentration), system requirements (flow rate, stack configuration), and cost considerations (efficiency, material cost, lifetime). However, we are currently only starting to understand CDI operation on a quantitative and kinetic basis. Ongoing research is not only dedicated to further optimizing the pore size distribution and chemical composition of already known carbons, but also expands to novel materials and complex pore and electrode architectures [20–22].

In this review we summarize the basics and theory of CDI. We discuss the range of carbon materials used for CDI, and provide guidelines and strategies for a rational design of porous carbon electrodes for desalination applications. Note that in Sections 3–7 the terminology macropores and micropores is based on that used in porous electrode theory [23–26], with the term "macropores" denoting the electrolyte-filled continuous interparticle space in between carbon particles, serving as transport pathways for ion transport across the electrode, while the term "micropores" is used for all the pore space within the carbon particles (intraparticle porosity). In Section 8 the formal IUPAC terminology for porous material characterization is used where macro-, meso-, and micropores are distinguished based on the pore sizes in a porous material [27].

2. Historical background of CDI 1960–1995

In this section we present an overview of the early phase of CDI development as summarized in Fig. 2. We define this early phase to last until 1995, when carbon aerogel CDI electrodes were developed. A detailed discussion of carbon electrode development for CDI from 1995 onward is presented in Section 8.

Pioneering work on the concept of water desalination, called "electrochemical demineralization of water" at that time, was performed by Blair, Murphy and co-workers in the early late 1960s, and continued until the late 1960s [28–31]. During that period, electrodes were classified according to their "ion-representatives", and it was assumed that ions could only be removed from water when specific chemical groups present on the surface could undergo either reduction or oxidation, followed by the creation of an ionic bond between the ion in solution and the ionized group on the carbon surface. According to a study by Blair and Murphy [28] most of the graphite-like materials and other forms of carbon, when used as an electrode material, were cation-responsive, due to the presence of the quinine–hydroquinone couple and other supposedly cation-selective surface groups. This was the reason

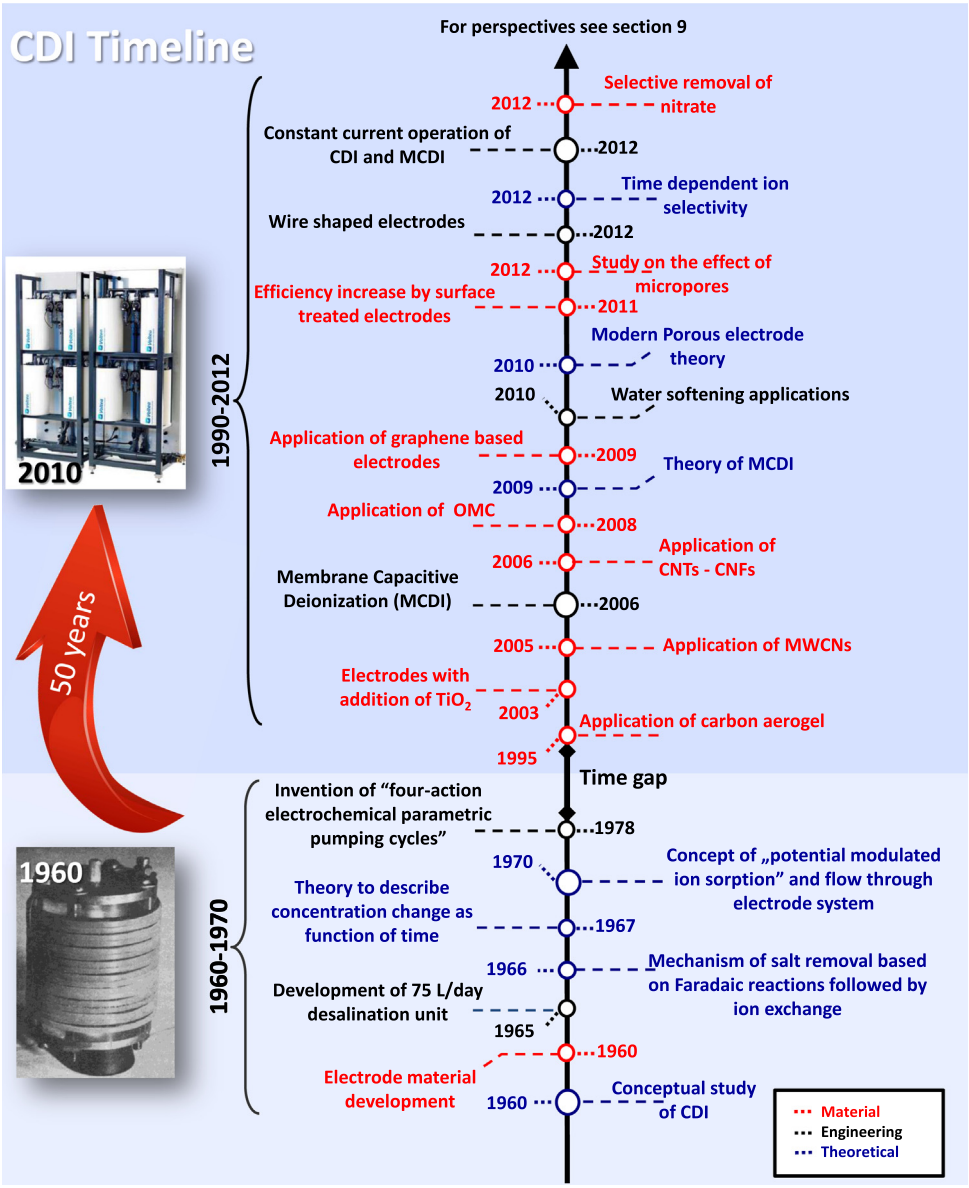

Fig. 2. Timeline of scientific developments of CDI, indicating milestones since the inception of CDI in 1960.

why during this phase of CDI development much attention was focused on the development of a method to distinguish between the cation- and anion-selective nature of the electrodes, and on the preparation of an anion-responsive electrode for instance by incorporation of an organic molecules [29].

Some years later the mechanism of "electrochemical demineralization" was studied using Coulometric and mass balance analysis by Evans and Hamilton [32]. This study started off the discussion on the extent of ion adsorption in the absence of an external voltage difference. Evans et al. [33] also made an attempt to explain the fundamental mechanism of ion removal by CDI. Evans stated that for

the first step in water demineralization Faradaic reactions are required on the cathode side, to adsorb hydrogen and to generate hydroxyl ions. In the next step, basic conditions created by hydroxyl ions provide appropriate conditions for the ionization of weak acid groups, followed by the demineralization reaction based on an ion-exchange mechanism. During the regeneration step, the voltage was reversed with the aim to decrease the local pH, and in that way to release previously removed ions. Based on this mechanism, it was believed that to obtain a functional demineralization cycle, the voltage difference has to be reversed during the regeneration cycle, and it was believed that the efficiency of the salt removal was determined by the concentration of surface groups. As will become clear from subsequent sections in this review, these classical views on the fundamentals of water desalination by porous electrodes have by now become obsolete and have been replaced by the view that can be briefly summarized as follows, namely that the capacitive storage of ions in the electrical double layer is the most important effect, and thus, carbon-based electrodes are suitable both as anode and cathode, while Faradaic reactions are no longer considered to be of primary importance in driving the CDI process.

The first detailed study using a mathematical description of the demineralization process based on a capacitive mechanism was presented by Murphy and Caudle [30]. In this work mass balance and transport equations are combined to describe the salt concentration as function of time, and the model is used to describe experimental data obtained under several operating conditions. A different study by Murphy et al. [31] focused on surface properties of carbon materials used as electrode material after chemical treatment, for example, treated with a mixture of concentrated sulfuric and nitric acids, and describes their influence on the process efficiency. Murphy et al. [31] concluded that the cation-responsive electrode behaves as ion-exchanger because of the carboxyl groups incorporated in the surface after acid treatment. More detailed studies on the mechanism and transport processes accompanying electrochemical demineralization were reported by Evans et al. [33] and Accomazzo and Evans [34].

In 1968, a study by Reid et al. [35] demonstrated the commercial relevance and long term operation of a demineralization unit without substantial loss of salt adsorption capability over time. Moreover, it was demonstrated that besides sodium and chloride ions, calcium, magnesium, sulfate, nitrate, and phosphate ions can be effectively removed.

A breakthrough in the study of the concept of electrochemical demineralization was made in the early 1970s by Johnson et al. [4], where the theory of "potential-modulated ion sorption", known nowadays as Electric Double Layer theory (EDL), was identified as the actual mechanism responsible for ion removal, and the use of asymmetric half-cycle operating conditions was introduced. The use of this operational mode is important since it showed that by using unequal half-cycle times or by optimizing the cell voltage during the desalting step, one can improve the system performance without reversing the polarity. In the same study the authors stressed that Faradaic reactions that may occur at the interface between the solid conductive material and the solution may cause electrode degradation, and from the performance efficiency point of view, these processes are not essential when the current flow is mainly capacitive. Moreover, for the first time, a simple cost study indicated the economical feasibility of CDI, if only stable electrodes can be produced. A further study by Johnson and Newman [5] describes the development of a porous electrode model to analyze ion adsorption in porous carbons, and their charge–voltage dependence, see Section 5.3. This work concluded that the ion capacity of the electrode depends on the electrical capacity of the double layer, the available surface area, and the applied cell voltage.

Following the concept of EDL theory, extensive studies on this and other topics were initialized by Soffer, Oren and co-workers in the early 1970s, and still continue up to the present time [6,36–40]. The work presented in Ref. [36] focuses on developing a new technique to investigate double layer effects in porous electrodes. In the same work the authors concluded that even the smallest pores in the size range of 0.5–3 nm are wetted and contribute to the ion removal process. In 1978, in a study by Oren and Soffer [6] the idea of "four-action electrochemical parametric pumping cycles" was introduced as an effective method to obtain a precise separation between just desalinated water and concentrate. This concept, as described in more detail in Section 3.2 was further investigated in Refs. [37,38].

Starting from the 1990s, an increasing number of publications focused on developing an effective carbon material for water deionization. Amongst them, carbon aerogel materials developed by Farmer

et al. attracted the most attention [41]. Due to its monolithic structure, large internal surface area and good conductivity, carbon aerogel electrodes were considered as an improvement over traditional systems using activated carbons. Further study on the applications of carbon aerogels to remove various salts, for example $NaNO_3$, are described in Refs. [42,43]. Modern developments in the application of carbon materials for CDI are discussed in Section 8.

3. Experimental approaches to operation and testing of CDI

In the experimental study of CDI, many choices are available on what system to study, and by what method of testing. Important questions in the study of CDI are:

- What choices can be made for the method of testing of a CDI electrode or cell?
- What CDI cell geometries can one choose from?
- Which are the possible operational modes?

These three questions are addressed in this section. In Section 3.1 we discuss the basic choice between either using an experimental approach related to the electrochemical analysis of Faradaic systems (often using three different electrodes, of which only one is the porous electrode to be tested), or to follow an approach focusing on desalination performance, using a two-electrode cell with both electrodes consisting of porous carbon. We continue in Section 3.2 with listing various of the possible CDI designs that can be chosen based on the "two-porous-electrode" cell design, and discuss in Section 3.3 which different feedwater compositions can be used in CDI-testing. Section 3.4 discusses two CDI experimental layouts used in literature. The detailed analysis of the CDI cycle in terms of salt adsorption and charge is presented in Section 3.5. In Section 3.6 we introduce the important option of adding ion-exchange membranes to the CDI system, and in Section 3.7 the common method of constant voltage operation is explained and a comparison is made between desorption at zero voltage and at reversed voltage. Finally, in Section 3.8 the distinction is explained between the classical constant-voltage mode of operation and the novel mode of constant-current operation.

3.1. Electrochemical experimentation vs. desalination using a two-electrode cell pair

For the characterization and testing of CDI electrodes, two different approaches have been described in literature. The first approach is to perform electrochemical (EC) analysis, in general based on a setup consisting of a working, counter, and reference electrode. In this approach only current and voltage signals are measured, and not the actual change of salt concentration, and the water containing the salt ions is not necessarily flowing along or through the porous carbon electrode (which is the working electrode). All three electrodes are typically different, with only the working electrode made of the CDI material to be tested [20,44–46].

In a quite different approach, water containing salt is flowing along or through a cell pair consisting of two porous carbon electrodes usually made of the same material and equal in mass and dimensions, between which a cell voltage is applied. A third (i.e., reference) electrode is not used. The degree of desalination as well as the current responding to a certain cell voltage can be measured in this setup (see Section 3.5). In the coming sections we focus on this second approach, where water is desalinated using cell pairs consisting of two porous electrodes. Section 6.2 discusses one particular mode of EC testing using a symmetric porous electrode cell pair.

The use of the first approach (EC testing using a three-electrode setup) finds its roots in similar testing of single electrodes for supercapacitor applications, and in the study of (planar) electrodes where Faradaic reactions take place. In a three-electrode experiment, the voltage of the electrode under study is measured relative to a reference electrode, as function of the current running between the working and counter electrode. Several well-known techniques are available to modulate the voltage- and current-signals, the two of which most often used for CDI are: (1) cyclic voltammetry (CV) where the (working) electrode potential is swept in time following a triangular pattern between a lower and higher set-point in voltage, and the resulting current is plotted in a CV-diagram [20,44]; and (2)

electrochemical impedance spectroscopy (EIS), where a small voltage signal, sinusoidally changing over time, is varied in a large window of frequencies, and the responding current (also sinusoidally varying, but with a time-lag) is analyzed to construct Nyquist plots and other representations that allow one to derive the magnitude of resistances and capacities in the electrode [45,47].

Though these techniques are well established [48], their application to porous electrodes is more complicated than for flat electrodes, and analysis requires understanding of distributed charge/resistance networks [49,50]. Classical analysis of data obtained from these methods assumes that the local resistances in the electrode are not changing as a function of time and position in the electrode. However, this condition is not met in CDI where desalination is the key objective, leading to strong salt concentration changes with place and time in the electrode, as we will discuss in Sections 5.3 and 6.3. Therefore, we argue in Section 6 that EC testing should be based on high-ionic strength conditions of the electrolyte (e.g., >0.5 M) as long as mathematical methods to analyze CV and EIS curves obtained in low salinity solutions have not yet been developed for porous electrodes.

Therefore, in the remainder of this section we focus on the second experimental approach discussed above, namely testing of a symmetric two-porous electrode cell, using the cell voltage applied between the two electrodes as the primary electrical signal. We note that this second approach is also more reminiscent of actual operation and desalination using CDI, which is another reason to use this approach.

3.2. Geometries for CDI testing based on a two-electrode layout

Most experimental work on CDI uses a design with two porous carbon film electrodes with a typical thickness between 100 and 500 μm, placed parallel to one another in such a way that a small planar gap is left in between the electrodes through which water can flow along the electrodes. This design is the classical CDI-geometry, and goes under various names, such as "flow-through capacitor technology" or "flow-by" CDI and is schematically sketched in Fig. 3a. In this "flow-by" CDI geometry, a typical electrode for laboratory scale experiments is in the range of 5×5 cm^2 to 10×10 cm^2. Such electrodes can be constructed either as freestanding thin films, or can be coated directly onto a flexible current collector such as graphite foil [9,51]. It is possible to test a single cell pair, or to construct a stack of multiple cell pairs. In that case, each current collector layer is contacting two porous

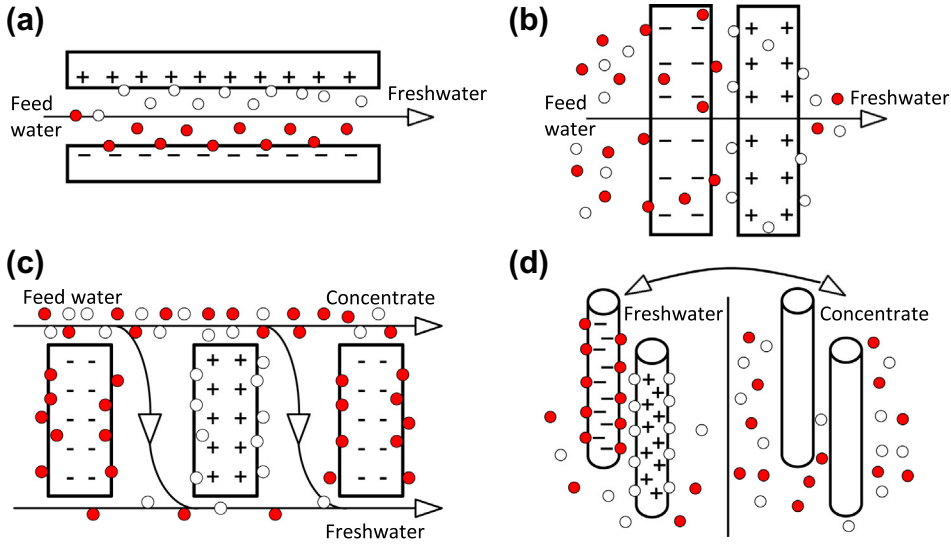

Fig. 3. Overview of most relevant CDI system geometries. (a) Flow-by mode, (b) flow-through mode, (c) electrostatic ion pumping, and d) desalination with wires.

electrodes (one on each side) and, thus, the sequence of anode–cathode is reversed from one cell to the next in the stack. Typically, each electrode is the same as the other in a cell pair, though cell pairs with electrodes with different synthesis conditions have been described in Refs. [52–57]. Recently [58], a different kind of asymmetric cell geometry was introduced, namely to use cathode-to-anode mass ratios not of one, but of two and three (and vice versa, of one-half and one-third), and compare desalination performance with the symmetric system where the two electrodes have equal masses.

The open channel between the electrodes, through which the water flows, can be an open channel, then typically at least 1 mm in thickness, or can be constructed from a spacer material, being a porous thin layer, of thickness typically between 100 and 300 μm. The geometry is normally not such that a purely one-dimensional flow pattern arises, but instead water flows from one edge of a square channel to an exit point at the opposite corner [43], or from a hole in the center of a square cell radially outward to leave the cell on all four sides [59]; the direction of this flow pattern can also be reversed.

Instead of the water flowing along the electrodes, that is, the "flow-by" mode, it is also possible to direct the water *straight through* the electrodes, a method applied by Newman and Johnson in Refs. [4,5] and further developed by Suss et al. [18], see Fig. 3b. In this design the feed water is pumped perpendicular to the layered structure, that is, straight through the larger pores in the electrodes. This flow condition has the advantage of a faster system response (rate of desalination) than flow-by CDI because instead of the CDI system being limited by the diffusive time scale (based on the time required for ions to diffuse from the spacer channel into the electrodes), now the process can be accelerated to work at the much faster RC time scale [18].

Another approach is called "electrostatic ion pumping" [60], see Fig. 3c, a method related to the classical technique of "parametric pumping" [6,13,37,38], two methods both having the advantage that (semi-continuously) two separate streams are produced from different exit points: a freshwater stream from one end of the device and a concentrate stream from the other end. In classical parametric pumping, the feedwater is injected about halfway along the length of the relatively long spacer (water) channel. In this method, while water is being fed continuously through the inlet hole in the middle of the column, the cell voltage between the two electrodes is applied during a certain period of time and turned off during another period of time. During the period of applying the cell voltage, a valve is opened on one end of the channel (valve A) and another valve closed on the opposite end of that channel (valve B), allowing desalinated water to come out at end A. During the period of zero cell voltage, valve A is closed and valve B is opened so that concentrate can be extracted through B. Electrostatic ion pumping [60], see Fig. 3c, is a modified approach because the one long channel used in parameter pumping can be considered to be cut up in smaller electrodes which are stacked together.

A new design employs movable carbon rod electrode wires [61], see Fig. 3d, thereby avoiding the sequential production of freshwater and concentrate from the same device for different periods of time, as in flow-by CDI and flow-through CDI, and avoiding the need to reverse the water flow direction as in electrostatic ion pumping. Instead, the freshwater and concentrate streams are separated at all times, right from the start. Thus, in contrast to the standard mode for CDI it does not have the disadvantage of the required precise switching of the effluent stream into freshwater and into concentrate, and the inadvertent mixing of just-produced water with the untreated water, an effect that may occur right after switching the voltage. In the wire-based approach, cell pairs are constructed from wires, or thin rods, with anode wires positioned close to cathode wires. An array of such wire pairs is lowered into the water and upon applying a voltage difference between the anode and cathode wires, salt ions will be adsorbed into their counter electrodes. The wire approach requires no spacer layer as long as the wires are sufficiently rigid, or at least one set of wires is coated with an ion-exchange membrane. After adsorbing salt, the assembly of wires is lifted from the compartment (or stream) that is desalinated, and immersed into another water stream, upon which the cell voltage is reduced to zero and salt is released. After salt release, the procedure can be repeated; thus, two continuous streams are obtained, one in which feed water is steadily converted into freshwater and one where feed water is continuously becoming more saline. The saline stream (into which adsorbed salt is released) can also be of a different source as the water to be desalinated. But when there is only one source of feed water, then by upfront splitting the feed water stream in a certain ratio of volumes, the water recovery of the process is automatically determined. Here, water recovery (WR) is the ratio of

freshwater volume over inlet volume, an important determinant to analyze performance of a water desalination process, see also Section 7.

3.3. Feedwater composition

The feed water used in CDI experiments can have very different compositions – ranging from analytical grade water with specified amounts of ions, to the complex compositions of brackish natural water or industrial process or waste water. First of all, it is important to decide whether or not to do experiments in air-saturated water. If so, it is advisable to make sure the oxygen- and CO_2-content is known, kept constant and reported. Oxygen- and CO_2-free water can be obtained by using a nitrogen blanket in the water storage (recycle) vessel, or by bubbling nitrogen gas through this tank.

In general, we can differentiate between the following types of feed water:

1. Real water (diluted sea water, tap water, ground water, waste or process water from agriculture or industrial sources). This water will contain many different ions, monovalent as well as divalent, and with some ions being amphoteric (i.e., their charge dependent on pH, such as HCO_3^- or HPO_4^{2-}). It will also contain colloidal matter, such as humic acids.
2. Water of a synthetic composition simulating a "real" water source, but which is free of organic pollutants, solid particles, and the like.
3. Water containing only a single salt solution, such as NaCl or KCl. This is most commonly the choice for laboratory-scale experiments in the literature.

When "real" water is chosen (option 1), one must decide on what pre-treatment to use to remove particulate and biological matter, and organic pollutants. Another consideration is that the use of ionic mixtures in options 1 and 2 leads to the requirement that the effluent freshwater produced must be analyzed using (off-line) individual ion detection methods, such as ion chromatography or inductively coupled plasma optical emission spectroscopy. However, in option 3, when utilizing only single salt solutions, the measurement of the conductivity of the effluent water is sufficient (ideally combined with pH measurements). In single salt solutions, we can choose for an electrolyte where the diffusion coefficients, D, of the anion and cation are (almost) equal such as for KCl, or choose for a salt where D_{cation} and D_{anion} are rather different such as for NaCl.

Each of these three types of water has its own advantages and disadvantages when used as feedwater in CDI experiments, and the choice between them must be made based on the objectives of the actual study. For fundamental CDI experiments to determine, for example, the salt adsorption capacity of an electrode material, option 3 using a single salt solution is the most straightforward to analyze, because the desalination performance can be followed in time and on-line using a conductivity meter. We note, however, that because of the complex composition of natural and industrial water, CDI performance under real conditions may be very different from what has been determined based on "clean" single salt solution experiments.

3.4. "Single-pass experiments" vs. "batch-mode experiments"

For all CDI cell designs, in order to measure the actual water desalination by CDI, we need to measure the change of ion concentration over time. This can be done by taking water samples and analyzing the ion composition. This is also the required procedure for studies with ion mixtures, such as for most real water sources or complex artificial mixtures, see Section 3.3 [26]. Only if a single salt solution (such as NaCl or KCl) is used, simple on-line measurement of the water conductivity suffices.

For the layout of a CDI experiment and in particular for the location of the conductivity probe, that is, where the conductivity is actually measured, two methods are possible: In the single-pass (SP)-method (Fig. 4a) water is fed from a storage vessel and the salinity (conductivity) of the water leaving the cell is measured directly at the exit of the cell or stack [12,58,62,63]. In this method the measured effluent salinity will start to drop soon after applying the cell voltage. Later on, however, the effluent (measured) salinity rises again to the inlet value, because the electrodes have reached their adsorption capacity. The effluent water is either discarded or can be recycled to a reservoir container. This

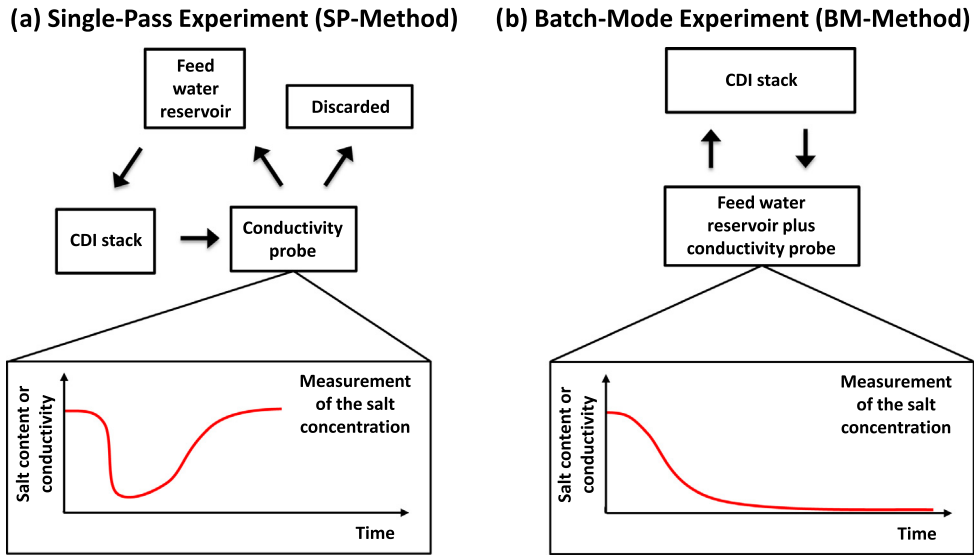

Fig. 4. Schematic of two designs for CDI experiments. (a) Single-pass experiment (SP-method): The water conductivity is measured at the exit of the stack, or cell, and the outflow is discarded afterwards, or recycled to the large feed water reservoir. (b) Batch-mode experiment (BM-method): The conductivity is measured in a (small) recycle beaker.

reservoir needs to be large to ensure that concentrations here only change very slightly within the adsorption half of the cycle, say less than 1%, to make sure that the influent concentration remains virtually constant during the cycle. The total amount of removed salt molecules can be calculated from numerical integration of the effluent concentration vs. time data (taking the difference with the feed concentration, and multiplying by the water flow rate Φ) [12,14,26,58,59,62].

In another common approach, which we call the batch-mode (BM) method (Fig. 4b), the recycling reservoir is much smaller, and it is in this container where the water conductivity is measured [9,22,64]. The volume of the recycling reservoir needs to be small because otherwise the change in salinity is low and cannot be measured accurately. In this experiment, the measured salinity drops steadily and does not have a minimum; instead it levels off at a final, low, value. The difference in salinity between the initial and final situation can be multiplied by the total water volume in the whole system to calculate the amount of ions removed from the water.

The analysis by the BM-method (Fig. 4b) is simpler than by the SP-method (Fig. 4a). However, one problem in the BM-method is that the equilibrium salt adsorption is measured for a different (final) reservoir concentration in each experiment, and this value is unknown a priori. Thus, in the BM method it is difficult to compare data for equilibrium adsorption at the same salt concentration, for example, for a range of cell voltages. The reason is that with increasing cell voltage, desalination increases and thus the salt concentration in the system decreases. And thus, in this experimental design it is more difficult to make a parametric comparison between theory and experiment. This problem does not arise with the SP-method because here we measure all properties (effluent salinity, electrical current) at well-defined values of the salinity of the feed stream. This is one advantage of the SP-method, the other being that it is more reminiscent of a real CDI application with water to be treated only passing through the device once, instead of being recycled multiple times, which will be less efficient.

3.5. Experimental data analysis

In this section, we briefly describe how to analyze (M)CDI data for salt adsorption, charge, and energy in the SP-method as discussed in Section 3.4. The analysis is based on an adsorption/desorption

cycle that has reached dynamic equilibrium (DE), where every cycle is the same as the last one, and equal to the next one. After equilibration of the cell, the DE state is often reached after two or three cycles. In the DE state, the salt adsorption in one part of the cycle must be equal to the desorption in the other part. Likewise the charge that is being stored (by transferring electrons from one electrode via the external circuit to the other electrode), will be returned when discharging the cell. A small electrical leakage current may make the total charging current somewhat higher than the discharging current. Not taking degradation mechanisms into account and as long as the operational settings do not change, the system response in the DE state should continue ad infinitum.

For practical CDI relevance, it is important to report experimental results of the DE cycle, and not results of runs prior to reaching the DE and certainly not of the very first "run-in" cycle after assembly of the cell with fresh material, as these runs can give quite markedly different desalination performance, due to transient effects of salt accumulation in the cell and electrodes. Also, the desalination degree in the first few runs will be influenced by the chemisorption of ions in the carbon, ions which will not be desorbed when the voltage is reversed [9,65,66]. These transient, start-up effects are interesting in their own respect, but for CDI it is more important to present DE results because CDI is meant to run continuously for many cycles, and the performance of start-up cycles is usually not representative of continuous operation.

In Fig. 5 we sketch how to analyze a complete DE CDI cycle for salt (left-hand side) and for charge (right-hand side), either for constant voltage (CV) operation (upper row) or for constant current (CC) operation (second row), an operational mode that will be discussed in Section 3.8. The salt adsorption and charge in an (M)CDI-cycle can be derived from data of effluent salt concentration and electrical current vs. time, as shown in Fig. 5. For salt adsorption, the difference between the feed and effluent salt concentration is integrated over time for either the adsorption period or the desorption period,

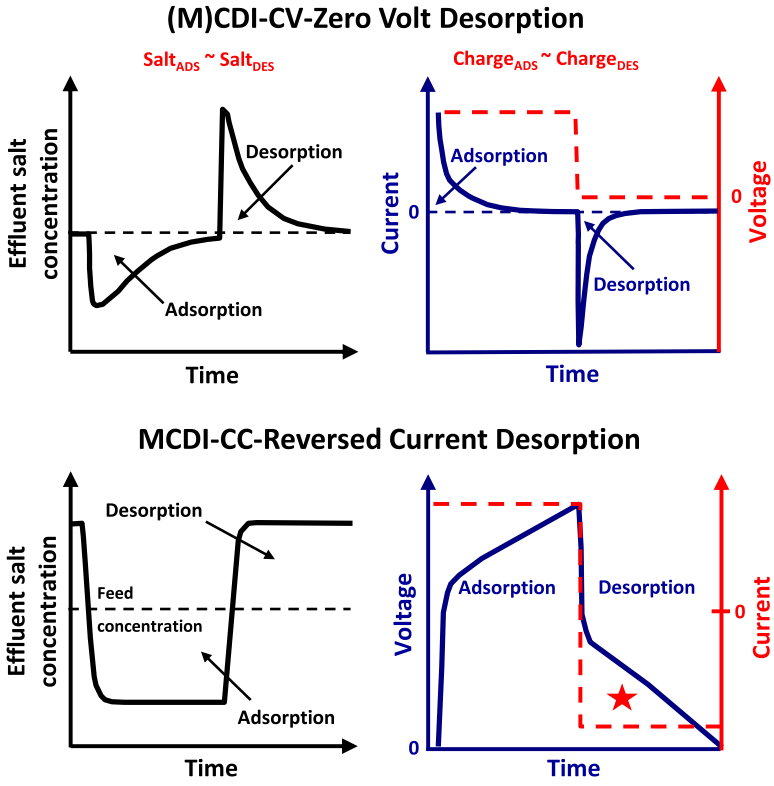

Fig. 5. Cycle analysis (single pass method) for constant voltage (CV), and constant current (CC) operation of (M)CDI. Both the effluent salt concentration and current signals are analyzed.

and multiplied with the water flowrate running through the cell; likewise, for charge, the current is integrated over time. In addition, energy consumption is calculated on the basis of integrating the power (product of cell voltage and current) over the adsorption step. During desorption at constant current, it is possible to recover part of the energy, see area marked by the red star in Fig. 5.

3.6. Membrane(-assisted) Capacitive Deionization (MCDI)

One of the most promising recent developments in CDI is to include ion-exchange membranes (IEMs) in front of the electrodes, called Membrane Capacitive Deionization (MCDI). IEMs can be placed in front of both electrodes, or just in front of one. With only one IEM, the overall positive effect on salt adsorption is less pronounced than in the case of using two IEMs. In the present section we only discuss data of MCDI containing two IEMs. IEMs have a high internal charge because of covalently bound groups such as sulfonate or quarternary amines, and therefore allow easy access for one type of ion (the counterion) and block access for the ion of equal charge sign (the co-ion). As we will explain below, including IEMs in the cell design significantly improves desalination performance of the CDI-process. In general, IEMs have a selectivity for ions of one charge sign relative to ions of another charge sign. In a further modification, the membrane can be made to have a selectivity between ions of the same sign class: for instance between nitrate and chloride (both monovalent anions) [67]. The membranes can be included as stand-alone films of thicknesses between 50 and 200 μm, or can be coated directly on the electrode with a typical coating thickness of 20 μm [8–12,68], see Fig. 1b.

Where does the advantage of MCDI over CDI come from? In MCDI, just as in CDI, upon applying a cell voltage in the ion adsorption step, counterions are adsorbed in the electrical double layers (EDLs) formed within the intraparticle nanostructure (micropores) inside the porous carbon electrodes, see Fig. 10, while co-ions are expelled from these micropores. In CDI, the co-ions ultimately end up in the spacer channel and reduce the desalination performance, that is, for the cell pair the ratio of salt removal over charge (the charge efficiency, Λ) is much less than unity (see also Sections 5.1.1, and Fig. 11). In MCDI, with ion exchange membranes placed in front of the electrodes, the co-ions that are expelled from the micropores are blocked by the membrane and cannot leave the electrode region. Consequently, they will end up in the interparticle pore space within the electrode (macropores, see Fig. 10) and accumulate there, which increases the macropore co-ion concentration to values beyond those in the spacer channel. Because of required charge neutrality in the macropores, this accumulation of co-ions there leads to an accumulation of counterions in the macropores as well. Thus, in MCDI, not only are counterions adsorbed in the EDLs in the micropores, but an additional part is stored in the macropores as well, where the salt concentration will ultimately be higher than in the spacer channel, see Fig. 14a. Therefore, the macropores play an important role in increasing the salt adsorption capacity of MCDI relative to CDI. In contrast, in CDI the salt concentration in the macropores is lower during ion-removal (not higher), while upon reaching equilibrium the salt concentration there becomes the same as that outside the electrode, that is, the same as in the spacer channel, and thus the macropores have no salt storage capacity in CDI [12].

The advantage of MCDI over CDI is clearly shown in the results presented in Fig. 6 (compare bars a–c, and b–d) which shows that MCDI absorbs more salt per cycle than CDI. The two modes of operation (ZVD, RVD) will be explained in Section 3.7.

3.7. Constant voltage (CV) operation of (M)CDI: zero-voltage (ZVD) vs. reversed-voltage (RVD) desorption

Up until this point we have considered (implicitly) that in a desalination-release cycle of (M)CDI the adsorption step is at an applied non-zero cell voltage and the desorption step at zero voltage. This operational mode we call (M)CDI-CV-ZVD for ''constant-voltage, zero-voltage desorption'' and is the standard operational mode in the scientific literature on CDI. However, experimentally one is free to use different cell voltage levels. For example, cycling between V_{cell} = 0.6 V (adsorption) and 0.3 V (desorption) has been described previously [40].

In this section we compare results of the CV-ZVD-mode of operation with results where during desorption the voltage level is changed to values opposite in magnitude to that during adsorption, that is, ''reversed-voltage'' desorption, or RVD. We show in Figs. 6 and 7 the advantage in desalination per

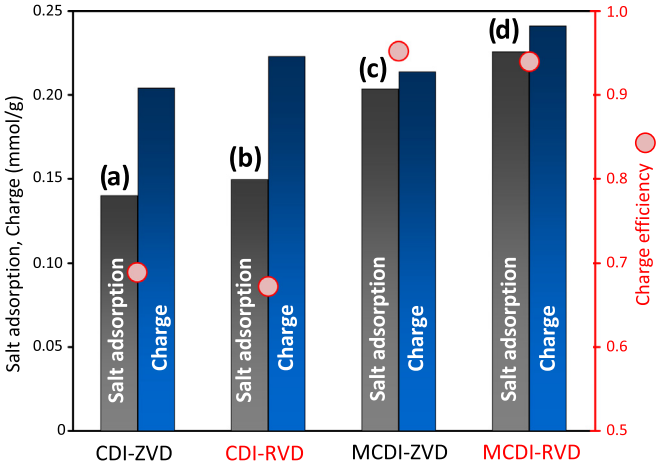

Fig. 6. Salt adsorption and charge per cycle, and charge efficiency (total cycle duration 600 s) for (a) CDI-CV-ZVD, b) CDI-CV-RVD, (c) MCDI-CV-ZVD, and (d) MCDI-CV-RVD. V_{cell} = ±1.2 V, $c_{salt,in}$ = 20 mM. Abbreviations explained in Section 3.7.

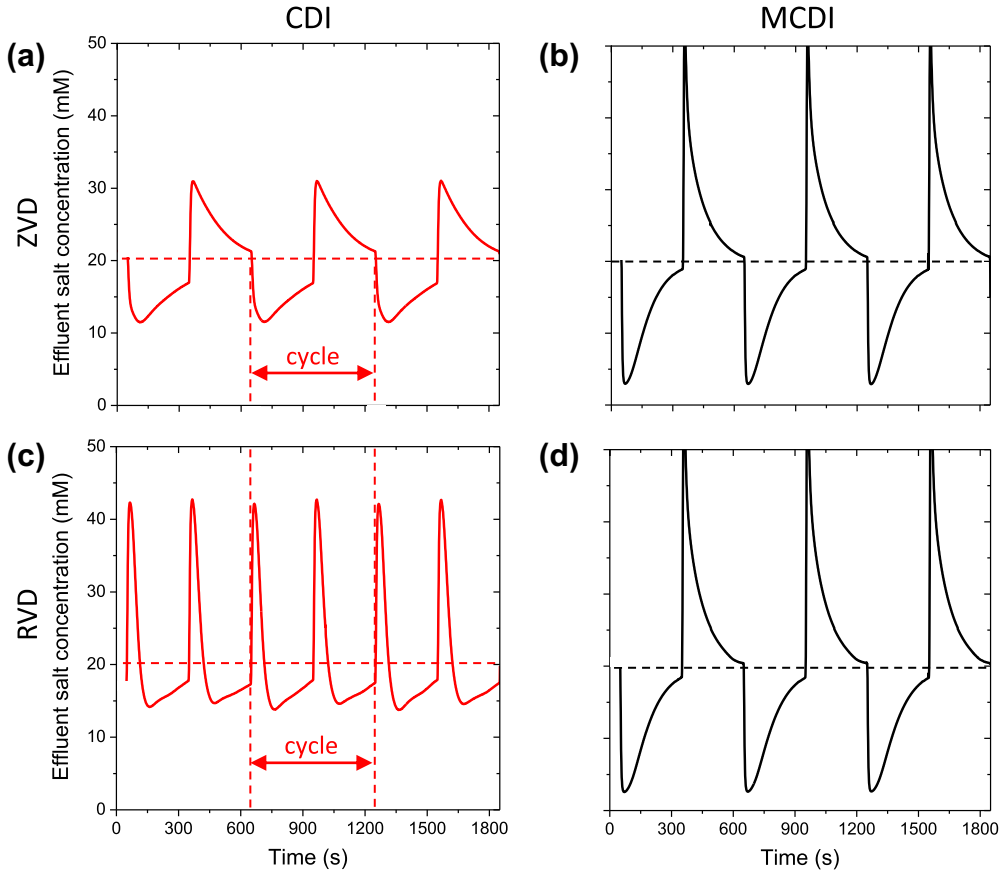

Fig. 7. Effluent salt concentration during three consecutive desalination/release cycles in four different modes of CDI-operation as explained in the main text of section 3.7 (a) CDI-CV-ZVD, (b) MCDI-CV-ZVD, (c) CDI-CV-RVD, and (d) MCDI-CV-RVD.

cycle when using RVD operation. For MCDI this operational mode has already been presented in Ref. [12]. In Ref. [12] we have argued that RVD-operation is not possible for CDI (i.e., without membranes) for reasons discussed below. However, as we will show next, that conclusion was premature and instead, quite unexpectedly, we find that CDI-CV-RVD is most certainly possible.

But first, let us answer the question, why is there an advantage of operation in RVD-mode? In CDI and MCDI in general, during standard ZVD desorption, counterions are expelled from the electrodes into the spacer channel and this depletion of counterions from the electrode region continues until the micropores become uncharged and the salt concentration in the macropores is approaching that in the spacer channel.

Now, in MCDI-CV-RVD, not only are the counterions removed to the point that the electrode is charge-neutral again, but counterion desorption continues, first of all from the EDLs in the micropores, in which now the co-ions are attracted as countercharge, and secondly from the interparticle macropores, of which the salt concentration drops dramatically to reach values close to zero at the end of the desorption step, see Fig. 14b, to be discussed later. Thus we have a very effective "clean-up" of the counterions from the electrode structure. Consequently, in the subsequent adsorption step of the next cycle, the counterion adsorption rate and capacity are increased compared to operation at ZVD-conditions, as can be seen from Fig. 6. MCDI-CV-RVD is possible because once the counterion is released from electrode "A" into the spacer channel, even though it may now feel an attractive force for adsorption in the opposite electrode "B", it is because of the membrane located there that it is blocked from entry in electrode "B", and is thus flushed out of the cell.

In CDI it has been argued that with a reversed voltage during desorption, because of the absence of membranes, the ions that are released from electrode "A" will be quickly adsorbed in the other electrode "B", and therefore it is not possible to work at RVD-conditions in CDI-CV because not much salt is effectively released into the effluent stream [12,14]. However, this prediction turned out to be wrong and we find that CDI-CV-RVD is most certainly possible, with even a higher adsorption capacity per cycle than in CDI-CV-ZVD, see Fig. 6. The reason must be that the expelled counterions actually do have sufficient chance to leave the stack via the spacer channel before being adsorbed in the opposite electrode. Interestingly, as a consequence of RVD-operation in CDI, in one "original" cycle consisting of first applying a positive cell voltage for a certain time and then a negative cell voltage (both durations 300 s for the data of Fig. 7), in CDI-CV-RVD, there will be *two* adsorption phases and *two* desorption phases condensed into one original cycle (of 600 s in total), or in other words, the cycle frequency in CDI-CV-RVD is twice that in ZVD-mode. This phenomenon of "frequency doubling" can be observed in Fig. 7, when comparing panel a with c. Note that in Fig. 6 we report desalination for CDI-CV-RVD as achieved within the timeframe of the "original" cycle of 600 s.

All four operational modes that have now been discussed are compared in Fig. 6 which shows that for salt adsorption, MCDI-CV-RVD > MCDI-CV-ZVD > CDI-CV-RVD > CDI-CV-ZVD. Although both for MCDI and CDI, using RVD enhances the total salt adsorption per cycle, it decreases the charge efficiency, which is the ratio of salt adsorption to charge per cycle [69]. In general, as will be discussed in Sections 5.1.1 and 7.2, when considering charge efficiency, MCDI is preferable over CDI, because both for ZVD and RVD mode, the charge efficiency Λ is above 0.9 for MCDI, while for CDI, it is generally below 0.8.

3.8. Constant current (CC) operation of (M)CDI vs. constant-voltage (CV) operation

Practically all published work on CDI uses one of the above experimental procedures based on a constant cell voltage (CV-operation) applied during ion adsorption, which is reduced abruptly during the ion desorption step resulting in salt release.

An operational mode quite different from CV-operation is constant current operation (CC) [14]. As sketched in Fig. 5, and in more detail in Fig. 8, for CV operation, during the desalination step the effluent water first decreases in salinity level, and then the salinity increases again. However, this may not be the most practical operational mode for actual devices when the production of freshwater with a constant composition (salinity) over time is required. This is achieved in CC-operation where the effluent salt concentration level remains at a fairly constant value, namely at a constant low value during adsorption, and at a constant high value during desorption, see Fig. 8 (right hand side for MCDI-CC).

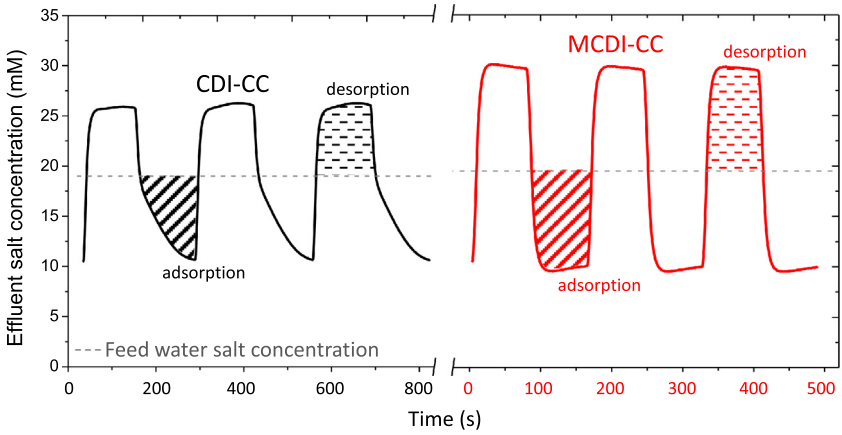

Fig. 8. Effluent salt concentration for constant-current (CC) operation of CDI and MCDI. Inlet salinity of NaCl 20 mM, flow rate 7.5 mL/min per cell. During adsorption, a current of 37 A/m^2 is applied, while the desorption current is −37 A/m^2. The current is reversed from positive to negative when the cell voltage reaches the upper limit of $V_{cell,max}$ = 1.6 V after which we switch to the ion desorption step until we return to a zero cell voltage.

Another advantage of CC operation is that one can precisely tune the effluent salt concentration level by adjusting the electrical current, or water flow rate, as control parameters [14].

One question is, to achieve a constant effluent salinity by CC-operation, are membranes required? To us, the answer is "yes", which we base on the finding that CC operation works only in MCDI and not in CDI. Instead, in CDI-CC the effluent salinity changes throughout the adsorption step, indicating that the salt adsorption rate is not constant, even though we operate in CC-mode, see Fig. 8, left-hand side. This is due to the fact that in CDI the electrical current is partially compensated by counterion adsorption and for the other part by co-ion desorption, as will be discussed in detail in the next sections [12,17,59]. The co-ion desorption effect decreases at high voltages and then the current is directly proportional to water desalination rate, but this is not yet the case at low cell voltages. Thus the salt adsorption rate by the full cell pair changes as function of time and this is why in CDI-CC the effluent salinity does not quickly level off to the desired constant low plateau, see Fig. 8 (left hand side for CDI-CC). For CC operation in combination with membranes (MCDI-CC, see Fig. 8, right-hand side), constant levels of the effluent salt concentration are quickly reached after start of a new adsorption step, because the co-ions are kept within the electrode structure and only counterions carry the ionic current. Thus, membrane-assisted CDI (MCDI) is required to obtain a constant effluent concentration in CC operation [14].

4. Conceptual approaches to understand the phenomenon of CDI

In the previous section we have analyzed a wide range of experimental possibilities for CDI. In the present section we discuss various conceptual approaches to describe CDI performance. Two related questions in this respect are:

1. How to understand the fundamental phenomenon that porous electrodes are able to adsorb salt under the application of an external voltage?
2. How to quantify experimental data for CDI, that is, what is the right theoretical modeling framework?

In the present Section 4 we highlight various conceptual approaches that have been developed with the aim to answer these questions. In Section 5 we will discuss in more detail those approaches that can be used to quantify and predict the outcome of a CDI experiment, for example, desalination, charge and energy.

4.1. Understanding of CDI using the concept of operational voltage windows

To describe the behavior and the performance of porous carbon electrodes in a CDI cell, one approach is based on a general description of electrochemical processes, and points out the importance that each electrode's potential must be positioned appropriately relative to a reference potential, or within a voltage window, required to have optimized ion adsorption and minimal Faradaic, parasitic electrode reactions [17,70]. Instead, if the potentials are not chosen correctly, then ion adsorption is not optimized.

Because the optimum electrode potential depends on the material's potential of zero charge (PZC), modifying the PZC, for example, by oxidation or reduction of the carbon materials can improve the resulting CDI performance. This can be done by reducing the positive electrode in a way that its PZC is shifted negatively and likewise the negative electrode can be oxidized to positively shift its PZC. As a result, after applying a voltage difference to a previously short-circuited CDI-system, both electrodes will work in a voltage window where expulsion of co-ions is limited, and adsorption of counterions is dominant, due to introduced potential shifts of both electrodes in opposite directions. The electrical potential of both electrodes can also be optimized by the use of a third electrode (reference electrode) which can lead to a higher charge efficiency and salt adsorption capacity [71].

4.2. Modeling based on charge-transfer between the electrodes

In a different approach, classical electrostatic double layer (EDL) theory for capacitive, ideally-polarizable, electrodes is the starting point to describe the charge–voltage and salt-voltage characteristics of the cell. In a first approximation it is assumed that the charge is only related to electronic charge in the carbon electrode, and to ionic charge (ions in the aqueous phase), compensating one another exactly, see Fig. 10. In this first-level approach surface charge due to chemical ion adsorption or carbon redox chemistry, see Fig. 9, is neglected, and, thus, when the material is not charged, there is a

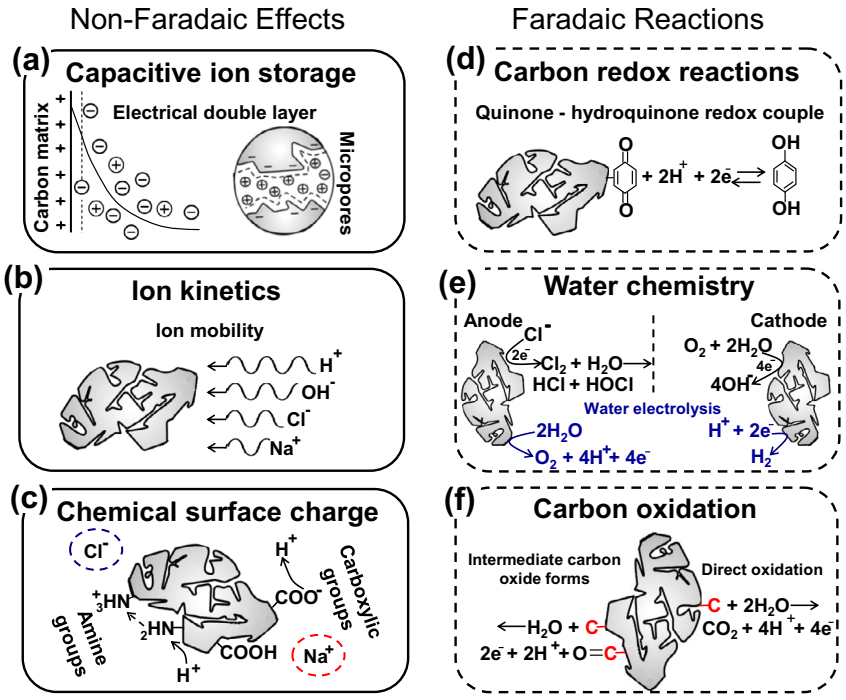

Fig. 9. Overview of important electrochemical reactions and processes in CDI electrodes. Effects (a–c) can be classified as non-Faradaic, and (d–f) as Faradaic processes.

zero voltage drop across the EDL. Electrokinetic modeling based on the Nernst–Planck equation can be used to quantify the dynamics of the process. Though neglected in a first approximation, the effects of chemical ion adsorption and carbon redox chemistry (see Section 4.4), can be incorporated in more detailed models [25].

In the EDL approach, the focus is not on how voltage windows are chosen relative to a reference electrode, but on how much charge is transferred from one electrode to the other, and how this impacts ion concentrations inside the porous electrodes (EDL structure) and the resulting local voltage drops across the EDL, that is, only local voltage *differences* play a role, not absolute potentials (relative to a reference electrode). This review follows the EDL-based approach which is discussed in much more detail in Section 5. Using similar concepts, Section 6 describes EC testing based on a pair of carbon electrodes where only purely capacitive processes occur. A one-dimensional electrosorption transport model is provided by Perez et al. [72], and a more detailed transport theory combined with EDL modeling in a two-dimensional geometry of the pores and spacer channel is found in Jeon et al. [73].

4.3. Isotherm-based modeling

A third approach for CDI modeling is to quantify experimental data for salt adsorption in the electrodes as function of salt concentration in the external bath (recycle volume) using one of several adsorption isotherms, such as those based on the Langmuir- or Freundlich-equation [65]. From the fitted parameters such as equilibrium constant K, information can be extracted on the interaction energy between ion and substrate. The fitted isotherms can also be used to predict adsorption at other values of the reservoir ionic strength.

Problematic in this approach is that it does not describe the fact that in CDI anions and cations are separated into their respective counter-electrode when they are removed from the water. Instead, isotherm-based modeling describes the adsorption of the whole salt molecule as if onto one and the same sample of carbon material. Consequently, the impact of several parameters cannot be included in this description, such as the role of the cell voltage. This approach neither describes how much charge is required for a certain salt adsorption (i.e., the charge efficiency is not predicted, see Section 5) nor how this approach can be extended to describe asymmetric electrodes (unequal mass of anode to cathode) [58].

4.4. Overview of electrochemical reactions and processes at the carbon/electrolyte interface

In Sections 3 and 4.2 we have focused on the capacitive effects of ion storage in the electrical double layer (EDL) formed inside the carbon micropores. However, the EDL effect is by far not the only electrochemical process playing a role in CDI. In Fig. 9 we summarize in six panels possible electrochemical processes that can play a role in CDI, their importance dependent on parameters such as applied voltage, electrode material, oxygen content of the water, and pH. Some of these processes are at the heart of the CDI phenomenon (A and B) while others are effects which need to be minimized, such as those leading to the formation of chemical byproducts or to pH-fluctuations of the produced water. Some of the effects lead to a reduction in the (desalination) efficiency, while others may in the long run even result in system performance loss. Therefore, all possible electrochemical processes must be understood in order to optimize electrode performance stability, energy efficiency, and to reduce pH-fluctuations. It may also be possible to make positive use of certain effects, such as effects (C) or (D) in order to improve CDI performance (energy efficiency) in novel ways. In general, the six processes that we identify below can be split up in two groups: non-Faradaic processes (effects A–C below), and Faradaic reactions (D–F). The distinction is that in the latter group, electrons participate in electrochemical reactions with reactants and products either part of the carbon/electrolyte interface (D), or present in the electrolyte phase (E and F). Let us list the six categories one by one, see Fig. 9.

4.4.1. Non-Faradaic effects

(a) First of all, *capacitive ion storage* is the phenomenon of the formation of an electrical double layer (EDL), where upon applying a charge, ions are captured electrostatically and stored capacitively

in the diffuse layer formed next to the carbon interface, see Sections 3, 4.2 and 5.1. The formation of the capacitive EDL is at the heart of the CDI process.

(b) *Ion kinetics* refers to the influence of the difference in mobility of the various ions on EDL formation. Ions (salt ions, protons, hydroxyl ions) are transported from the spacer channel via macro- and mesopores into the micropores, see Sections 5.2 and 5.3. High rates of ion transport are essential in CDI, but as indicated, the high mobility of the H^+ and OH^- ions (relative to salt ions) may play a role, leading to reduced adsorption of salts in the EDLs, and to pH fluctuations when H^+-adsorption is different from OH^--adsorption. Note that here we suggest that pH fluctuations may be simply due to the effect of differences in ion mobility, as an alternative to explanations based on electrochemical reactions such as water splitting to be discussed below.

(c) By *chemical surface charge* we describe the presence of charged groups at the carbon/electrolyte interface, groups responsible for the natural charge of carbons. Such groups are typically carboxylic (to render the material negatively charged) or based on amine-functionalities (to give the material a positive charge). When both such groups exist on the carbon, the material will be amphoteric which implies that dependent on the local pH near the carbon surface it may be positively or negatively charged, and thus there is a pH beyond which the material is negatively charged, and below which it is positive, that is, the carbon has a pH of zero charge. The charge of these groups depends on their intrinsic pK-value and on the local pH in the micropores [25], which depends on the local electrical potential, and the transport rates of H^+ and OH^- into and out of the pores [58,74]. Therefore the micropore pH can be hugely different from that in bulk solution, and thus the charging state of these groups can vary dramatically during a CDI cycle. These changes in charging state lead to a net H/OH adsorption and to pH-fluctuations in the flow channel. These H/OH adsorption/desorption fluxes will also influence the transport of salt ions, which can be modeled within the Nernst–Planck–Poisson framework [25,26,75].

4.4.2. Faradaic reactions

(d) *Carbon Redox Reactions* is the term to describe that certain carbon surface groups are able to change their redox state without the development of charge separation between surface and solution. The archetypical example for carbon is the quinone (Q) to hydroquinone (HQ) conversion, where two =O bonds in the quinone group on the carbon "react" with two electrons and two protons to form two –OH-groups (HQ). The presence of these groups on the carbon will lead to electronic charge storage in the desalination/release cycle, without the adsorption of salt ions (such as Cl^- or Na^+). Instead, by this mechanism protons are chemically adsorbed in the cathode upon carbon reduction from Q to HQ. Thus, the Q-to-HQ reaction may lead to pH fluctuations in the CDI spacer channel.

(e) *Water chemistry* By the term "water chemistry" we summarize all electrochemical processes where components in the water react at the carbon surface, with the products not staying at the surface but dissolving into the electrolyte. These components are mainly the water and its H^+/OH^- charge carriers, Cl^- and dissolved O_2. Water splitting (water electrolysis) is understood to limit the CDI process to voltages below the limit of 1.23 V beyond which a significant electrical leakage current may be expected with hydrogen gas and oxygen gas developing. However, the situation is found not to be so strict and operation well below 1.23 V is possible in practice, perhaps because the CDI process is not running in steady-state and local ion concentrations in the electrode are not at free solution values. Also, the reverse of water splitting is possible with oxygen dissolved in the water undergoing reduction at the cathode side, causing a pH increase of the effluent stream [63]. Oxidation of chloride ions at the anode followed by disproportionation of chlorine gas into hypochlorite is also of importance [63].

(f) Finally, *carbon oxidation* describes the possibility that the carbon itself not just catalyzes chemical reactions as described in (e) but sacrificially takes part in a conversion process, being increasingly oxidized and, it has been suggested, electrochemically converted ultimately into CO_2 leading to electrode mass loss and collapse of CDI performance [13,17].

This finalizes our summary of six categories of possible electrochemical effects that can take place in CDI electrodes. Even though this is already a fairly long list, we are aware that other (electro)chemical effects may also occur in CDI electrodes. Still, the list already suggests that in terms of quantitative study and the theoretical modeling of CDI, much work is still to be done, because until the present day only effects (a) and (b) have been considered to some extent in full-scale theoretical models to

describe the CDI desalination cycle. Effects (c–f) have not yet been included in these CDI transport models (effect (c) to some extent in Ref. [25]).

An important point to make is that it is not the case that when, for example, effect (e) occurs in the one electrode, it will have to happen to an equal (but opposite) extent in the other electrode. On the contrary, it may well be that one effect of the list is important in the cathode, and a very different one in the anode. Thus, it is not the case that an electron-transfer from carbon to water in one electrode (Faradaic electrochemical reactions) must be compensated 1-to-1 by another Faradaic reaction in the other to conserve electron balance. This is only true in a steady-state process, and CDI is not steady-state at any moment. Instead, a Faradaic reaction in one electrode can be compensated by a capacitive effect without electron-transfer in the other electrode. The only constraint in the CDI system is that the (electronic) current running into the one electrode is the same in magnitude as the electronic current running out of the other.

5. Theory of ion transport and adsorption in CDI

In Section 4 we discussed in general terms approaches to conceptually understand CDI. In the present section we will discuss in more detail theoretical concepts to quantitatively describe ion transport and ion storage properties of carbon electrodes for CDI. The literature on ion and water transport in porous media is vast and we do not attempt a review of this field (cf. Refs. [76,77] for an introduction with references). Instead, here we will introduce several mathematical routes that have shown to be effective tools in describing equilibrium and transport properties in CDI.

5.1. Electrostatic double layer models

5.1.1. Introduction

In this section we focus on describing salt adsorption and charge storage in the micropores within the carbon particles using the concept of the electric double layer (EDL). Basically, the EDL-model describes that across an interface (in our case, the carbon/electrolyte interface in the pores inside the carbon particles) there can be charge separation, with some excess charge in one phase (i.e., the electronic charge in the carbon matrix) locally charge-compensated by charge in the other phase (in our case due to the ions in the electrolyte-filled pores). These two components of charge sum up to zero, that is, as a whole, the EDL is uncharged. The concept of the EDL dates back to Helmholtz [78] who assumed in the 19th century that all surface charge (either electronic charge in a conductor, or chemically bound surface charge) is directly charge-compensated by countercharge adsorbed to (“condensed onto”) the surface; put in other words: the condensed layer of counterions directly compensates the surface charge. In this context, counterions are not to be mistaken with co-ions: counterions are the ions of opposite charge as that of the surface (which in our case is the electronic charge in the carbon, which can be of both positive and negative sign) and which are, therefore, attracted to the surface. In contrast, co-ions have the same charge sign as the surface and will be repelled away from the surface.

If the Helmholtz-model would hold, this would be an ideal situation for CDI: for every electron transferred from one electrode to the other, one cation would be transferred into the cathode to compensate the negative electronic charge there (assuming that all ions are monovalent), while one anion would be transferred into the anode to compensate for the positive electronic charge there, and as a result effectively one full salt molecule would be removed from the spacer channel. Thus, the charge efficiency Λ (to be defined below) would be unity: one salt molecule is removed for each electron transferred from one to the other electrode. Note here that in CDI the definition of anode and cathode is based on the charging step (when we adsorb salt): the cathode is where the cations go to during charging. This is opposite to the definition in battery and supercapacitor applications, where anode and cathode are defined based on where the ions go during electrode *dis*charging.

Unfortunately, the Helmholtz-model insufficiently describes the EDL structure in porous CDI electrodes. Instead, we must consider that ions *do not* condense in a plane right next to the surface, but remain diffusively distributed in a layer close to the surface, as described by the diffuse, or

Gouy–Chapman (GC) layer [79,80]. This diffuse layer must be combined by an inner (or compact) layer in between the electrode (the carbon matrix) and the diffuse layer; this inner layer is also called Stern layer or Helmholtz layer, and does not contain charge. Combination of the diffuse layer and (what is now called) Stern layer dates back to Stern in 1924 [81]. The diffuse layer does not have a precise width, but instead, ion concentrations progressively decay with increasing distance from the surface. The Debye length λ_D is a characteristic distance for the counterion concentration and potential to decay by a factor of e (~2.7) (in the low-voltage limit of the theory and for a planar single surface). For a NaCl solution of 10 mM ionic strength, the Debye length is approximately $\lambda_D \sim 3.1$ nm at 20 °C. As a rule of thumb, we can consider the diffuse layer to have ended after 2- or 3-times the Debye length.

The above approach, as depicted graphically in Fig. 10a, assumes that the diffuse layer extending from one surface is not "overlapping" with that of a nearby opposite surface. If, however, this is the case, then the diffuse layer does have a finite extension, namely of half of the distance between the two surfaces. This half-space contains all diffuse countercharge. Of course we have the same situation for cylindrical pores, or pores of other geometries with a finite space for the diffuse layer to form. This situation of "EDL overlap" will typically be the situation for the micropores (Ø < 2 nm) in activated carbon particles as the average pore size is generally smaller than the Debye length.

As discussed, in the Gouy–Chapman (GC) model (Fig. 10a) the ions are not surface-adsorbed in a condensed layer as considered by Helmholtz, but remain in solution because of their thermal motion. At equilibrium, the ion concentration profiles can be described in first approximation by the Boltzmann distribution which is at the basis of the Poisson–Boltzmann equation. One of the key predictions of the Gouy–Chapman theory for the diffuse layer is that to compensate surface charge, two routes are available. The first is counterion adsorption in the diffuse layer (the diffuse part of the EDL), while the second option is co-ion desorption, which implies that ions that were close to the surface in the absence of charge, are now being expelled because they have the same charge sign as the surface charge that builds up. This effect is disadvantageous for CDI, because now for each electron transferred between the two electrodes, only an extra, say, 0.6 or 0.8 ions are estimated to be stored in each electrode (relative to the situation without charge), and (with the same process also occurring in the other electrode) there will be only 0.6 or 0.8 salt molecules removed from the water flowing through the spacer channel (we consider a monovalent salt in the present analysis). Thus, the charge efficiency Λ will drop significantly below 100% to values of 60–80%.

Unfortunately, the situation sketched above is by far not the worst situation, because the charge efficiency can drop even further, all the way to zero. Zero salt adsorption is possible because at low

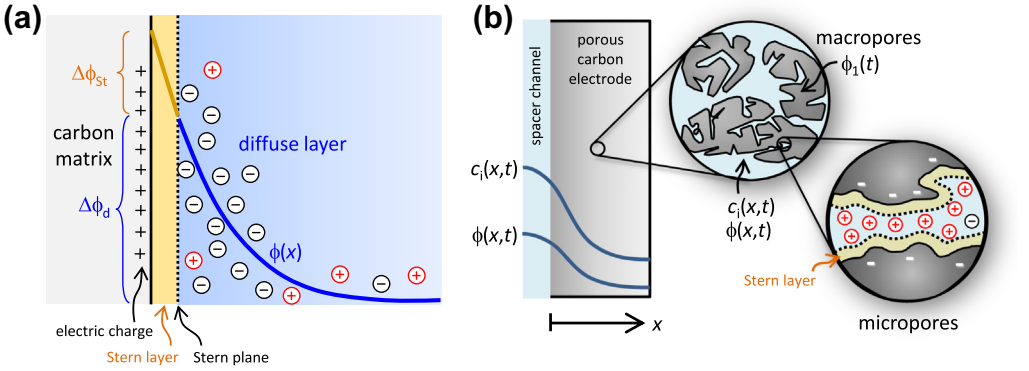

Fig. 10. Models for charge and ion storage in porous CDI electrodes. (a) Structure of the electrical double layer (EDL) according to the Gouy–Chapman–Stern theory for a single planar EDL. (b) Two-porosity-model for the electrode [12,14,23,58]. Both macro- and micropores are electrolyte-filled, and in both we assume locally averaged ion concentrations (within the micropores described by the Donnan model). The large and continuous interparticle pores (macropores) transport salt across the electrode thickness and are charge neutral, with salt concentration c, while in the (intraparticle) micropores the excess ionic charge is charge-compensated by electrical charge located in the carbon matrix.

voltages we approach the Debye–Hückel (DH) limit, a limit that is reached when the EDL voltage drops below the thermal voltage V_T, which is $V_T = k_B T/e = RT/F \sim 25.7$ mV at room temperature. In the DH-limit, electronic charge is compensated for 50% by counterion adsorption and for 50% by co-ion desorption, that is, co-ions that were in the electrode micropores prior to applying the electrical charge, are now expelled from the micropores. Consequently, the electrode cell pair consisting of the two porous electrodes (one in which the electrical charge is positive, the other negative) removes exactly zero salt from the water channel that is in between the electrodes. Data in the literature quantitatively underpin this effect, namely that with increasing cell voltage not only (1) the charge increases relatively linearly (as expected), but (2) also the charge efficiency increases, from zero to unity [59]. As salt adsorption is the product of these two parameters, it increases more than linearly with increasing cell voltage, or charge, see Fig. 11.

In CDI we typically work at cell voltages above 1.0 V, and thus, for a symmetrical cell design the EDL-voltage will be above 0.5 V, which is about 20 times the "thermal voltage", very far from the DH limit. For such high voltages, GC-theory would predict that for each extra electron transferred between anode and cathode, we are very close to removing a complete salt molecule from the water, because in each electrode we have only counterion adsorption and no longer any co-ion desorption because all co-ions initially present have already been expelled and there are none left. Thus, we expect the charge efficiency to be close to $\Lambda \sim 1$. Unfortunately, this is not the case. The origin of this discrepancy is the importance of the Stern layer which is the thin dielectric layer in between the charged surface and the start of the diffuse layer, as depicted in Fig. 10. This "start of the diffuse layer" (or Stern *plane*) can in first approximation be considered as the closest-approach-plane for the centers of the ions to the charged carbon surface, with the thickness of the Stern *layer* corresponding to the (hydrated) radius of the ion, for example, 0.3 nm (see Fig. 10a). Across this dielectric layer (which is uncharged of its own, that is, does not contain ions), the voltage drop can be very high. Our estimates are that it is not improbable that 80% of the applied voltage drops across this layer for the microporous carbons currently used for CDI. However, note that this does not imply that 80% of the energy invested in water desalination by CDI will be lost in this way, as the energy associated with the Stern layer is simply stored and can be completely recovered when the cell is discharged again. Thus, the Stern layer does not *contain* charge but it is a dielectric layer separating two regions of opposite charge, acting as a capacity that is charged and discharged. Finally, it is important to realize that in the simplest GCS-model as depicted in Fig. 10a the intersection of Stern and diffuse layer, which is the Stern *plane*, neither contains any charge nor (electro-)adsorbed ions. Instead, the Stern plane only denotes the closest-approach-distance for ions to come to the surface.

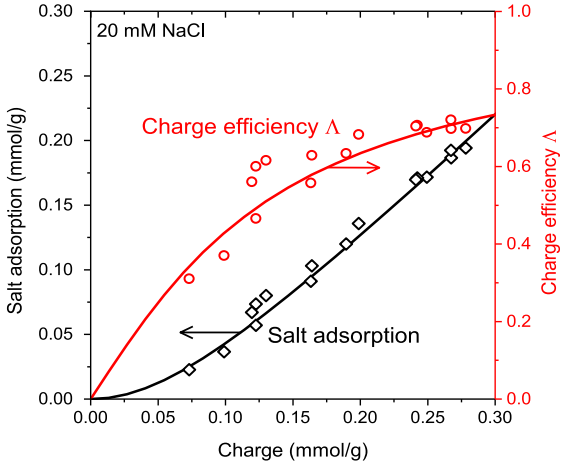

Fig. 11. Effect of co-ion desorption from electrical double layers on salt adsorption in a symmetric two-electrode cell pair made of activated carbon containing electrodes, as quantified by the charge efficiency Λ (salt adsorption/charge-ratio). Data reproduced from Refs. [12,59], see also Fig. 12.

The two concepts discussed above, namely the diffuse layer of diffusely distributed ions in the electrolyte-filled pores, and the dielectric Stern layer separating the diffuse layer from the carbon matrix structure, will be used in the further theory. Note that the Donnan model, discussed in Section 5.1.3, assumes that the diffuse layer has properties independent of the distance from the Stern plane, but otherwise this "Donnan part" of the model is similar to the diffuse Gouy–Chapman layer.

5.1.2. Gouy–Chapman–Stern theory for non-overlapping EDLs

Electrostatic double layer (EDL) theory is most often applied to derive a relation between stored charge (density) and the voltage difference across the EDL, that is, the voltage difference between the conducting electrode material ("matrix", or "carbon" in our case) and a location outside the EDL. "Outside the EDL" is defined as a position sufficiently far away from the surface that local charge neutrality is regained and thus (for a 1:1 salt) the concentration of cations equals that of the anions. The necessary distance depends on many factors but, for example, for a 10 mM salt solution a distance of 10 nm will be more than sufficient. EDL-theory is an equilibrium theory and equilibrium formally assumes that no further changes occur over time. One might suppose that such a theory cannot be applied for a dynamic process like CDI where – by definition – the transport rate of ions into the EDLs is always significant. Still, in the EDL layer of a few nanometers in thickness, local equilibrium can be assumed: even though there are significant ion transport fluxes across the electrode during the process of desalination, the charge–voltage (and salt-voltage) relations that describe ion concentrations in the micropores are very well described by assuming local equilibrium in the EDL layers. Formal derivations for the validity of this assumption are given in Ref. [82], with the main reason simply the very short (nm-scale) typical thickness of the EDL across which equilibration will be very fast, relative to the time-scale of seconds and minutes in a full CDI-cell with typical dimensions of the electrode layers of more than 100 μm and full cell dimensions of 10s of cm's.

The majority of literature on EDL-theory focuses on the amount of stored charge in the EDL. However, for CDI we are more interested in the total number of ions stored in the EDL. This "salt storage" has been studied in much less detail than the classical charge–voltage relationship of EDLs. Interestingly, the same EDL-model that predicts the charge vs. voltage relation also predicts the salt vs. voltage relation. An important effect is that at low voltages across the EDL, the capacitance for *charge* storage is non-zero (i.e., the slope of the charge vs. voltage-curve is non-zero), but the capacitance for *salt* storage will be zero. This effect implies that CDI is inherently a non-linear process [24]: voltages are required across the diffuse part of the EDL that are at least a few times the thermal voltage (V_T, which is ~25.7 mV at room temperature) to have water desalination by porous electrodes.

The equilibrium ratio of salt removal (in a 1:1 salt solution) vs. charge using a two-electrode setup, is called the charge efficiency, Λ. Experiments reported in Ref. [59] show that at low cell voltages (the applied voltage between the two electrodes), the charge efficiency Λ approaches zero, and only approaches unity, which is the theoretical maximum, at cell voltages well above V_{cell} = 1.0 V, and only at low enough ionic strength (see Fig. 11 for c_{salt} = 20 mM). Note that "charge" in this definition is the charge Σ expressed in the same dimension as salt removal, either in moles, moles/area, or moles/gram electrode. To convert from charge Σ_F in the more common dimension of C (Coulomb) per area or per gram, to Σ, we must divide by Faraday's number, F = 96,485 C/mol. In the sections below, both Σ and Σ_F are used. Also the pore charge density, to be discussed below, σ_{mi}, is expressed in mol/m^3 = mM, and can likewise be derived from the volumetric charge density in C/m^3 by dividing by Faraday's number. Also, experiments with the Electrochemical Quartz Crystal Microbalance (EQCM) can be used to determine the charge efficiency of single electrodes, as in this method both charge and the mass of adsorbed ions is measured [83,84].

Several of the above concepts, such as the difference between ion adsorption and charge storage, are depicted in Fig. 12, conceptually based on a classical figure that was first presented by Soffer and Oren in 1983 [37], see also Ref. [85]. In Fig. 12 we show the adsorption into the carbon pores of cations and anions from a monovalent (NaCl) solution, as a function of the electrode charge. Ion concentrations are defined per unit carbon micropore volume which is estimated for the activated porous carbon tested to be ~0.75 mL/g. The data are calculated from the measured charge and salt

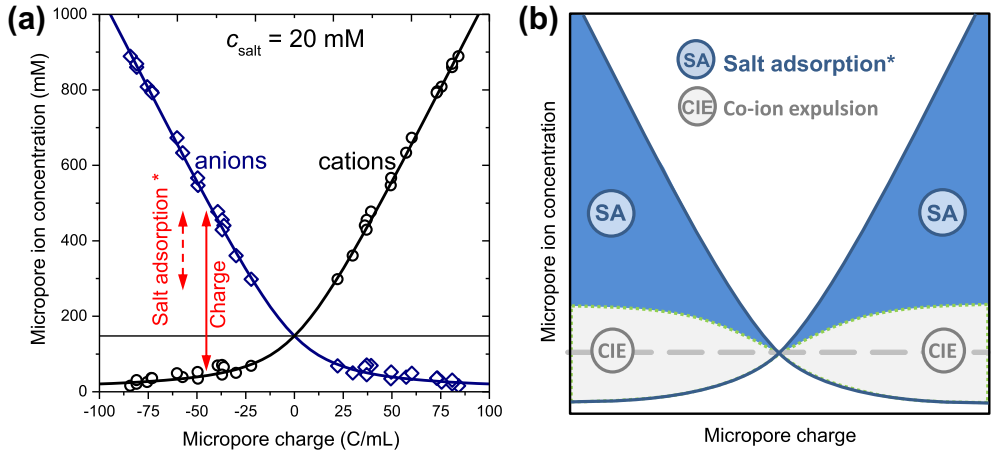

Fig. 12. (a and b) Typical curves for anion and cation equilibrium adsorption in the micropores of activated carbon electrodes, based on data from Ref. [12], expressed as moles of ions adsorbed per volume of micropores. Theoretical lines are based on the modified-Donnan model. Note that the micropore charge is always higher than the salt adsorption. (* Salt adsorption relative to the situation of zero charge.)

adsorption in a two-electrode setup [12,59,86]. To construct Fig. 12 both theoretically (here based on the modified Donnan-model to be discussed in Section 5.1.3), and experimentally, the assumption of symmetry is made, which implies that the anion adsorption (cation desorption) in the anode equals the cation adsorption (anion desorption) in the cathode; this also implies that the applied cell voltage is assumed to be equally divided over both electrodes. Our experimental work reported in Ref. [58] suggests that this assumption is very appropriate, at least for electrodes based on activated carbon powders that have not undergone modifications to introduce specific chemical groups. Fig. 12 shows that when we increase the micropore charge from zero, that the counterion adsorption increases with the same amount as the co-ion desorption, and thus the net salt adsorption in the micropores will be zero. With further increasing charge the co-ion desorption levels off and we reach the limit that for each increment in charge, an equal increment in counterion adsorption can be expected. This is the ideal situation that for each (additional) electron transferred between the electrodes, an (additional) full salt molecule is removed from solution. Consequently, Fig. 12 suggests that it may be favorable to operate CDI not by discharging from a charge of say 100 C/mL back to 0 before starting a new cycle, but that a cycle where we go from, for instance, +100 C/mL charge back to +50 C/mL charge (with reversed numbers in the opposite electrode) may be advantageous.

A large range of models are available to describe the structure of the EDL at planar surfaces and in the pores of charged materials and electrodes. The literature is extensive and we will not attempt a review. In the context of CDI and supercapacitors, advanced EDL-models describing ion removal and charge have been set up [87–92]. In the next two sections we will summarize two more simple mean-field approaches that can be used in two important limits, namely (1) the limit that the typical pore size (radius) is much larger than the Debye length, where we use the Gouy–Chapman–Stern (GCS) theory, and (2) the opposite limit where the pore size is small relative to the Debye length. For the latter, the EDLs overlap strongly and we can use a "modified Donnan" (mD) approach. These two models have the important property that they are mathematically sufficiently tractable to be implemented readily in larger-scale transport models, as we will show in Sections 5.2 and 5.3. More complicated EDL models may not allow one to do this easily.

Thus, in case we have a porous material with pores sufficiently large compared to the EDL-thickness, we can assume that the EDLs do not overlap and we can use the classical Gouy–Chapman–Stern (GCS) theory developed for a single ("isolated"), planar (flat) electrode. This limit is approached both in high salt concentration (short Debye length), or for very large pores (macropores). In that case the general Boltzmann relationship gives the ion concentration at position x away from the carbon

surface, as function of ϕ, the dimensionless potential relative to that in the neutral bulk solution (macropores), where the ion (salt) concentration is $c_{salt,mA}$, as

$$c_j(x) = c_{salt,mA} \cdot \exp(-z_j \cdot \phi(x)) \tag{1}$$

with z_j the ionic charge number (ion valence), and ϕ defined as the dimensional voltage V divided by V_T. Eq. (1) is valid for ions as point-charges in the mean-field approximation, and can be integrated across the diffuse layer to obtain for the surface charge density, σ, in mol/m^2,

$$\sigma = 4\lambda_D c_{salt,mA} \cdot \sinh\left(\frac{1}{2} \cdot \Delta\phi_d\right) \tag{2}$$

where λ_D is the Debye length, given by $\lambda_D = 1/\kappa$, with the inverse Debye length, κ, given by

$$\kappa^2 = \frac{2F^2 c_{salt,mA}}{\varepsilon_r \varepsilon_0 RT} = 8\pi\lambda_B c_{salt,mA} N_{av} \tag{3}$$

with $\varepsilon_r\varepsilon_0$ the dielectric permittivity of water (=78·8.854 × 10^{-12} C/Vm), R the universal gas constant, T temperature, λ_B the Bjerrum length, given by $\lambda_B = F^2/(4\pi\varepsilon_r\varepsilon_0 RT \cdot N_{av})$, and N_{av} Avogadro's number. The Bjerrum length is λ_B = 0.72 nm at room temperature. The surface charge density, σ, is defined in moles of charges per unit area of the electrolyte/carbon interface and can be multiplied by F to obtain the surface charge density in C/m^2.

From Eq. (1) we can also derive the total excess concentration of ions stored in the EDL, given by Refs. [59,82]

$$w = 8\lambda_D c_{salt,mA} \cdot \sinh^2\left(\frac{1}{4} \cdot \Delta\phi_d\right). \tag{4}$$

Next we define the charge efficiency, Λ, as an experimentally accessible parameter for any CDI cell geometry, as given by [59,82]

$$\Lambda = \frac{\Gamma_{salt}}{\Sigma} \tag{5}$$

where Γ_{salt} is the removed amount of salt upon applying a cell voltage (e.g., in moles per gram of all electrodes together) and Σ is the total charge transferred (obtained from Σ_F in C/gram divided by F). This equation can be used for any CDI experiment, as long as the current (which can be integrated in time to obtain Σ_F) and the salt removal are measured (see Section 3.5 for a description of various methods). Thus, Eq. (5) is equally valid for symmetric as for asymmetric CDI cells, and likewise is valid for electrodes where redox reactions play a role.

The charge efficiency is an equilibrium property; thus, measurements require sufficient time for desalination to come to an end after a certain cell voltage has been applied. To adequately describe the salt/charge ratio while the CDI-process is continuing, one option is to use the term "dynamic charge efficiency" [14]. Typically, we define charge efficiency for an experiment where we step up the cell voltage from zero to a certain value. However, it is also possible to go from a certain non-zero cell voltage $V_{cell,1}$ to a second value, $V_{cell,2}$ and base Λ on the resulting change in Σ and Γ [37]. One can also develop alternative definitions, such as a differential charge efficiency, which can be defined in many different ways, for example, as the slope in a plot of Λ vs. V_{cell}, or the slope in Λ vs. σ, and so on. In a transport model one can use a differential charge efficiency to relate the ions flux into an electrode, to the current, as in Ref. [93]. In the present work we focus on the equilibrium charge efficiency Λ and use it to describe an experiment with a cell voltage of zero, V_{cell} = 0, as reference.

The charge efficiency cannot only be measured, but can also be predicted based on EDL-theories. In this section we do this on the basis of the "single-plane" GCS-theory. Additional to the assumptions underlying the GCS-theory we will also assume that we describe an experiment with two equal electrodes and that the magnitude of the diffuse layer voltage, $\Delta\phi_d$, is the same in each electrode; thus, we assume ideal symmetry of the CDI cell pair [58]. In that case, we can use (1) $\Sigma = \sigma \cdot a$, where a is the specific electrode surface area in m^2 per gram of electrode, and (2) $\Gamma_{salt} = w \cdot a$, based on the fact that

for a symmetric cell pair the total adsorption of ions in one electrode equals the total adsorption of *salt* molecules in the cell pair (at least for a symmetric monovalent salt). Combining these definitions with Eqs. (2), (4), and (5) results in (see Ref. [59])

$$\Lambda = \tanh\frac{\Delta\phi_d}{4}. \tag{6}$$

Eq. (6) predicts that according to the GCS model, the charge efficiency Λ only depends on the diffuse layer voltage, $\Delta\phi_d$. In the GCS-model, we must finally consider the Stern layer voltage, $\Delta\phi_{St}$, which relates directly to the charge, σ, according to

$$\sigma \cdot F = C_{St} \cdot \Delta\phi_{St} \cdot V_T \tag{7}$$

with C_{St} the Stern layer capacity (in F/m^2). To complete the calculation of the equilibrium GCS-model, we need to relate the applied cell voltage V_{cell} to $\Delta\phi_d$ and $\Delta\phi_{St}$. Assuming a symmetric cell, this relation is $V_{cell}/(2 \cdot V_T) = |\Delta\phi_d + \Delta\phi_{St}|$. As mentioned, we have assumed throughout this section that the EDL-structure in the one electrode equals that in the other electrode except for the obvious difference in sign. For an ideal NaCl solution and for electrodes made of porous carbon, this assumption finds strong experimental support in the work described in Ref. [58]. For electrolytes containing both monovalent and divalent ions, this assumption will no longer be correct [26].

This finalizes our treatment of the Gouy–Chapman–Stern model valid for a non-overlapping, planar, EDL-structure. In the next section, we consider the modified Donnan model, valid in the opposite limit, where the EDL-thickness is much larger than the typical pore size.

5.1.3. Modified Donnan theory for fully overlapped EDLs

In the previous section we discussed the GCS-model applicable when EDLs are not overlapping. However, applying this theory to experimental data using standard electrodes made of porous activated carbons, we found [59] that at high cell voltages this theory predicts co-ion expulsions from the EDL that are beyond the amount of co-ions initially present in an electrode. This anomaly is due to the fact that the GCS-theory cannot be applied to micropores where the Debye length is of the order of, or larger than, the pore size. This problem is resolved when the mD-model is applied for CDI. The mD-approach is valid in the limit of strongly overlapped EDLs, and was shown to work well to describe many data sets for salt adsorption and charge storage in CDI, see Refs. [14,25,26,58,94].

The mD-model can be used to theoretically describe the equilibrium salt adsorption and charge in microporous carbons, and assumes that the electrical double layers (EDLs) inside the carbon particles are strongly overlapping, to the point that we can assume that the potential in the micropores becomes constant (i.e., does not vary with position in the pore). This will be a valid assumption when the Debye length is much larger than typical micropore sizes, which are often in the 1–2 nm range. In this limit, it is possible to make the "Donnan" assumption that the electrolyte inside the carbon particles has a constant electrical potential. Obviously this is an approximation of the detailed structure of the EDL in microporous carbons [92,95], but the Donnan approach has the advantage of being mathematically simple, while it has shown to accurately describe data both for charge and salt adsorption. Because of its simplicity, it can easily be included in porous electrode mass transport theory [23,25,26], while it will not predict larger co-ion expulsions than physically possible. The latter prediction, as mentioned before, is a severe complication of the GCS-theory when applied to microporous carbons.

The basic approach as set out above, however, does not yet describe well various data sets for salt adsorption and charge in microporous carbons. To that end, we must make two quite natural modifications [95]. The first is to include the Stern layer in between the location of the electronic charge (residing in the carbon matrix), and the ions present in the electrolyte-filled micropores. The Stern layer reflects the fact that the ionic charge cannot come infinitely close to the electronic charge, for instance due to the (hydrated or dehydrated) ion size, or because the electronic charge is not exactly located at the edge of the carbon material, for example, because of an atomic "roughness" of the carbon/electrolyte interface. The second modification to the basic Donnan approach is to include a chemical attraction energy for the ion when the ion transfers from outside to inside the carbon particles,

described in the theory by a term μ_{att}. Thus, in this way we consider an additional, non-electrostatic, attraction for the ion to go into a pore, even in the absence of electronic charge, as has been experimentally observed [96].

The mD-model containing these two modifications, see Refs. [14,26,58,62] is described by the following equations. First of all, the concentration of ion j in the micropores inside the carbon particle is given by

$$c_{j,mi} = c_{salt,mA} \cdot \exp(-z_j \cdot \Delta\phi_d + \mu_{att}) \tag{8}$$

where "mi" stands for the intraparticle (micro)pores (the pores inside a carbon particle), and "mA" for the macropores, being the transport pathways outside the particles, (see Fig. 10b). In the macropores, the anion and cation concentration are equal (local electroneutrality) because we only consider a monovalent salt solution at present, and thus $c_{j,mA}$ can be replaced by the macropore salt concentration, $c_{salt,mA}$, which will be a function of time and position (depth) within the electrode, just like $c_{j,mi}$. In Eq. (8), $z_j = +1$ for the cation and $z_j = -1$ for the anion, while $\Delta\phi_d$ is the Donnan electrostatic potential difference between micro- and macropores, that is, between inside and outside the carbon particle. It may be noticed that Eq. (8) is very similar to Eq. (1) in Section 5.1.2 except for the extra term μ_{att}, with the Donnan potential now replacing the local potential, ϕ. Note that Eq. (8) will be used for the whole micropore volume, whereas Eq. (1) was only used to describe the ion concentration in a plane at distance x from the electrode surface, and was integrated over x to obtain the charge–voltage and salt-voltage relations given by Eqs. (2) and (4). In the mD-model, this integration is not necessary, and instead summing up Eq. (8) for both ions directly gives the total ion density in the pores:

$$c_{ions,mi} = c_{cation,mi} + c_{anion,mi} = 2 \cdot c_{salt,mA} \cdot \exp(\mu_{att}) \cdot \cosh(\Delta\phi_d). \tag{9}$$

Though it is possible to consider the fact that μ_{att} will be different for anions and cations (and may depend on other factors), in the present work we will assume that they are the same. In future work it may be possible to derive from dedicated experiments with different salt solutions the individual values of μ_{att} for each ion separately.

The local ionic micropore charge density, σ_{mi}, likewise follows from Eq. (8) as

$$\sigma_{mi} = c_{cation,mi} - c_{anion,mi} = -2 \cdot c_{salt,mA} \cdot \exp(\mu_{att}) \cdot \sinh(\Delta\phi_d). \tag{10}$$

This volumetric ionic micropore charge density (dimension mM = mol/m^3), σ_{mi}, relates to the Stern layer potential difference, $\Delta\phi_{St}$, according to

$$\sigma_{mi} \cdot F = -C_{St,vol} \cdot \Delta\phi_{St} \cdot V_T \tag{11}$$

where $C_{St,vol}$ is a volumetric Stern layer capacity (in F/m^3). We can define the charge efficiency of the EDL as the total ion concentration, $c_{ions,mi}$, relative to the value at zero charge (zero $\Delta\phi_d$), divided by charge, which according to Eqs. (9) and (10) then leads to

$$\Lambda = \frac{c_{ions,mi} - c^0_{ions,mi}}{\sigma_{mi}} = \tanh\frac{\Delta\phi_d}{2} \tag{12}$$

where superscript "0" refers to the total ion adsorption at a cell voltage of $V_{cell} = 0$. Eq. (12) is valid for an experiment where the initial and final salt concentrations outside the EDL are the same (Fig. 4a). Eq. (12) is slightly, but notably, different from the prediction based on the GCS-model as given by Eq. (6).

For a symmetric CDI cell, the measurable parameters of equilibrium charge Σ_F ($=\Sigma F$) and salt adsorption Γ_{salt} (relative to salt adsorption at zero applied voltage, that is, at $V_{cell} = 0$ V) per gram of both electrodes together, can be related to $c_{ions,mi}$ and σ_{mi}, as follows [14,26,58,62]:

$$\Gamma_{salt} = \frac{1}{2} \cdot p_{mi}/\rho_e \cdot \left(c_{ions,mi} - c^0_{ions,mi}\right), \quad \Sigma_F = -\frac{1}{2} \cdot F \cdot p_{mi}/\rho_e \cdot \sigma_{mi} \tag{13}$$

where ρ_e is the electrode density (mass per unit total electrode volume) and p_{mi} the micropore volume relative to the total electrode volume. Note that the ratio p_{mi}/ρ_e is equal to the micropore volume per gram of carbon powder (as, for example, measured by nitrogen adsorption) times the

mass fraction of carbon powder relative to the total electrode mass (e.g., 85%). The ratio of Γ_{salt} over Σ is equal to the charge efficiency Λ. It is important to note that Eqs. (12) and (13) assume symmetry: the double layer structure in the cathode is equal to that in the anode, except for the difference in the sign of charge; thus μ_{att} must be the same for the cation and the anion. More general theories including differences in μ_{att} as well as the natural charge of the carbon (dependent on local pH) and redox reactions should be developed in the future. Extensions for electrodes with unequal mass of the the two electrodes are given in Ref. [58]. Finally, as for the GCS-model, for equilibrium, the applied cell voltage V_{cell}, defined as a positive number, relates to $\Delta\phi_d$ and $\Delta\phi_{St}$ according to $V_{cell}/(2 \cdot V_T) = |\Delta\phi_d + \Delta\phi_{St}|$.

5.2. Simplified dynamic CDI transport model for batch-mode experiment

Next we describe a simple dynamic CDI process model including the mD-model of the previous section, valid for a batch-mode experiment (see Section 3.4) where the water leaving the CDI-cell is flowing to a recycle vessel and from there fed back into the CDI-cell (see Fig. 4b). Assuming relatively low desalination "per pass", we can make the assumption that throughout the cell the salt concentration is the same everywhere (though it will decrease in time), and is the same as in the recycle vessel. As we will show, this model can be solved using simple spreadsheet-software, using the forward Euler method, see Box 1. This model assumes symmetry at several points, namely that the EDL-structure in the anode is the same as that in the cathode, except for the obvious difference in sign. The presented model describes CDI and does not include the membranes, required for a description of membrane-assisted CDI (MCDI).

We will develop this transport model on the basis of the modified Donnan (mD) model (Section 5.1.3) as this seems to be the most suitable EDL-model for CDI. When desired, it can also be set up based on the GCS-model.

The model is based on a cell balance for the ionic charge density in the intraparticle micropores, σ_{mi}, which relates to the current density J running from electrode to electrode, as given by

$$v_{mi}\frac{d\sigma_{mi}}{dt} = J \cdot A, \tag{14}$$

where J is defined in mol/m^2/s, and where A is the electrode area (that is, the area of the spacer channel covered by the porous electrode, either anode or cathode), and v_{mi} is the micropore volume in all electrodes of the same sign (i.e., all anodes, or all cathodes). The volume v_{mi} excludes the volume of the interparticle macropores in the electrode, which is included in v_{tot}. To obtain the current as measured externally in A (Ampère), we can multiply $J \cdot A$ by Faraday's constant, F. The current J depends on the driving force for transport, $\Delta\phi_{tr}$, which is the applied cell voltage minus the voltages in the EDLs in both electrodes, and it will depend on the resistance, to which there are contributions both in the spacer channel and within the electrode. The resistance in the spacer is a linear resistance as all charge effectively has to transfer from one electrode across the channel to the other. Within the electrode, however, the situation is very different because charge will be stored in a distributed fashion, and the ion concentration profile increasingly penetrates into the electrode (see Sections 5.3 and 6.3): initially there is hardly any resistance in the electrode as ions will be stored right next to the interface with the spacer. It is only with the passing of time that the ions will need to travel a constantly increasing distance to reach unsaturated pores. To describe all these effects, porous electrode theory is required which will be treated in the next section.

In a simplified transport model, the macropore concentration is assumed constant across the electrode and an ionic electrode resistance is included [12,97]. Without membranes, we can combine this resistance inside the electrode with that in the spacer channel. To describe the current–voltage relation, we will not assume a constant resistance but include how the resistance increases when the salt concentration goes down. We assume that at each moment in time the salt concentration within the electrode macropores (the transport pathways in the electrode) is the same as in the spacer channel. Therefore, we can use a single relation between J, $\Delta\phi_{tr}$, and c (with c being the salt concentration, assumed equal in spacer channel, macropores, and recycle vessel), resulting for J in

$$J = k \cdot c \cdot \Delta\phi_{tr}, \tag{15}$$

where k is an effective total transport coefficient (in m/s) and $\Delta\phi_{tr}$ is the dimensionless voltage drop that drives transport, that is, the voltage between the outer region of the EDLs in the one electrode and in the other electrode. This voltage drop, $\Delta\phi_{tr}$, relates to the cell voltage, V_{cell}, and the EDL-voltages according to

$$V_{cell}/V_T = (\Delta\phi_{St} + \Delta\phi_d)_{anode} + \Delta\phi_{tr} - (\Delta\phi_{St} + \Delta\phi_d)_{cathode} = \Delta\phi_{tr} + 2 \cdot |\Delta\phi_{St} + \Delta\phi_d|, \tag{16}$$

where the second equality is based on the assumption of symmetry of the EDL-structure in anode and cathode. Vertical lines denote that the absolute value of the EDL-voltages is used. By combining Eqs. (10), (11), and (15) with Eq. (16) we obtain a relation for J as function of σ, c and V_{cell} according to

$$J = kc\left\{\frac{V_{cell}}{V_T} - \frac{2 \cdot \sigma_{mi} \cdot F}{C_{St,vol} \cdot V_T} - 2 \cdot \operatorname{asinh}\frac{\sigma_{mi}}{2 \cdot c \cdot \exp(\mu_{att})}\right\} \tag{17}$$

which can be substituted directly in Eq. (14).

Finally, we set up a balance stating that the total number of moles of salt molecules in the system is conserved,

$$v_{tot}c_0 + v_{mi}c_{ions,mi,0} = v_{tot}c + v_{mi}c_{ions,mi} = v_{mi}\gamma \tag{18}$$

where v_{tot} is the water volume in the whole system, including the recycle vessel, tubing, spacer channel and macropores, but excluding micropores. Volumes v_{mi} and v_{tot} as well as area A must either be based on a single cell, or on the full CDI-stack. In Eq. (18), subscript "0" refers to time zero, the moment before the voltage is applied. To understand Eq. (18), one must realize that the number of moles of *ions* in the micropores of *one electrode*, $v_{mi} \cdot c_{ions,mi}$, equals the number of moles of *salt* molecules in the micropores of *both* electrodes taken together. As shown in Eq. (18), we describe the total amount of salt molecules in the system, divided by the micropore volume, v_{mi}, by the parameter γ.

The micropore ions concentration is obtained by combining Eqs. (9) and (10) which leads to

$$c_{ions,mi} = \sqrt{\sigma_{mi}^2 + (2 \cdot c \cdot \exp(\mu_{att}))^2} \tag{19}$$

which can be combined with Eq. (18) to result in

$$c = \frac{\sqrt{b^2 - 4\beta(\sigma_{mi}^2 - \gamma^2)} - b}{2\beta}, \quad \beta = (2\exp(\mu_{att}))^2 - \left(\frac{v_{tot}}{v_{mi}}\right)^2, \quad b = 2\gamma\frac{v_{tot}}{v_{mi}}. \tag{20}$$

Thus, we have set up a CDI model based on a single differential equation, Eq. (14), expressing micropore charge density, σ_{mi}, as function of current J, together with auxiliary relations for the salt concentration, c, and current density, J, according to Eqs. (17)–(20). Just as in Refs. [58,62] we will not use a constant Stern capacity to fit the data, but use a function where $C_{St,vol}$ increases with increasing charge, a classical observation [62,98,99], which we describe empirically by using $C_{St,vol} = C_{St,vol,0} + \alpha \cdot \sigma_{mi}^2$. Next we will demonstrate how this set of equations can be solved in simple spreadsheet software [example sheet available upon request from the authors] and we show a comparison of theoretical results with example data.

To solve this model, total saltwater volume v_{tot}, micropore volume (of all electrodes of one sign), v_{mi}, and electrode geometrical area A (of all electrodes of one sign) are obtained from the experimental geometry and carbon analysis (e.g., pore volume in mL/g from nitrogen sorption, times the mass of porous carbon in the electrode, results in v_{mi}). From fitting of the mD-model to equilibrium data we obtain parameter estimates for $C_{St,vol,0}$, α, and μ_{att}. Fitting to the time-dependent part of the data, the only remaining parameter is then the transfer coefficient, k, to fit all possible data sets.

Box 1 Solving the simplified dynamic CDI model using spreadsheet software.

A simple procedure allows us to solve Eqs. (14), (17), and (20) as function of time in standard spreadsheet software, using the Euler Forward method.

- Step 1. Assign columns for the parameters t (s), c (mM), σ_{mi} (mM), and J (mol/m^2/s).
- Step 2. Make a separate list of constants: k, V_{cell}, v_{tot}, $C_{St,vol,0}$, α, F, μ_{att}, v_{mi}, β, and A.
- Step 3. Make a list of time values from 0 to a certain final time, with time-steps Δt.
- Step 4. For time zero we know that (1) c is equal to c_0 and (2) that $\sigma_{mi} = 0$ and $c_{ions,mi} = c_{ions,mi,0}$ from Eq. (19). Based on these parameters, we can calculate γ, b and β from Eqs. (18) and (20). Also, J can be calculated at time zero using Eq. (17).
- Step 5. A value for σ_{mi} at the next moment (at the next "time-line") follows from Euler Forward's method based on Eq. (14): $\sigma_{mi,i} = \sigma_{mi,i-1} + J_{i-1} \cdot \Delta t \cdot A/v_{mi}$ where subscript "i" refers to the actual time-line, and "i−1" refers to the previous time-line.
- Step 6. For the actual time-line "i" we now calculate c using Eq. (20), based on σ_{mi} from the same time-line "i", and next we calculate J using Eq. (17), based on c and σ_{mi} from the same time-line "i".
- Step 7. We copy the equations for c, σ_{mi}, and J from Steps 4 and 5 down to the final time.
- Step 8. We can now plot the salt concentration c as function of time, t.
- Step 9. It is important to compare results for various values of the timestep Δt, and only when Δt is small enough that it does not influence the outcome of the calculation, then we can use the calculation outcome (we find good results with $\Delta t = 1$ s).

In Fig. 13 we present example data obtained in the same stack of $N = 8$ cells as described in Refs. [14,58,59,62] using activated carbon electrodes (Norit Supersorb 50) with electrodes each of mass 0.58 g and with each cell having $A = 33.8$ cm^2 projected (geometric, outer) surface area, using a spacer of $L_{sp} = 250$ μm thickness and an open spacer porosity of $p_{sp} = 0.5$, after compression of the stack. Of the electrode mass, 85 mass% is AC (activated carbon), and the micropore volume of pores <1 nm measured by Nitrogen Sorption is 0.22 mL/g AC. The water flow rate is 60 mL/min for the stack.

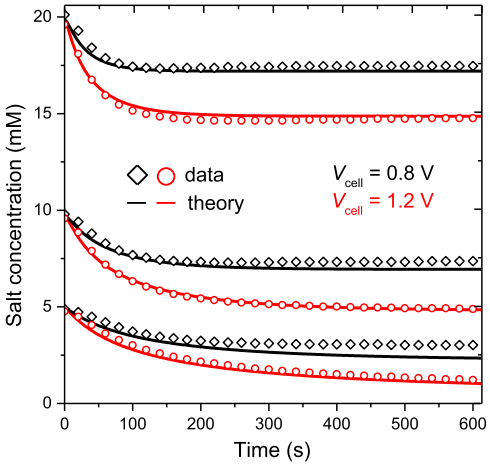

Fig. 13. Salt concentration vs. time in batch-mode CDI-experiment (see Fig. 4b) for three values of initial salt concentration, and in each case for two values of the cell voltage. Lines: theory, dots: experimental data.

We present data at an initial salt concentration of $c_{salt,0}$ = 5, 10 and 20 mM, and at cell voltages of V_{cell} = 0.8 and 1.2 V. We have the following geometrical input parameters for the whole system (stack level calculation): v_{tot} = 200 mL, v_{mi} = 0.86 mL, and A = 270 cm^2. We can fit the theory to the data quite well using the following set of fitting parameters: $C_{St,vol,0}$ = 0.21 GF/m^3, α = 19.2 F m^3/mol^2, μ_{att} = 1.5 kT, and k = 1.5 μm/s. Note that in Fig. 13 we have shifted the experimental data to the left by 20 s for all data sets, necessary because of the slight delay between transport of water from the stack to the recycle vessel and mixing there. From the fit of theory to data we can rather confidentially estimate the system transport coefficient as $k \sim 1.5$ μm/s. Comparing this with an ideal spacer transfer coefficient of $2 \cdot D \cdot p_{sp}/L_{sp} \sim 7$ μm/s ($D_{avg} \sim 1.7 \times 10^{-9}$ m^2/s for NaCl), we can estimate that the resistance in the electrode is ~2 μm/s (assuming simple addition of resistances, R, with $R \propto 1/k$), and thus the resistance in the electrode is more than 3× higher than in the spacer channel. This is a very tentative analysis, and for a full analysis the CDI system must be modeled by porous electrode theory, as will be explained in the next section.

5.3. Porous electrode theory for CDI applied to Membrane-CDI with an ion-selective blocking layer

In this section we present a detailed model for transport and storage of ions in a porous electrode, based on a monovalent salt solution (for extensions to mixtures see Refs. [25,26]). Porous-electrode theory was originally developed for systems where a constant and high salt concentration in the transport pores could be assumed, which together with assuming a linear EDL capacity resulted in classical transmission line theory [49,50,100], see also Section 6.2. Newman in his papers with Tobias [101] and Johnson [5] extended this model to CDI by also describing ion transport across the electrode, leading to the prediction of local salt depletion in the electrode pores and prediction of desalination in the transport channel. Recently this approach was used again by Suss et al. [18]. In these works, to couple the local charge flux into the EDLs (micropores) to the local EDL salt flux, the Helmholtz-model was assumed. This implies that these two fluxes are set equal to another; that is, it is assumed that for each additional electron stored in the electrode, locally one cation is taken from solution and immobilized, without any co-ion expulsion. This model simplification basically sets the local charge efficiency to unity, and thus does not describe that charge flux and salt flux can be very different. The model also makes an artificial choice about which is the ion to which the electrode has the 100% selectivity. Upon reversing the voltage this selectivity must be assumed to step-change from 100% selectivity for, say, the cation, to 100% selectivity for the anion (see Fig. 1 in Johnson and Newman, Ref. [5]). These approaches based on the Helmholtz-model do not describe CDI of mixtures, as there is no mechanism in the theory to include, for example, the prevalence of Ca^{2+} over Na^+ in the EDLs.

These problems are solved when using porous electrode theory as recently developed by Biesheuvel and Bazant in Refs. [23,24] and extended in Refs. [25,26], see also Refs. [102,103]. The key feature is to include a realistic EDL model to relate electrode charge to EDL salt adsorption, and via surface conservation laws relate these to the EDL charge flux and ion (salt) fluxes.

The porous electrode theory describes as a function of the depth in the electrode (x) and time (t) the following coupled variables: the concentration in the interparticle macropores, c_{mA}, the potential there, ϕ_{mA}, the charge density in the intraparticle micropores, σ_{mi}, and the net salt adsorption in the micropores. The latter variable will be described using an effective salt concentration, c_{eff}, which is a summation over all pores of the total ion concentration (divided by 2 to get a salt concentration), defined per unit total electrode volume, thus

$$c_{eff} = p_{mA} c_{mA} + \frac{1}{2} p_{mi} c_{ions,mi} \tag{21}$$

where p_{mA} is the macroporosity of the electrode and p_{mi} is the microporosity (per volume unit of total electrode). All these parameters depend on depth x and time t, and only after sufficient time they level off to their final, equilibrium, value when gradients through the electrode become zero. Equilibrium properties are described by the set of equations given for the mD-model in Section 5.1.3.

In the following one-dimensional example calculation, we consider a monovalent salt solution with both ions having the same diffusion coefficient, D. This D is an effective diffusion coefficient for

transport in the macropores, which contains a contribution of pore tortuosity. We will not consider transport outside the electrode, but we will consider the presence of an ion-selective membrane layer between spacer and electrode to simulate membrane-CDI.

Outside the membrane, we assume a constant salt concentration, c_{sp}. The membrane in front of the electrode is assumed to be 100% permselective, that is, only counterions can go through; we also neglect a transport resistance within the membrane. In that case the total potential drop from spacer across the membrane (including the two EDL Donnan edges of the membrane) to a point in the macropores located at the edge with the membrane is

$$\Delta\phi_{mem} = \ln\frac{c_{sp}}{c_{mA}} \tag{22}$$

which is based on a cation-exchange membrane (otherwise a minus-sign must be added), with c_{mA} the macropore salt concentration in the electrode, right next to the membrane. Within the electrode the salt mass balance is given by

$$\frac{\partial c_{eff}}{\partial t} = p_{mA} D \frac{\partial^2 c_{mA}}{\partial x^2} \tag{23}$$

with x the position across the electrode, $0 < x < L$, where L is the electrode thickness, and D the ion diffusion coefficient in the interparticle macropores. Furthermore, the micropore charge balance is given by

$$p_{mi}\frac{\partial \sigma_{mi}}{\partial t} = 2 p_{mA} D \frac{\partial}{\partial x}\left(c_{mA}\frac{\partial \phi_{mA}}{\partial x}\right). \tag{24}$$

At each position in the electrode, the macropore potential ϕ_{mA} is related to that in the carbon matrix, ϕ_1, according to

$$\Delta\phi_d + \Delta\phi_{St} = \phi_1 - \phi_{mA}, \tag{25}$$

with expressions for $\Delta\phi_d$ and $\Delta\phi_{St}$ given by Eqs. (10) and (11). Boundary conditions are as follows: at the backside of the electrode (closed off for ion and water flow) we have $dc_{mA}/dx = 0$ and $d\phi_{mA}/dx = 0$. Initial conditions are a certain value for the macropore concentration c_{mA}, and with $\sigma_{mi} = 0$ everywhere in the electrode, we can use Eqs. (9) and (21) to determine c_{eff} at time zero. To simulate a real experiment where we apply a certain cell voltage between two electrodes (with the spacer channel in between), we make a step-change in voltage between that in the spacer channel ϕ_{sp} (just outside the membrane) relative to that in the carbon matrix, ϕ_1. This difference $\phi_{sp} - \phi_1$ is quickly stepped up at time zero from zero to $\Delta\phi_{step}$. In the carbon matrix we assume a constant potential ϕ_1; thus, we neglect a possible electrical resistance in the carbon, in the current collectors, and in the connecting wires. At the front-side of the electrode where it contacts the membrane, the potential ϕ_{mA} relates to that in the spacer channel according to: $\phi_{mA} = \Delta\phi_{sp} + \Delta\phi_{mem}$, with $\Delta\phi_{mem}$ a function of c_{mA} at that position, see Eq. (22).

The final boundary condition follows from the assumption of a perfectly selective cation-exchange membrane in front of the electrode, which implies that the total anion number in the electrode is conserved, that is, the anion flux through the membrane is zero. This implies that at the membrane/electrode edge ($x = 0$) we have as a final boundary condition: $dc_{mA}/dx|_{x=0} = c_{mA}(x=0) * d\phi_{mA}/dx|_{x=0}$. This is in principle a valid boundary condition. However, we find that this is numerically troublesome and it is better to use instead a different constraint, namely that of total anion conservation in the whole electrode: $\int_0^L c_{mA}\left(p_{mA} + p_{mi}\cdot 2c_{mA}e^{2\cdot\mu_{att}}\Big/\left(\sigma + \sqrt{\sigma^2 + (2c_{mA}e^{\mu_{att}})^2}\right)\right)dx = \text{constant}$, where we have implemented Eq. (10) in Eq. (8) for the anion concentration in the micropores ($z_i = -1$).

Next we show an example calculation for the macropore salt concentration c_{mA} as a function of position x and time t during ion adsorption after a step-change of $\Delta\phi_{step} = -30$, for $\mu_{att} = 0$, $p_{mi} = p_{mA} = 0.30$ and $C_{St,vol} = 0.15$ GF/m^3. The value of $\Delta\phi_{step} = -30$ corresponds to applying a negative voltage of -770 mV to the electrode relative to the midplane (i.e., $V_{cell} = 1.44$ V). As Fig. 14 shows, after applying this voltage, macropore concentrations increase in time. This is because anions cannot leave the electrode region and as they are expelled from the micropores they must end up in the

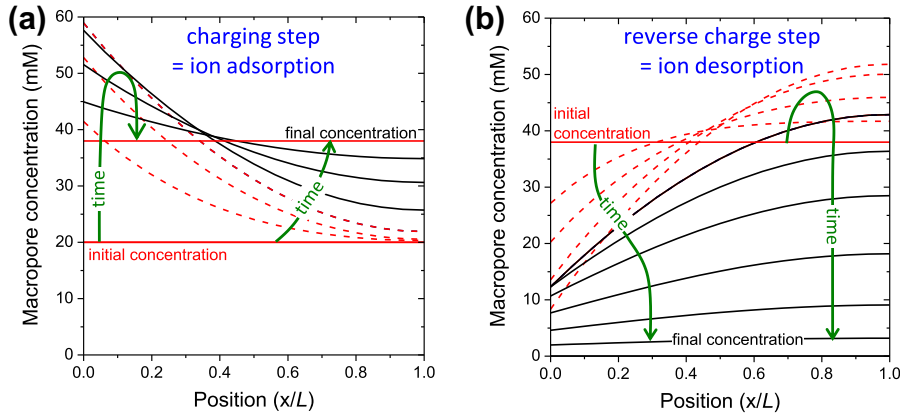

Fig. 14. Calculation results of 1D dynamic porous electrode model for MCDI with a cation exchange membrane located at $x = 0$ perfectly blocking for anions. (a) Macropore salt concentration profiles as function of time (direction of arrows) during application of −770 mV voltage to the electrode relative to the spacer channel, and (b) After subsequent increase of the potential to +770 mV.

macropores, which therefore also adsorb extra cations, compared to the situation without the membrane [10,12]. In Fig. 14 we show the effect of increasing the electrode voltage, not simply back to $\Delta\phi_{step} = 0$, but further, to an opposite polarity of $\Delta\phi_{step} = 30$, that is, ions are now desorbed at reversed voltage, a very effective operational mode as discussed in Section 3.7. As can be observed, the salt concentration in the macropores drops tremendously during this stage, and gets very close to zero (to reach a value of about 30 μM), making further ion transport in the electrode problematic because of the low conductivity. In a final calculation (not shown) the cell voltage is reduced to zero again, and the macropore salt concentration returns to the starting value without noteworthy gradients across the electrode (i.e., the concentration increases equally rapid everywhere).

Important other parameters that follow from the calculation are salt adsorption and charge. The micropore charge increases to beyond 1000 mM during charging, slightly below the value for the cation concentration in the micropores (with the anions in the micropores at a concentration of 1.4 mM). These numbers for the micropore concentration imply that the macropore-to-micropore Donnan potential was never higher than ~3.3 thermal voltage units, or about $\Delta\phi_d \sim 85$ mV during charging. During discharge at reversed voltage, the micropore charge goes from positive to negative, to reach a minimum value of $\sigma_{mi} \sim -40$ mM.

Clearly, these effects of strong transients in the ion concentrations across the electrode are very important in the study of the dynamics of CDI and membrane-CDI, as we will also discuss in more detail in Section 6.3 for the case of CDI without membranes. Simple analysis based on RC-networks or other theories that assume a constant resistance in the electrode will fail completely for (membrane-)CDI, because as we have shown here, ion concentrations (and thus resistances for ion transport) change dramatically across the electrode, and are also very time-dependent, while the salt adsorption capacity of the EDLs is highly non-linear.

An important assumption in this modeling approach is that ion transport from macropore to micropore is sufficiently fast to be close to equilibrium, that is, transport resistances in the system are due to ion diffusion and electromigration through the macropores across the thickness of the electrode. An extended model accounting for a local transport resistance between macro- and micropores can be based on describing the individual ion adsorption fluxes into the carbon micropores j_i by $j_i = k_{\rightarrow} \cdot c_{mA} \cdot \exp(-z_i \cdot \alpha\ \Delta\phi_d) - k_{\leftarrow} \cdot c_{mi,i} \cdot \exp(z_i \cdot (1-\alpha) \cdot \Delta\phi_d)$, where α is a transfer coefficient ($0 < \alpha < 1$) and the kinetic adsorption and desorption constants, $k_{\rightarrow}$ and $k_{\leftarrow}$, relate to μ_{att} according to $\mu_{att} = \ln(k_{\rightarrow}/k_{\leftarrow})$. For high values of the kinetic constants, or low values of the flux j_i, the equilibrium Donnan model is recovered. With this final remark we end this section on the mathematical modeling of ion transport and capacitive storage in CDI.

6. Electrochemical analysis of CDI

6.1. Introduction

Electrochemical (EC) analysis is an essential tool to evaluate the performance of porous electrode systems. Many options are available of what current or voltage signals to apply in EC analysis, and of what experimental system to test. The experimental system is often one of the following two. The first option is to test a single porous electrode in combination with a counter- and a reference electrode (''three electrode setup''). The other option is to test two porous electrodes as one another's counter-electrode. The use of a reference electrode is not obligatory in this second option, and solely the cell voltage difference between the two electrodes is externally controlled or measured (''two electrode setup''). This second option is most resembling of actual CDI operation (likewise for supercapacitors), and we will, therefore, discuss this second system.

The main question is then: can we use the standard toolbox of EC test methods (galvanostatic cycling, cyclic voltammetry, impedance spectroscopy, etc.) also for realistic CDI conditions? The problem here is that CDI is often applied for water of a low ionic strength which is initially below 200 mM (and often even below 50 mM) and this value decreases further during desalination. These are concentrations much lower than those used in standard EC analysis where the salt concentration is typically 1 M or higher. So, does it make sense to use the same methods and the same analysis approach when we do EC analysis for water of say 20 mM ionic strength?

Of course, one can still run the same type of experiment, and using an appropriate theory we can obtain important information on local resistances and capacities. However, the application of standard theoretical tools developed for testing at high ionic strength, based on constant RC theory for porous electrodes [49,50], seems undesirable as these methods assume constant capacities and resistances, as well as equal ion diffusion coefficients, and for water desalination neither of these assumptions is very much applicable; instead, capacities are non-linear and resistances for ion transport are highly place- and time-dependent, as we will illustrate in Section 6.3. Applying a theory that does not account for these effects will easily lead to erroneous conclusions. In such situations the transmission line-theory completely fails and we need to revert to solving a porous electrode model based on several coupled PDEs [23–26]. Analytical solutions are not readily available for this problem and thus it seems that EC analysis in low ionic strength aqueous solutions with ions of different diffusion coefficients will require novel dedicated software making use of exact porous electrode theory, for example, along the lines of that presented in Section 6.3.

Is EC analysis for CDI then not possible? On the contrary: EC analysis for CDI is certainly possible and important but to be able to use standard theoretical tools, we need to test at high ionic strength conditions, and ideally with a salt with equal ion diffusion coefficients, such as KCl. Analysis of a two-electrode cell pair along this lines is described in the next section.

6.2. Voltage square-wave chronoamperometry for CDI electrode characterization at high ionic strength

CDI electrodes can be characterized by EC testing making use of RC porous electrode theory (''transmission line-theory''). The starting point of this theory is that at high ionic strength conditions, the diffuse (or, Donnan) layer potential is sufficiently low such that we are in the low-potential limit where we have no net salt (electro-)adsorption in the EDLs, see Eq. (4). This, together with the assumptions of equal ion diffusion coefficients and that of a perfectly dissociated 1:1 salt, leads to the prediction that we have no gradients in salt concentration inside and outside the electrode. For the effect of unequal ion diffusion coefficients, see Eqs. (2) and (4) in Ref. [25]. Making these assumptions allows us to modify Eq. (24) to

$$\frac{\partial \sigma_{\mathrm{mi}}}{\partial t} = \frac{2 p_{\mathrm{mA}} c D}{p_{\mathrm{mi}}} \frac{\partial^2 \phi_{\mathrm{mA}}}{\partial x^2} \tag{26}$$

where c is the constant salt concentration in macropores and outside the electrode. Implementing $\sigma_{\mathrm{mi}} \cdot F = -C_{\mathrm{St,vol}} \cdot \Delta\phi_{\mathrm{St}} \cdot V_{\mathrm{T}}$ and $(\Delta\phi_{\mathrm{d}} +)\Delta\phi_{\mathrm{St}} = \phi_1 - \phi_{\mathrm{mA}}$ and assuming ϕ_1 (the electrode potential) not to vary in time, we can rewrite Eq. (26) to

$$\frac{\partial^2 \phi_{mA}}{\partial x^2} - RC\frac{\partial \phi_{mA}}{\partial t} = 0 \tag{27}$$

which is the classical equation for the transmission-line model, where according to our porous electrode theory the dimensionless group RC is given as the product of $R = V_T/2Fp_{mA}cD$ for the resistance per unit length (in Ω m), and $C = C_{St,vol}p_{mi}$ for the volumetric capacitance (in F/m^3). Eq. (27) can be solved analytically for all kinds of applied voltage or current-signal [49].

In the present work, we will use Eq. (27) for an experiment where we apply a step-change in cell voltage between two equal porous electrodes, and measure the resulting current signal (abbreviated here as SW-CAM, for "square-wave chronoamperometry") for porous electrodes made by a standard casting technique, see Ref. [62], from Norit Supersorb-50 activated carbon (Norit B.V., The Netherlands). We will analyze a two porous-electrode setup, with a spacer layer in between the electrodes (electrode thickness L = 340 μm, electrode mass density ρ_e = 0.50 g/mL). Assuming symmetry, we only need to solve Eq. (27) for one electrode, while across the half-spacer layer we then have a constant resistance, $R_{tot,ext}$.

Boundary conditions for Eq. (27) are that at the inner edge of the electrode ($x = L$) we have $d\phi_{mA}/dx = 0$ while at the electrode/spacer interface we have

$$\frac{I_e \cdot R_{tot,ext}}{V_T} = \phi^* - \phi_{mA}|_{x=0} = -\frac{L}{Bi}\frac{\partial \phi_{mA}}{\partial x}\bigg|_{x=0} \tag{28}$$

where I_e is the current density (in A/m^2) and the Biot-number describes the ratio in electrode resistance over external resistance, given by $Bi = RL/R_{tot,ext}$, where the electrode resistance per unit length, R (in Ω m), is given above, and $R_{tot,ext}$ is the external resistance over half of the channel (in Ω m^2). In Eq. (28), ϕ^* is the dimensionless voltage step-change applied to the half-cell. The analytical solution for the current density I_e as function of time after applying a step-change in voltage is [49],

$$I_e(t) = I_{e,0} \cdot \sum_{n=0}^{\infty} \frac{2 \cdot Bi}{Bi^2 + Bi + \lambda_n^2} \exp(-\lambda_n^2 \cdot t/RCL^2) \tag{29}$$

where the values of Λ_n are the roots of the transcendental equation $\lambda_n \cdot \tan \lambda_n = Bi$, and where the initial current density is

$$I_{e,0} = V_{cell}/2R_{tot,ext} \tag{30}$$

where V_{cell} is the voltage applied between the two electrodes.

The advantage of the SW-CAM technique is that based on a set of curves at various values of V_{cell} we obtain a data set which can be analyzed in various ways to make several "checks and balances" to analyze step-by-step whether the assumptions underlying the analysis are correct. We will discuss these various steps next. As we show, using SW-CAM we can independently and robustly derive values for R, C and Bi, and we can analyze these numbers to evaluate the system.

First of all, the starting data of current density I_e vs. time t, see Fig. 15a, must fulfill several properties, namely that I_e starts off high and must drop to zero, both in the first step where we apply a voltage difference between the two electrodes (charging step), as well as in the second step where the voltage is reduced to zero again (discharging). At each switching moment, the current must instantly step up or down, as indeed observed in Fig. 15a. The higher the voltage, the higher currents must be.

Next we integrate the current signal with time, and after dividing by the electrode thickness we obtain the charge σ^* (per unit total electrode volume), as plotted in Fig. 15b vs. cell voltage. Two requirements can here be checked for validity: first of all whether the charge increases in proportion to voltage, implying that the capacity, C, does not depend on voltage, a basic requirement in the transmission line theory. Secondly, the total charge, σ^*, transported in the one direction during the charging step must be close to the total charge transported back in the discharging step, and thus the two values derived for charge σ^* at each voltage must be the same. Both these requirements can be observed in Fig. 15b to hold true. Taking the slope of σ^* vs. V_{cell} and multiplying by a factor 2, we obtain the value for the capacity C required in the transmission line theory, which in this case is C = 34.7 MF/m^3. We can also multiply this number by the electrode mass density

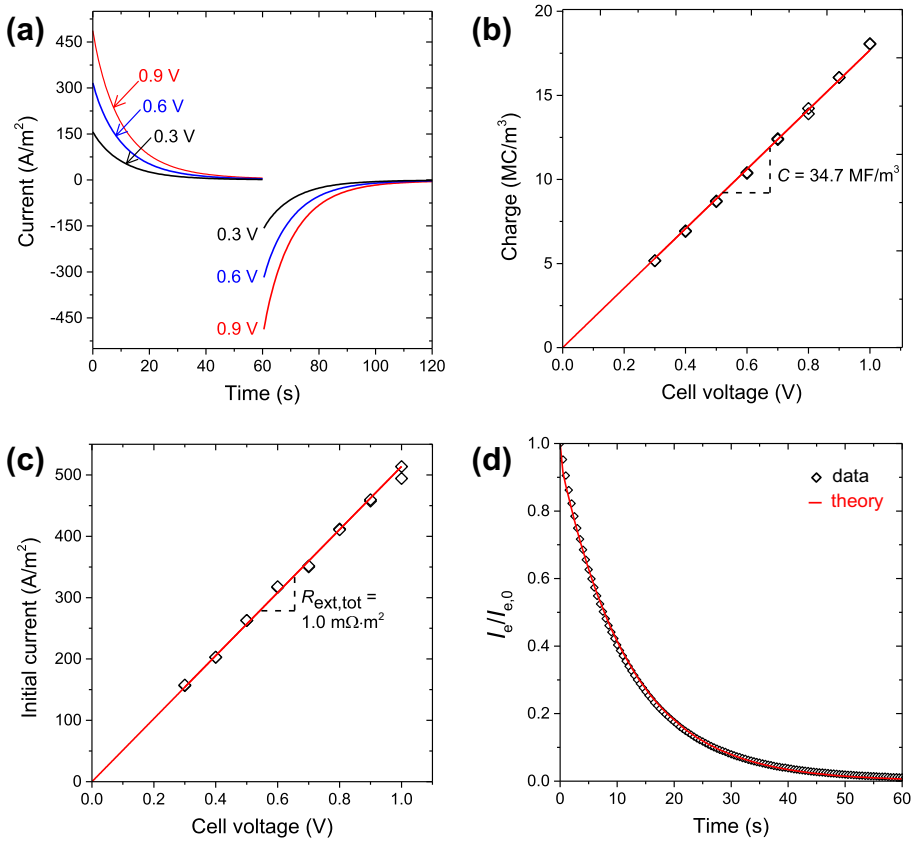

Fig. 15. EC analysis using square wave chrono-amperometry of a two-porous electrode cell filled with 0.5 M KCl solution. (a). Transient current signals after applying a cell voltage step change, V_{cell}, and again after the voltage is reduced to zero. (b). Electrode charge in C/m^3. From the slope we can derive the capacity C. (c). Initial current vs. V_{cell}. (d). Mastercurve of dimensionless current vs. time for the data sets of panel (a) and comparison with theory (Bi = 0.15).

ρ_e and obtain for the capacity ~70 C/g, which is a fairly standard number for the single-electrode capacity. This number can be divided by 4 to get the actual *system* capacity such as reported in Refs. [59,104]. For 500 mM NaCl solution and a different electrode material, a value of 23 C/g system capacity was measured in Ref. [104], while for the same system C = 19 C/g was reported for a salinity of 20 mM salt.

Next we can analyze the initial current $I_{e,0}$. As Eq. (30) shows, we expect $I_{e,0}$ to be proportional to V_{cell}, and indeed Fig. 15c shows this to be true. From the slope of $I_{e,0}$ vs. V_{cell} we can derive the external resistance to be $R_{tot,ext}$ = 1.0 mΩ m^2. This linear resistance, derived from the initial current, can be due to an ionic resistance (spacer channel) or an electrical resistance (wires, current collector, etc.), but in any case it must be outside the porous electrode. The analysis does not lead to the identification where the resistance is located, either in the spacer channel or in the wires or current collector. However, the analysis given below suggests that the ionic resistance in the spacer channel cannot account for the observed value of the linear resistance $R_{tot,ext}$ and thus it is likely due to an electronic effect.

Having established these two numbers, $R_{tot,ext}$ and C, the only parameter yet to derive is the volumetric resistance R of the porous electrode. But, first, as shown in Fig. 15d, we test a final prediction of the theory, namely that we can collapse all curves of I_e vs. t onto a *mastercurve* by dividing the current I_e by the initial current $I_{e,0}$, see Eq. (29). This renormalization has been made in Fig. 15d

and shows that both for the charging and the discharging step a perfect collapse of all data sets for $I_e(t)$ is obtained. Now, fitting the theory, Eq. (29), to this collapsed set of data-curves gives the following result. Namely, that for Bi above 0.15 we do not get a good fit, with the theoretical curve first dropping too quickly and around 10–30 s, dropping off too slowly [not shown]. For Bi $\leqslant$ 0.15 the fit is actually quite good, but not perfect. There is no influence of the value of Bi on the theoretical curve (and thus neither on the quality of the fit) when Bi $\leqslant$ 0.15 because for such low Bi-numbers, the resistance in the system is now completely in the linear part (described by $R_{ext,tot}$). This has the consequence that a simple exponential curve, $I_e(t)/I_{e,0} = \exp(-t/\tau)$, describes the data just as well, with $\tau = R_{ext,tot}CL = 11.5$ s. The choice for Bi = 0.15 is interesting (a lower value would describe the data just as well) because this value follows exactly when we take ideal ionic conductivities in the macropores and neglect tortuosity effects; that is, we apply $R = V_T/2Fp_{mA}cD$ with $p_{mA} = 0.30$, $c = 500$ mM, and $D = 2 \times 10^{-9}$ m^2/s, which results in an electrode volumetric resistance of $R = 0.44\ \Omega$ m. It is difficult to imagine that R can theoretically be even lower, because we already assumed perfect equilibration of the voltage through the carbon matrix, that is, zero electrical resistance in the porous electrode. Thus, the only remaining volumetric resistance is in the electrolyte-filled pores and $R = 0.44\ \Omega$ m must then be the lowest possible resistance, unless unaccounted for effects of enhanced ion transport play a role [105].

If indeed, apparently, the ionic resistance in the electrode can be described by the theoretical formula based on the free diffusion coefficient, then for the spacer channel we may expect the same, and thus we can calculate the spacer layer contribution to $R_{tot,ext}$ as $R_{tot,ext,th} = V_T L_{half\text{-}spacer}/2Fp_{spacer}cD$, which assuming $p_{spacer} \sim 0.50$ results in $R_{tot,ext,th} \sim 0.066\ m\Omega\ m^2$ ($L_{half\text{-}spacer}$ is 250 μm) which is about 15 times below the experimental value of $R_{ext,tot}$, suggesting that in this particular experiment the linear external resistance is in the electrical circuit/current collector, not in the ionic solution in between the electrodes.

In conclusion, SW-CAM allows us to accurately test the properties of capacitive porous carbon electrode cells and calculate the electrode capacity and the various contributions to the observed resistance. In the present case the linear (external) resistance is determining the total resistance and analysis suggests that we can assign this resistance to an electric (not ionic) effect, while we can also tentatively conclude that the distributed (volumetric) resistance within the electrode may be close to the ideal value based on an ion transport resistance that is only determined by the free solution ion diffusion coefficients. This finalizes our exposition of the derivation of the various constants in the transmission line theory based on the SW-CAM technique. In conclusion, the SW-CAM technique is a robust, precise and very informative method to perform EC-analysis on two-electrode capacitive cells in aqueous solutions. To demonstrate that under conditions of lower ionic strength, strong concentration gradients develop in CDI electrodes, we make a theoretical analysis in the next section for realistic parameter settings.

6.3. The development of salt shock waves in CDI electrodes

To demonstrate the relevance of using full porous electrode theory instead of "RC-network" style models when describing porous electrodes in contact with solutions of low and moderate salinities (as typical in CDI) we present in this section calculation results based on the same model as explained in Section 5.3, but now excluding the membrane, that is, we model "normal" CDI in the present section. In front of the electrode we consider a stagnant diffusion layer (mass transfer film) through which the ions must diffuse, of equal thickness as the electrode, which contacts a bulk solution of constant salt concentration.

This calculation is the same as presented in Fig. 9 of Ref. [23] and uses the mD model and the parameter settings $\delta_{mD} = 1.25$, $p_{mA} = p_{mi} = 0.30$ and $\mu_{att} = 1.5$ kT. The difference is that presently we will use a higher electrode voltage of $\phi = V/V_T = 25$, defined relative to the flow channel. This number translates to about 0.6 V applied over the half-cell and thus 1.2 V over the cell pair, a very realistic cell voltage in CDI.

Calculation results show clearly how after application of the voltage, the macropore salt concentration, c_{mA}, in the electrode, see Fig. 16a, rapidly drops to reach very low values (down to about 1 ppm of the initial value). Subsequently, the macropores are slowly replenished again from the open side of the

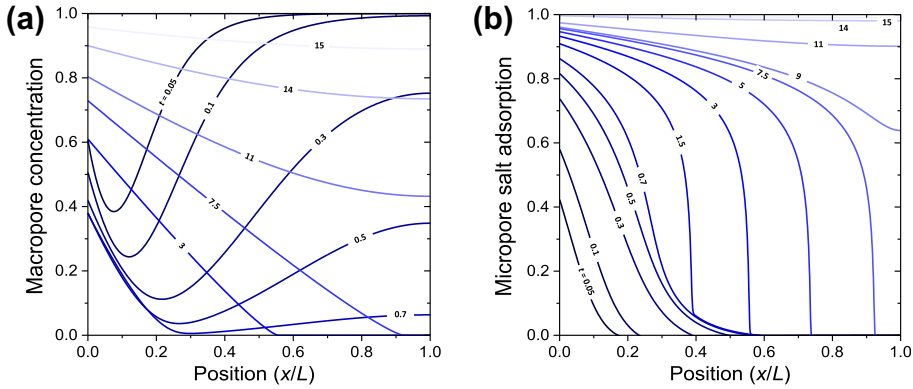

Fig. 16. (a) Macropore ion concentration c_{mA} (relative to bulk salt concentration) as function of electrode position and time (inset numbers) after applying a step-change in voltage across the electrode. (b) Micropore salt adsorption (minus adsorption at zero voltage, and relative to equilibrium value). Inset numbers give dimensionless time which can be recalculated to dimensional time by multiplying with L^2/D, where L is the electrode thickness.

electrode (located at $x = 0$) until the electrode macropores will again be saturated. An even stronger non-linear effect is shown when we plot the micropore salt adsorption, that is, $c_{ions,mi}$ of Eq. (19), vs. place and time in Fig. 16b [minus the value at zero voltage, and rescaled to the equilibrium value]. Here the formation of a shockwave in the electrode is clearly observed, that is, a desalting front is established in the electrode which slowly moves inward (to the right in Fig. 16), until it dissolves at the backside of the electrode, and the system moves to the equilibrium situation. It is at the position of the shockwave, x^*, that salt (diffusing into the electrode from the outside) is locally adsorbed, with hardly any salt adsorption to the left of x^* and zero to the right. The development of such a shock is not predicted by RC network modeling, and thus these calculations clearly show that to theoretically describe desalting by CDI, a full porous electrode theory including a realistic microscopic EDL model is essential.

7. Energy requirements of CDI

7.1. Thermodynamic minimum energy consumption of desalination

Desalination of water is a process in which the ionic content of the water is demixed, and thus the entropy of the system decreases. This implies that we always needs an energy input. Desalination starts with feed water (volume flow rate $\Phi_{v,feed}$, salt concentration c_{feed}) which is separated in two product streams, one being the fresh (dilute) water ($\Phi_{v,fresh}, c_{fresh}$), and the other being the concentrate ($\Phi_{v,conc}, c_{conc}$), with $\Phi_{v,feed} = \Phi_{v,fresh} + \phi_{v,conc}$ and $c_{feed} \cdot \phi_{v,feed} = c_{fresh} \cdot \phi_{v,fresh} + c_{conc} \cdot \phi_{v,conc}$. Desalination performance is often defined by the freshwater concentration and by the water recovery (WR), which is the ratio of $\phi_{v,fresh}$ over $\phi_{v,feed}$.

Water desalination leads to an increase of the system free energy, ΔG. This requires an energy input which is at least equal to this value ΔG. This is the minimum energy input for desalination, independent of the chosen process. In practice the energy requirements will be significantly higher. The objective of material and engineering studies in water desalination is to design a process for which the energy input is as close as possible to ΔG, see Fig. 17.

To describe ΔG as a function of the desalination performance (recovery and freshwater concentration), the general equation, valid for ideal thermodynamics for the ions in the water, is

$$\Delta G = G_{fresh} + G_{conc} - G_{feed}, G_i = RT\phi_{v,i}c_i \ln c_i \tag{31}$$

where c is the total dissociated ion concentration in the water. For instance, for a monovalent fully dissociated salt like NaCl, c is twice the salt concentration, c_{salt}. For water, ideal thermodynamics quite

Fig. 17. Schematic representation of thermodynamics in an ideal water desalination technology. G denotes Gibbs free energy in each stream. The difference, $\Delta G = G_{fresh} + G_{conc} - G_{feed}$, is the minimum energy required for desalination to take place.

closely describes the exact energy consumption, even up to the concentration of sea water ($c_{salt} \sim 500$ mM). Eq. (31) predicts that for the desalination of seawater with $WR = 0.6$, we need exactly 1 kWh per m^3 of produced freshwater when $c_{salt,fresh} = 5$ mM.

Instead of Eq. (31), we can use several equivalent expressions, for example:

$$\Delta G = RT\phi_{v,fresh}(c_{feed} - c_{fresh})\left[\frac{\ln\alpha}{1-\alpha} - \frac{\ln\beta}{1-\beta}\right] \tag{32}$$

where $\alpha = c_{feed}/c_{fresh}$ and $\beta = c_{feed}/c_{conc}$[106,107]. The water recovery, WR, relates to concentrations according to $WR = (c_{conc} - c_{feed})/(c_{conc} - c_{fresh})$. For example, if the objective is to desalinate a 100 mM NaCl solution (brackish water) to 5 mM freshwater with $WR = 0.8$, then $c_{conc} = 480$ mM, which consequently gives $\alpha = 20$, and $\beta = 0.208$. As a result, making use of equation 32, the minimum energy required is 0.12 kWh/m^3 freshwater, which is much lower than the energy consumption of the state-of the-art desalination technique, for example, reverse osmosis at this salinity, see Fig. 19.

7.2. Energy consumption of MCDI and CDI in CC-ZVD and CC-RCD modes

The previous section outlined the thermodynamic minimum energy consumption of desalination. In this section, closer inspection of energy consumption of actual CDI and MCDI operation is discussed. As example, we give results for constant-current (CC) operation of MCDI and CDI both in the ZVD and RCD mode, as will be explained next, and is plotted in Fig. 18. Here we present data for desalination of a series of NaCl-solutions from 10 mM up to 200 mM. For the adsorption step, an electrical current of 1 A is applied to the whole stack ($\sim$37 A/m^2) until the cell voltage reaches 1.6 V; for the desorption

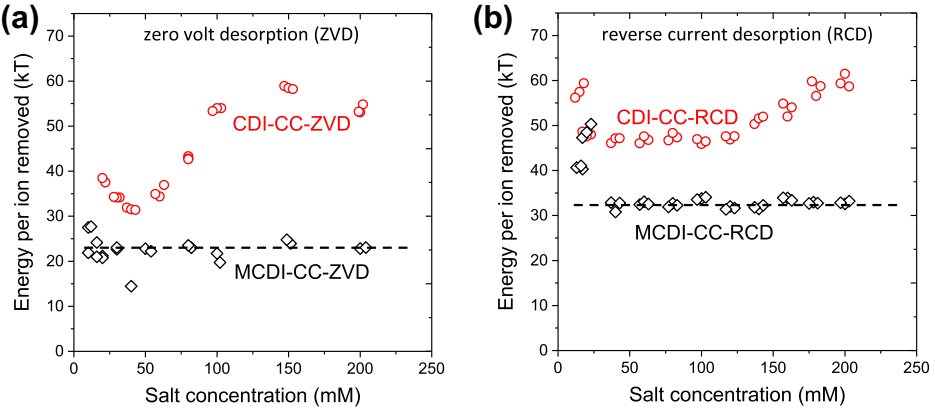

Fig. 18. Energy consumption per ion removed as function of salt concentration of MCDI and CDI in CC-ZVD and CC-RCD modes, see Ref. [14].

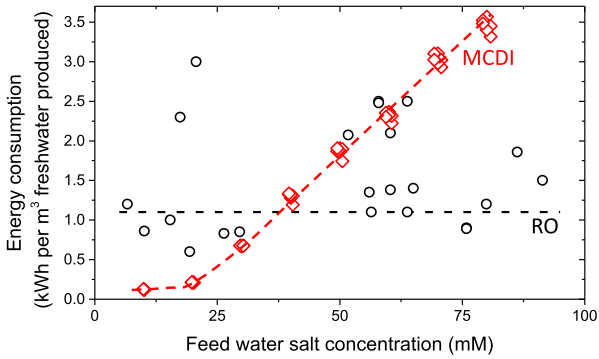

Fig. 19. Energy consumption of water desalination by MCDI and reverse osmosis (RO). Lines serve to guide the eye.

step, in the ZVD mode, a zero voltage is applied for 500 s, while in the RCD mode, a reversed current (−1 A) is applied until the cell voltage drops to 0 V again.

In Fig. 18 we present data for the energy consumption per ion removed for CDI and MCDI, which are calculated from the electrical energy input during desalination (ion adsorption step), obtained from multiplying the current in Ampère with the cell voltage in V, integrating over the duration of the adsorption step, and dividing by the total ion removal, as explained in Section 3.5. Note that this is the energy input during charging, part of which can be recovered from the energy release during discharging the cell (but only in RCD mode, not in ZVD mode). Interestingly, we see in Fig. 18 that for MCDI the energy consumption is lower than for CDI in both operational modes, and energy consumption for MCDI does not vary much with regard to the inlet salt concentration. In our setup, for MCDI a typical number for energy consumption is ∼20 kT per ion removed for the ZVD mode, and ∼30 kT per ion removed for the RCD mode. Once again, let it be stated that this is the energy per cycle without energy recovery.

Finally, results of a preliminary analysis are presented where MCDI is compared with reverse osmosis (RO), the state-of-the-art desalination technique. An experiment was conducted by desalinating a range of NaCl solutions of a starting concentration from 10 mM to 80 mM, to a freshwater concentration of 5 mM using a lab-scale MCDI setup, see Fig. 19. Operation is at constant current, RCD condition with $WR = 50\%$ ($V_{cell,end} = 1.6$ V, $I = \pm 37$ A/m^2). As the influent salt concentration increases, the energy consumption of desalinating the feed water to the 5 mM freshwater level also increases, as expected. Fig. 19 indicates that in the lower range of the influent salt concentration, approximately below 30 mM, the energy consumption of the MCDI system is lower than RO (data from literature on brackish-water RO).

8. Electrode materials for CDI

8.1. Introduction

As one can infer from the preceding sections, the porous electrode is a key component in all CDI systems, a situation similar to that in the field of capacitive energy storage devices. In both fields carbon is the material of choice for developing and making porous electrodes. We note that besides the material properties of the carbon, also other system settings, such as electrode thickness, spacer geometry, cell design, and operational settings are important factors which determine the CDI performance. In the following sections, we will review several carbon materials used for CDI, ranging from commercially used activated carbons to highly tunable carbide-derived carbons and highly ordered structures such as carbon nanotubes or graphene. Fig. 20 provides a selection of various carbons used for CDI applications.

CDI performance of carbon electrodes is not only related to the total pore volume, the pore size, and the pore connectivity, but is also related to electronic conductivity, electrochemical stability, and cost

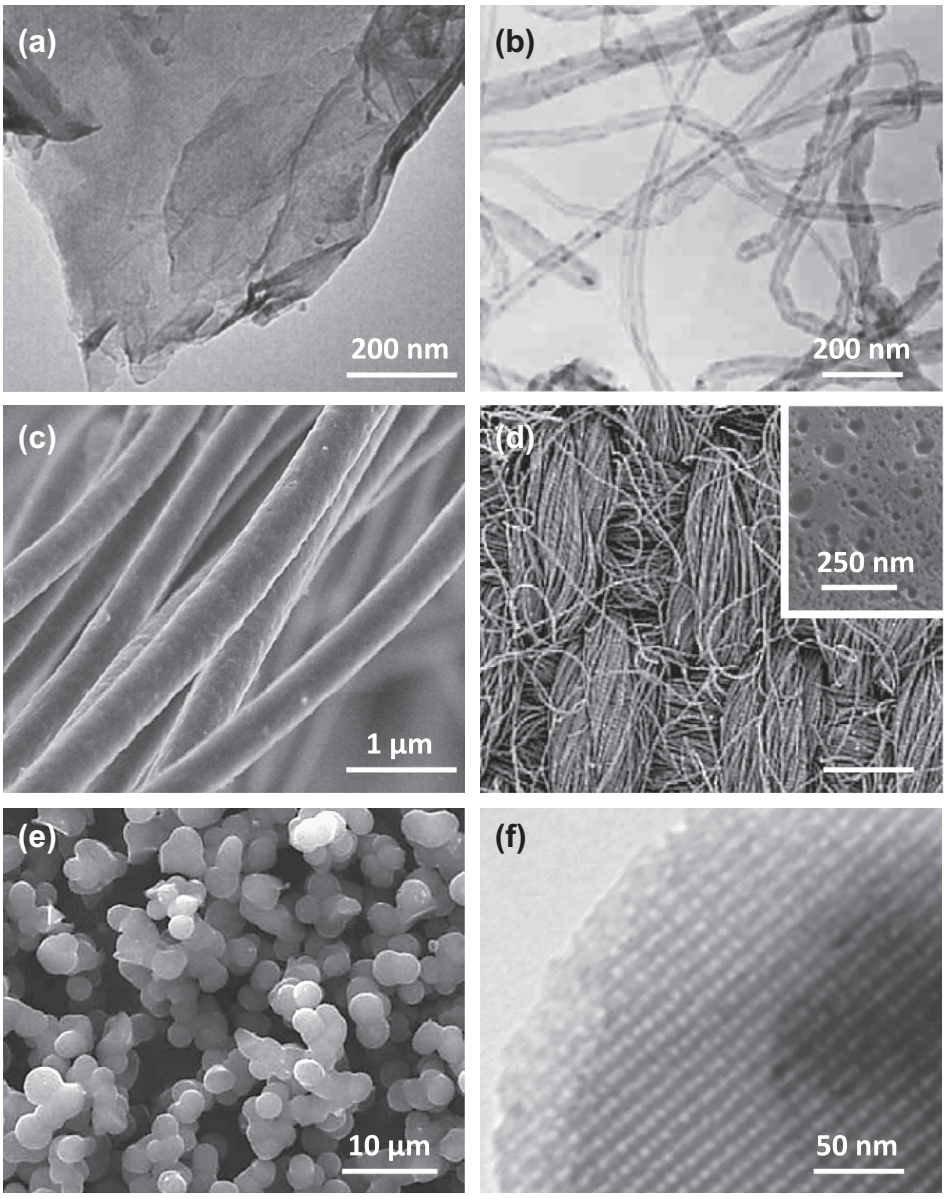

Fig. 20. Selection of carbon materials used for CDI. Graphene-like carbon flake (a, Ref. [56]), multi-walled carbon nanotubes (b, Ref. [108]), electrospun fibers (c, Ref. [109]), activated carbon cloth (d, Ref. [110]), carbon aerogels (e, Ref. [111]), and ordered mesoporous carbon (f, Ref. [47]).

considerations. The following list summarizes the most important requirements for CDI electrode materials and their relation to CDI performance, based on Ref. [39]:

1. *Large ion-accessible specific surface area*
   - Salt electrosorption capacity is related to the surface area.
   - However, not the entire surface area calculated from experimental methods may be accessible to ions.

2. *High (electro)chemical stability over the used pH and voltage range (no oxidation, etc.)*
   - Important to ensure longevity and system stability.
3. *Fast ion mobility within the pore network*
   - Bottlenecks or very small pores pose diffusional limitations and limit the kinetics.
   - This not only concerns the porosity within carbon particles, but also the pore structure of the entire CDI electrode, considering, for example, interparticle distances and electrode thickness.
4. *High electronic conductivity*
   - Metallic or metal-like electronic conductivity ensures that the entire electrode surface of all particles is charged without large voltage gradients within the carbon.
   - Only a high electronic conductivity ensures a low energy dissipation and low heating.
5. *Low contact resistance between the porous electrode and the current collector*
   - A low interfacial resistance is required to avoid a large voltage drop from the electrode to the current collector.
6. *Good wetting behavior*
   - Hydrophilicity ensures that the entire pore volume is participating in the CDI process.
7. *Low costs and scalability*
   - Cost considerations are important for large-scale applications.
8. *Good processability*
   - Shapeable into film electrodes: based on compacted powders, fibers, or monoliths.
9. *Large (natural) abundance and low CO_2 footprinting*
   - Availability and environmental impact considerations not only affect cost considerations, but also sustainability concerns.
10. *High bio-inertness*
    - Biofouling needs to be avoided for long-term operation in surface or brackish water.

Particularly important yet difficult to accomplish is combining a very high specific surface area (#1) with a high ion mobility (#3). A smaller pore size and a larger total number of small pores translates to a larger specific surface area (SSA; defined as surface area per mass). However, more small pores bring along transport limitations and steric hindrance as also the number of constrictions increases and the pore walls become more curved. The final and ultimate limit to the pore size is the bare ion size, for example, 1.16 Å for Na^+ and 1.67 Å for Cl^-. These numbers increase for solvated ions, with 3.58 Å for sodium and 3.31 Å for chloride [112]. Commonly, the majority of pores of most porous carbons will be significantly larger. Larger pores provide better transport pathways; however, they also decrease the total specific surface area.

Because of the importance of the pore structure and its effect on desalination performance, we first have to clarify the pore size terminology. The International Union of Pure and Applied Chemistry (IUPAC) defines pores strictly according to their size as follows (Refs. [27,113]; see also Fig. 21):

- *Macropores* larger than 50 nm
- *Mesopores* between 2 and 50 nm
- *Micropores* smaller than 2 nm

Since the term micropores may be associated with micrometer-sized pores, some authors have preferred the term "nanopores" for pore diameters smaller than 2 nm (e.g., Ref. [114]); however, we adhere strictly to the IUPAC definition. It is important to note that the IUPAC classification is independent of the choice of the porous material (e.g., carbon, metal, metal oxide), the kind of pores (e.g., closed-pore, open pore), or *where* the pore is actually located (inside a particle vs. between particles). As schematically shown in Fig. 21, open pores may be dead-end-pores (also called semi-open; that is a pore with only one open end which cannot contribute to percolation), interconnected (that is connected with another pore but not necessarily to the entire pore volume), or passing – and only closed pores cannot contribute to desalination.

It is important to note that the commonly used average pore size is insufficient to describe a complex pore structure and may even be misleading for many porous materials because it does not reflect

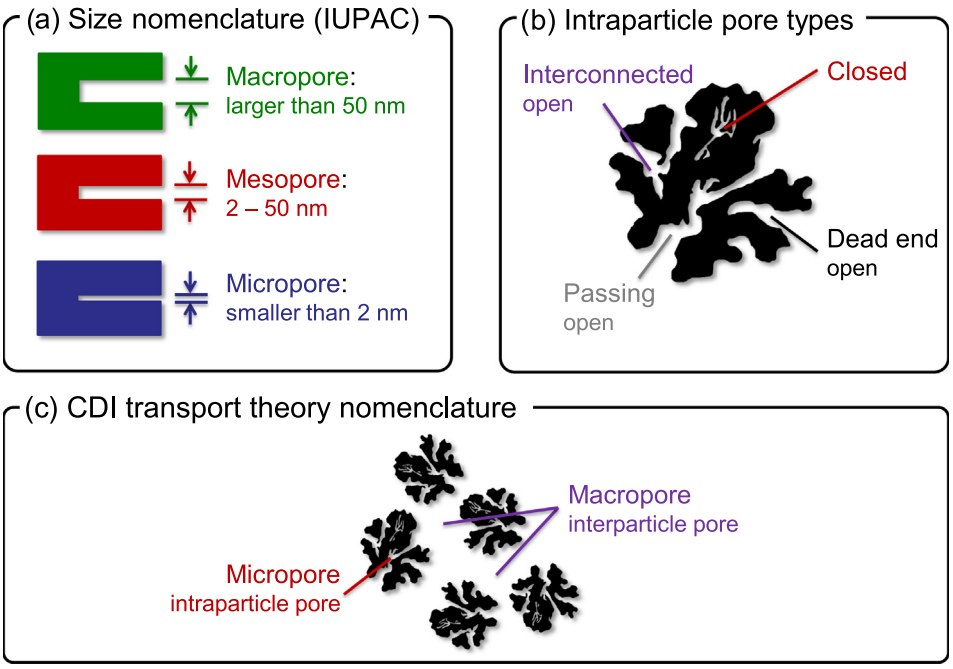

Fig. 21. Pore nomenclature according to IUPAC (a), classification of intraparticle pores (b), and nomenclature in porous media transport theory (c).

(i) the magnitude, and (ii) the modality of the pore size dispersion; that is, how narrow the pore size distribution centers around one or several maxima. Only carbons with a very narrow pore size distribution, such as carbon nanotubes (CNTs), some carbide-derived carbons (CDCs) [115], and many template-produced carbons [116], exhibit a meaningful pore size "average", whereas most activated carbons or hierarchic porous materials exhibit a much broader distribution of pore sizes.

We now have reviewed different kinds, sizes, and distributions of pores. However, it is also important to recall that pores have different shapes. The prevalent pore shape strongly depends on the carbon material, the synthesis conditions, and the post-synthesis procedure. Abstracted, the pore shapes may be approximated as spherical, cylindrical, or slit shaped as the simplest geometries. Many templated carbons exhibit highly ordered cylindrical pores [117], and for most activated carbons we assume slit-shaped pores. We note that also other structures are possible. One example is the space between dense nanoparticles which shows pore walls with a positive curvature [118]. The pore shape for one kind of carbon can also vary as a function of the synthesis temperature, as illustrated by the gradual transition from almost spherical pores to slit-shaped pores in CDCs [119].

Compared to the IUPAC definition, the literature on transport modeling in porous electrodes employs a very different definition of the terms micro- and macropores (cf. Sections 3–7): Here, micropores are any pores inside the porous particles that constitute the electrode, and macropores are the (interparticle) void space between these porous particles. This distinction reflects the large difference in size between the large interparticle and small intraparticles pores. In film electrodes composed of porous carbon powders, the size, number, and magnitude (i.e., pore volume) of such macropores depends on the film preparation and is governed by parameters such as particle size, use of polymeric binder, and film compaction.

In the following sections we focus on the influence of the properties of carbon particles (notably, pore structure) on CDI performance. To describe the pore structure in detail we adhere to the IUPAC definition which is commonly used for porous carbons (see Fig. 21). If not defined otherwise, we always refer to pores inside porous carbon particles (i.e., intraparticle pores). Only where explicitly

noted, we refer to interparticle pores (i.e., between particles). We also prefer the term intraparticle instead of interstitial [120] as the latter is a common term in crystallography and refers to atomic lattice defects.

For making CDI electrodes, we cannot use single carbon particles but need a film composed of such particles. Commonly, film electrodes for CDI are prepared similar to electrodes used for energy storage devices: carbon powders are mixed with a polymeric binder (usually ~10 mass%) and are usually blended with a conductive additive such as carbon black. The components are thoroughly mixed, rolled and dried, or directly cast on the current collector; the latter may be a graphite foil to avoid corrosion in saline water. A very elegant way to avoid the use of polymeric binder and possible wash-out of powder particles is the use of a porous monolith [121], an interwoven array of (porous) fibers [122], or carbon felts and fabrics [123,124]. When such structured electrodes are either not available or undesired (e.g., because of cost considerations), a film electrode made from individual particles can either be protected by a membrane (see Section 3.7) or mechanically stabilized by a porous separator which enables saline water flow.

8.2. Carbon materials

8.2.1. Activated carbons and activated carbon cloths

Among porous carbons, activated carbons (ACs) stand out, because they are by far the commercially most commonly used and usually the most cost efficient materials for many applications. Today, AC is the most common material found in water treatment systems and its use is already documented in early studies on CDI in the 1960/1970s (see Section 2). ACs are derived from natural sources such as coconut shells, wood, coal, starch, or synthetic sources such as resins or other organic precursors. The combination of a high SSA (1000–3500 m^2/g) and low costs (~0.50 €/kg) makes this material particularly attractive for widespread commercial applications [125]. Resin-derived AC can be synthesized as beads, fibers, or monoliths while most other ACs are usually powders composed of micrometer sized particles. For example, polyacrylonitrile (PAN) can be electrospun to form submicrometer thin carbon fibers with good desalination properties after being blended with 5 mass% of a conductive additive (carbon black) and activation in CO_2 (to increase the pore volume) [126]. The variety of precursor materials and synthesis conditions translates to an equally great variety in pore structures and surface chemistry of the resulting AC material. Thus, a detailed description of the properties, most importantly the pore structure, is important for any comprehensive understanding and comparison of the desalination capacity of AC electrodes [127]. As a general trend, an increase in the total pore volume/specific surface area results in a higher salt adsorption capacity.

A detailed study on ACs was presented by Zou et al. [128] where conventional AC, KOH activated AC, and TiO_2/AC composites were compared. The starting material was mesoporous AC with a SSA of 932 m^2/g and an average pore size of 4.2 nm. KOH activation was carried out so that the wetting behavior of the hydrophobic AC was improved by introducing hydrophilic surface groups to the system; this procedure yielded AC with a SSA of 889 m^2/g and an average pore size of 4.2 nm so that the SSA and pore size average remained largely unchanged after the activation compared to the starting material. TiO_2 coating resulted in a slightly lower SSA (851 m^2/g) and a somewhat smaller average pore diameter (4.1 nm). Both, KOH activated and TiO_2 infiltrated/coated samples had a slightly higher CDI performance compared to the starting material. For KOH-treated materials, the improved performance was explained by the more hydrophilic nature of the material, resulting in improved wetting. This is in line with a study by Ahn et al. [129] who indicated that charge transfer related to surface functional groups may also contribute to improved performance. It is still an open question if this aspect can explain the measured performance and how long-term stability will be affected by the presence of such surface functional groups which, over time, may chemically degrade.

The influence of Ti–O modification of activated carbon cloth (ACC) has been investigated by Ryoo et al. [130,131]. For these studies, ACC was derived from a phenolic precursor and the SSA of the material decreased from 1980 to 1180 m^2/g after loading with titanium(IV)-butoxide. After synthesis, chemical analysis confirmed the presence of titanium and oxygen groups, possibly in a tetrahedral configuration as indicated by X-ray photoelectron spectroscopy. Such Ti–O decorated ACC was found to show a higher salt electrosorption which was explained by the additional charge transfer during the

change of the oxidation state of titanium. In contrast, no significant change in the CDI capacity was found for metal-oxide coatings of Si–O, Zr–O, and Al–O [55]. Myint and Dutta [132] used seeded ZnO nanorods to decorate ACC electrodes for CDI applications, and Anderson et al. [133] used a sol–gel method to incorporate SiO_2 and/or Al_2O_3 nanoparticles in carbon electrodes.

Instead of utilizing metal oxide coatings, it is possible to modify the surface of ACC with a SSA of 1440 m^2/g by oxidation with HNO_3 or reduction by hydrogen annealing [71]. To mitigate the charge efficiency limiting effect of co-ion desorption around the potential of zero charge (PZC), the anode and cathode were chemically treated so that both electrodes would have a different PZC. While a reduced carbon electrode was found to be unstable and quickly re-oxidized in saline water, an asymmetric three electrode cell with one oxidized electrode, one untreated electrode, and one reference electrode showed a higher charge efficiency compared to a symmetric cell consisting of two untreated ACC electrodes.

A symmetric CDI cell with chemically modified ACC was studied by Oh et al. [110]. Oxidation of the carbon material with KOH or HNO_3 slightly decreased the specific surface area (−16% and −5% for KOH and HNO_3 treatment, respectively). In these experiments, the average pore size remained almost unchanged (±1 Å) compared to the untreated samples but still a higher salt electrosorption capacity was observed. This difference may be related to the activation of carbon via opening closed pores and, hence, new small pores were created inside the particles. The chemical treatment also improved the electrosorption kinetics.

8.2.2. Ordered mesoporous carbons

In contrast to the disordered arrangement of micropores in most ACs, ordered mesoporous carbons (OMCs) show a highly periodic hexagonal or cubic arrangement of mesopores which may improve the transport of salt ions through the pore network. OMCs can be derived via soft or hard templating and the literature on OMCs is extensive including several review articles (e.g., Refs. [116,134]). For hard templating, a template, such as a zeolite or ordered mesoporous silica, is infiltrated with a carbon precursor which then is carbonized. Then, in the final step, the initial template is chemically removed (e.g., with hydrofluoric acid) and OMC is obtained. The other approach, soft templating, is a relatively new method for the synthesis of OMC materials and it involves, for example, the self-assembly of triblock copolymers and the thermal removal of the latter; hence, the only solid phase left in the end is carbon which retains the ordered porous feature of the template. Depending on the synthesis conditions and possible activation, OMCs can have a very high SSA (>3000 m^2/g), but more typical SSA values are in the range between 750 and 1500 m^2/g. Thus, while the pore arrangement is very different, the SSA of OMC is comparable to many ACs.

OMCs synthesized from a modified sol–gel process with a SSA between 950 and 1594 m^2/g and an average pore size between 3.3 and 4.0 nm were studied by Li et al. [135]. Compared to AC, these OMCs had a significantly better CDI performance which has commonly been correlated with the presence of mesopores [22,135]. Zou et al. [22] for example, have stated that a pore size of around 3 nm should be considered particularly beneficial for ion transport with a high salt removal capacity (see Section 8.2.4 for a more detailed discussion on micropores and their contribution to the CDI performance). Even the OMC with the lowest SSA (950 m^2/g) showed a much better desalination capacity than AC with a comparably large SSA (845 m^2/g). This is in agreement with another study by Zou et al. [22] which showed that AC with a SSA of 968 m^2/g performs not as well as OMC with a SSA of 844 m^2/g. It is also possible that the disordered arrangement of small AC micropores obstructs fast ion transport so that a certain percentage of the total SSA may not fully contribute to the dynamic process of salt electrosorption; in contrast, almost the entire SSA of OMCs with their transport-optimized pore network may participate in the salt immobilization which results in an improved CDI performance. Now, when comparing different OMCs with small differences in SSA and pore size (1491 vs. 1594 m^2/g and 3.7 vs. 3.3 nm average pore size), the sample with the lower SSA had a significantly higher desalination capacity [135]. This may be related to differences in the carbon structure and the electrical conductivity because the OMC with lower resistance also gave the better CDI performance. As an alternative way for 3D structuring or hierarchic porosity and to increase desalination rates, Wen et al. [136] used a double-templating approach where macropores were created by an ordered assembly of silica spheres while triblock co-polymers were used as soft templates for OMC formed between the SiO_2 particles.

8.2.3. Carbon aerogels

Another group of carbons are carbon aerogels (CAs) [137] which combine a moderate SSA (typically 400–1100 m^2/g, but also up to 1700 m^2/g) [138] with a high electrical conductivity (25–100 S/cm) and a low mass density (<0.1 g/mL; see Ref. [39]). So far, CAs have been synthesized in the form of powders, small beads, thin films, and monoliths and they are composed of a network of rather dense carbon nanoparticles; thus, the very low density is not related to a low skeletal density of the carbon particles but to their very spacious arrangement. Most of the total SSA is usually related to interparticles pores (mesopores), but depending on the synthesis conditions there may also be micropores that are related to intraparticle porosity [139]. The latter may range from only 10 m^2/g or less, to more than 600 m^2/g [140]. Typical diameters of the rather round carbon nanoparticles range from 3 to 30 nm. Compared to CA, CDI electrodes based on carbon xerogels (CX) show after the synthesis a significant decrease of the initial porosity which can be used to achieve smaller pore sizes at lower cost [141]. The pore network for CA and CX formed between dense particles has pore walls with a positive curvature (also called exohedral pore structure). Such a pore geometry is different from most other porous carbons which have internal pores with a predominantly negative surface curvature. We note that materials with a positive surface curvature have been shown to improve the charge storage capacity per unit area compared to carbons with a negative pore curvature [118,142,143]. The common conclusion from work on carbon aerogels and xerogels has been that their pore size in the mesopore range is optimal for ion storage because electrical double layers do not overlap [144] and the mesopore size facilitates ion transport. Therefore, it is argued that such materials are particularly suitable for CDI applications (see also Sections 8.2.2 and 8.2.4).

A number of publications on CAs are dedicated to the electrosorption from mixed ionic solutions rather than investigating a single salt solution (such as NaCl). For instance, Farmer et al. [41,42] have studied CAs with a SSA of 600–800 m^2/g for CDI in mixed ionic solutions and a decay in salt electrosorption capacity of only ~5% over a period of several months was observed when using deaerated electrolytes. The electrosorption of several anions and cations (Na^+, K^+, Mg^{2+}, Rb^+, Br^-, Cl^-, SO_4^{2-}, NO_3^-) from natural river water was studied in Ref. [120] for CA with a SSA of 400–590 m^2/g and average pore sizes between 4 and 9 nm. It was found that monovalent ions with a smaller (hydrated) ion size were preferentially electrosorbed by CA electrodes. Farmer et al. also show that organic components in the water reduce the lifetime of CA CDI electrodes [145].

Considering the low mechanical stability of CA as a result of the very low bulk density, paste-rolling of CA with silica gel was studied by Yang et al. [138] as a method to improve the mechanical properties. Different carbon-to-silica mass ratios (100:0, 75:25, 50:50, 25:75) were investigated and a slight increase in CDI performance was observed when adding the silica gel.

8.2.4. Carbide-derived carbons

Unlike ACs, carbide-derived carbons (CDCs) can be synthesized to only exhibit extremely narrowly distributed micropores and no mesopores; but, unlike OMCs, pores in CDC are not arranged in an ordered fashion. CDCs are most commonly produced by etching of carbide powders in dry chlorine gas at elevated temperatures (200–1200 °C) but they can also be derived from monoliths, fibers, or thin films. The chlorine treatment followed by a subsequent hydrogen annealing to remove residual chlorine compounds yields a SSA typically between 1200 and 2000 m^2/g but activation may increase the SSA to values of up to 3200 m^2/g (cf. Ref. [115] for a review). Recently, the CDI capacity of CDCs derived from titanium carbide (i.e., TiC-CDC) has been investigated as a purely microporous material with pores smaller than ~1 nm [62]. Prior to the work of Porada et al. [62], micropores have largely been seen as a limitation for ion transport and the optimum pore size for carbons used for CDI was suggested to be in the mesopores range at 3–4 nm [22,135,144]. However, this study suggests that the pore volume associated with micropores is particularly attractive for CDI, and not, as it may be implied from studies on OMC, CA, and CX, the volume of mesopores.

8.2.5. Carbon nanotubes and graphene

Two of the latest additions to the carbon family, carbon nanotubes (CNTs; described by Sumio Iijima in 1991) and graphene (synthesized by Geim and co-workers in 2005) have already been investigated as materials for CDI electrodes. Both materials are characterized by having all (graphene) or

almost all (CNTs) surface area ion accessible because the area is on the outside of the material. This is in contrast to, for example, AC, where almost the entire surface area is within the particles. However, even when composed of 1D (CNT) or 2D (graphene) nanomaterials, the resulting CDI electrodes are by nature three-dimensional and will have a significant intraparticle porosity; for example, graphene sheets may become wrinkled and form slit-like pores even within one sheet. Depending on the synthesis conditions and post-synthesis treatment, a disadvantage of CNTs can be the presence of metal catalysts in the CNT material which may reduce the electrochemical stability of the resulting CDI electrodes making them susceptible to parasitic side-reactions.

The most commonly found CNTs are multi-walled CNTs. Zhang et al. [108] studied multi-walled CNTs from catalytic decomposition of methane with surface areas between 50 and 129 m^2/g and the sample with the highest SSA had the largest CDI capacity. In contrast to other porous carbons, these SSA values are low and as a result, the CDI performance is much smaller than for AC electrodes as shown by Wang et al. [146]. Electrodes for CDI composed of multi-walled CNTs (SSA: 47–129 m^2/g) [53] and multi-walled CNT/AC composites [147] have been studied and for pure CNTs, the CDI capacity increased with the amount of SSA. A series of CNT/AC ratios (from 1:0 to 0:1) were studied and it was shown that the CDI capacity continuously decreased as the CNT content was increased. Yet, the energy efficiency improved at high CNT loadings as the device conductivity benefits from a high CNT content considering the moderate conductivity of AC. In contrast, Ref. [148] shows that single-wall CNTs (455 m^2/g, average pore size: 4.8 nm) have a higher CDI capacity than double-wall CNTs (415 m^2/g, average pore size: 5.1 nm) [148] and both CNT varieties show a better desalination performance compared to AC with a significantly larger SSA (999 m^2/g, average pore size: 2.1 nm); yet, they are inferior to OMCs (SSA: 1491 m^2/g, average pore size: 3.7 nm).

Freestanding electrodes composed of either multiwall CNTs or composites of multiwall CNTs and polyacrylic acid (PAA) were obtained by Nie et al. [46] via electrophoretic deposition. Employing PAA was shown to improve the CDI performance as it acts as a cation exchange membrane (see Section 3.6 on membrane-CDI). Another composite electrode composed of PANI (polyaniline) and single-walled CNTs showed a slight increase in CDI performance (~10%) compared to films composed of pure single-wall CNTs. This improvement in desalination was explained by the increase in the mesopore volume but may also be related with the different electrochemical properties of the PANI-CNT composite material [44].

Purely graphene electrodes have been investigated by Wang et al. [149] and Li et al. [56]. In the latter study, CDI electrodes consisted of graphene flakes (or AC for comparison) added to graphite powder and polymeric binder in a 72:20:8 mass ratio. Initially, the graphene SSA was 222 m^2/g, but this value decreased to $\leqslant$50 m^2/g after treatment with sulfuric/nitric acid (for comparison: the AC had a SSA of 990 m^2/g). Graphene shows also differences in the kinetics of salt removal compared to other carbon materials. A study by Zhang et al. compared electrodes made from AC, mesoporous carbon, and mesoporous carbon/graphene composite electrodes [150] and it was reported that the latter had both a higher salt adsorption capacity and faster ion immobilization rates. This is also in agreement with another study by Zhang et al. on CNT/graphene composites [151].

8.2.6. Carbon black

Carbon blacks (CBs) are usually dense carbon nanoparticles with a low SSA (typically below 120 m^2/g) [152] and because of their high electrical conductivity, they are a common conductive additive to film electrodes composed of porous carbons. Indeed, as shown in Refs. [57,153], adding CB to CDI film electrodes made from AC significantly improves the salt removal in saline electrolytes with 670, and 1000 ppm NaCl. The very low SSA, however, limits the CDI performance of electrodes purely composed of CB particles, as shown in Refs. [6,37,38].

8.2.7. Overview of performance data of carbon electrodes for CDI

In Table 1 we summarize reported data from the literature for the important CDI property of salt adsorption per gram of electrode material. Here, data are given as function of salinity and cell voltage, per gram of both electrodes combined. The experiment in all cases is done in a symmetric cell with the two electrodes of the same mass and material. As can be read off from Table 1, reported numbers vary in a large range between ~0.7 and ~15 mg/g of adsorbed salt per gram of both electrodes combined.

Table 1
Overview of salt adsorption performance reported for different electrode materials applied for CDI.[a]

First author/journal/ publication year	Carbon material	Experimental conditions				Salt adsorption (mg/g)
		Initial salt concentration (mg/L)	Cell voltage (V)	Carbon content (%)	Operational mode	
J.C. Farmer/J. Electrochem. Soc./1996 [42]	Carbon aerogel	~50	1.2	nd	BM CDI	1.4
	Carbon aerogel	~500	1.2	nd	BM CDI	2.9
M.W. Ryoo/Water Research/2003 [131]	Ti–O activated carbon cloth	~5844	1.0	nd	BM CDI	4.3
K. Dai/Materials Letters/ 2005 [53]	Multi-walled carbon nanotubes	~3000	1.2	nd	BM CDI	1.7
X.Z. Wang/Electrochem. Solid-State Lett./2006 [146]	Carbon nanotubes-nanofibers	~110	1.2	100	BM CDI	3.3
L. Zou/Water Research/ 2008 [22]	Ordered mesoporous carbon	~25	1.2	78	BM CDI	0.68
L. Li/Carbon/2009 [135]	Ordered mesoporous carbon	~50	0.8	78	BM CDI	0.93
H. Li/Journal of Materials Chemistry/2009 [154]	Graphene	~25	2.0	100	BM CDI	1.8
Y.J. Kim/Sep. Purif. Techn./ 2010 [155]	Activated carbon	~200	1.5	nd	SP CDI	3.7
	Activated carbon	~200	1.5	nd	SP 0-MCDI	5.3
R. Zhao/J. Phys. Chem. Lett./ 2010 [59]	Commercial activated carbon electrode	~292	1.2	nd	SP CDI	10.9[b]
		~1170	1.4	nd		13.0[b]
H. Li/Env. Sci. & Techn./ 2010 [56]	Graphene-like nanoflakes	~25	2.0	80	BM CDI	1.3
H. Li/J. Electroanal. Chem./ 2011 [156]	Single-walled carbon nanotubes	~23	2.0	70	BM CDI	0.75
P. M. Biesheuvel/J. Colloid Inter. Sci./2011 [12]	Commercial activated carbon electrode	~292	1.2	nd	SP CDI	10.5
		~292	1.2	nd	SP 0-MCDI	12.8
		~292	1.2	nd	SP r-MCDI	14.2
J. Yang/Desalination/2011 [20]	MnO_2 activated carbon	~25	1.2	nd	BM CDI	1.0
G. Wang/Electrochimica Acta/2012 [109]	Carbon nanofiber webs	~95	1.6	100	BM CDI	4.6
B. Jia/Chemical Physics Letters/2012 [157]	Sulphonated graphite nanosheet	~250	2.0	72	BM CDI	8.6
D. Zhang/J. Mat. Chemistry/ 2012 [151]	Graphene-carbon nanotube	~29	2.0	90	BM CDI	1.4
H. Li/Journal of Materials Chemistry/2012 [158]	Reduced graphene oxide-AC	~50	1.2	nd	BM CDI	2.9
Z. Peng/Journal of Materials Chemistry/2012 [45]	Ordered mesoporous carbon–CNTs	~46	1.2	80	BM CDI	0.63
M. E. Suss/Energy Environ. Science/2012 [18]	Carbon aerogel monoliths	~2922	1.5	100	BM CDI	9.6
Z. Wang/Desalination/2012 [159]	Reduced graphite oxidate-resol	~65	2.0	80	BM CDI	3.2
S. Porada/ACS Applied Materials & Interfaces/ 2012 [62]	Activated carbon (Norit DLC Super 50)	~292	1.2	85	SP CDI	6.9
		~292	1.4	85		8.4
	Carbide-derived carbon	~292	1.2	85	SP CDI	12.4
		~292	1.4	85		14.9
	Norit DLC Super 50 (not published)	~25	1.4	85	SP CDI	6.1

[a] All experiments use NaCl solutions. SP: single-pass; BM: batch model. nd: no data. For SP, the given salinity is the inflow salinity. 0-MCDI: CDI including ion exchange membranes, with ion release at zero cell voltage; r-MCDI: with ion release at reversed voltage.

[b] After electrode mass correction by 10.6/8.5 g/g.

Table 2
Volumetric densities of a few selected functional CDI electrodes.

Carbon cloth electrode [71]	0.27 g/mL
Carbon aerogel electrode [18]	0.33 g/mL
Carbide-derived carbon electrode [62]	0.47 g/mL
Activated carbon (AC) electrode [62]	0.5 g/mL
Commercial AC electrode [12,59]	0.55–0.58 g/mL

For scientific studies on CDI electrodes, our suggestion is to always report the measured value of salt adsorption either in mg/g or in mol/g. We suggest that a proper CDI electrode should have an adsorption of at least 8 mg/g NaCl at a cell voltage of 1.2 V.

In Table 1, it can be observed that experiments done in the BM-method with low starting salinities, score very low on salt adsorption. This may be because during adsorption, the concentration in the system drops further, and there is a limited amount of salt in the system. Thus we suggest to do CDI experiments either using the SP-method, or, when using the BM-method, at a sufficiently high initial salinity, such that the salinity does not drop by over 50%. In Fig. 2 of Ref. [12], a dependence of absorbed amount of salt is observed as function of salt concentration. Especially below 5 mM (~292 mg/L) salt adsorption decreases. Therefore, we suggest varying the salinity in the experimental program instead of using only a single value for salinity.

Table 2 presents a few selected data for electrode mass densities. Adsorptions reported in Table 1 can be multiplied by these numbers to obtain the adsorption per mL of both electrodes combined.

9. Outlook: advanced CDI electrode materials and predictive modeling

The coming years will see the further development of CDI towards a mature technology with many applications also beyond water desalination. It is beyond the scope of this review to go into the details of such examples, such as the recovery of lithium from seawater, phosphate from agricultural sources, and valuable metal ions in metallurgical operations. The basic concept is either to capture and harvest valuable ions from a solution, or to remove undesired ions which may be harmful or poisonous.

Economic optimization of CDI requires the minimization of electrical energy usage and investment costs related to stack assembly and materials. To make this a rational optimization, a robust, reliable, and predictive CDI process model is required. Such a comprehensive model is not yet available but can be based on the elements laid out in this review. Particularly, a fully two-dimensional model should be developed that includes both the direction of flow through the CDI device, and the opposite direction of ion electrodiffusion into the electrode, and which can handle both constant voltage and constant current operation. Such a numerical tool can also be used to identify which of the various process options is the best (choosing for instance between flow-by CDI, flow-through, electrostatic ion pumping, or membrane-CDI).

Available CDI process models include the capacitive nature of ion storage but do not yet consider chemical (Faradaic) effects. It is important to develop theoretical methods that also address transport and adsorption of protons and hydroxyl ions (and the ongoing equilibration of $H_2O \leftrightarrow H^+ + OH^-$). This is important because a difference in removal of these ions leads to pH fluctuations in the spacer channel and, thus, in the pH of the freshwater produced. Also, these ions play a role in several of the Faradaic chemical effects in the electrode that were outlined before. Finally, understanding of pH-changes is important because pH fluctuations may play a role in possible scaling, for example, as a result of $CaCO_3$ precipitation.

On the materials side, further research will have to identify the most appropriate pore size and pore size distribution. Desalination with a high salt sorption capacity obtained with microporous carbons provides evidence against the common notion that only mesopores would yield a high CDI performance. However, transport limitations are commonly encountered in purely microporous particles. Ultimately, the goal is to create materials that combine a large number of micropores for ion immobilization with an intelligently designed hierarchical network of mesopores which act as optimized

transport channels. Thus, we have to consider the porosity and pore architecture of entire CDI electrodes rather than only the pore characteristics of individual porous particles to arrive at a CDI technology that combines a high salt adsorption capacity with high salt removal rates.

The choice for porous carbons or dense carbon nanomaterials for CDI electrodes is, as we have seen, well substantiated by the high CDI performance, the high tunability of carbon materials, and for activated carbons, the large abundance, availability and low to moderate costs. However, it should be noted that in principle other materials, such as polymers, ceramics, or metals, can also be used as CDI electrodes as long as they form a bicontinuous porous network and conduct electrical current. Advanced engineering of such materials would potentially enable the manufacturing of transparent, flexible, or castable electrodes with high specific adsorptions. However, such materials remain at the moment a mere theoretical possibility.

Cost considerations are of key importance to make CDI an affordable mass-market technology. At the moment, this leads one to consider activated carbons from natural sources as the materials of choice for the electrodes. Even within the class of activated carbons, the parameter space in which to optimize desalination is very large, and the potential for chemical modifications of the carbons, and the possible inclusion of nanoparticles within the electrode, has only just begun to be exploited for CDI.

A final major avenue to improve CDI systems is advanced electrode design. Present developments show a trend towards fiber mats or cloths and freestanding wires which have already shown their potential. Future systems may include monolithic foams or self-assembled hierarchical porous films. The next generation of CDI electrode design may use an asymmetry between the two electrodes regarding film thickness, porosity, material chemistry, and/or PZC. Such materials may potentially enable devices with a much more robust and more efficient CDI performance than current systems. Further improvements can also be obtained by advanced system engineering of CDI systems based on conventional carbon materials as illustrated recently by Jeon et al. [19]. Their novel MCDI system employs activated carbon (AC) flow electrodes and was applied to desalinate sea water. These results suggest this is a potentially robust technology for continuous CDI operation because the electrode material is constantly replenished.

In conclusion, in our view CDI is a challenging and exciting field and even after 50 years of development can still rightfully be considered an emerging technology. Many challenges remain in the understanding of the CDI process, and the search for improved electrode materials and CDI system solutions to enhance desalination performance continues.

Acknowledgments

This work was performed in the TTIW-cooperation framework of Wetsus, Centre of Excellence for Sustainable Water Technology. Wetsus is funded by the Dutch Ministry of Economic Affairs, the European Union Regional Development Fund, the Province of Friesland, the City of Leeuwarden, and the EZ/Kompas program of the "Samenwerkingsverband Noord-Nederland". We thank the participants of the theme "Capacitive Deionization" and "Advanced Waste Water Treatment" for their involvement in this research. The authors kindly thank Matthew Suss (Stanford University) for help with Section 6.3. V.P. acknowledges financial support *via* the Bayer Early Excellence in Science Award.

References

[1] http://www.un.org/News/Press/docs/2010/ga10967.doc.htm.
[2] Anderson MA, Cudero AL, Palma J. Capacitive deionization as an electrochemical means of saving energy and delivering clean water. Comparison to present desalination practices: will it compete? Electrochim Acta 2010;55:3845–56.
[3] Blair JW, Murphy GW. Saline water conversion. Adv Chem Ser 1960;27:206.
[4] Johnson AM, Venolia AW, Wilbourne RG, Newman J, Wong CM, Gilliam WS, et al. The electrosorb process for desalting water. Washington: U.S. Dept. of the Interior; 1970.
[5] Johnson AM, Newman J. Desalting by means of porous carbon electrodes. J Electrochem Soc 1971;118:510–7.
[6] Oren Y, Soffer A. Electrochemical parametric pumping. J Electrochem Soc 1978;125:869–75.
[7] Caudle DD, Tucker JH, Cooper JL, Arnold BB, Papastamataki A. Electrochemical demineralization of water with carbon electrodes. Washington: U.S. Dept. of the Interior; 1966.
[8] Lee J-B, Park K-K, Eum H-M, Lee C-W. Desalination of a thermal power plant wastewater by membrane capacitive deionization. Desalination 2006;196:125–34.

[9] Li H, Gao Y, Pan L, Zhang Y, Chen Y, Sun Z. Electrosorptive desalination by carbon nanotubes and nanofibres electrodes and ion-exchange membranes. Water Res 2008;42:4923–8.
[10] Biesheuvel PM, van der Wal A. Membrane capacitive deionization. J Membrane Sci 2009;346:256–62.
[11] Kim Y-J, Choi J-H. Improvement of desalination efficiency in capacitive deionization using a carbon electrode coated with an ion-exchange polymer. Water Res 2010;44:990–6.
[12] Biesheuvel PM, Zhao R, Porada S, van der Wal A. Theory of membrane capacitive deionization including the effect of the electrode pore space. J Colloid Interface Sci 2011;360:239–48.
[13] Bouhadana Y, Ben-Tzion M, Soffer A, Aurbach D. A control system for operating and investigating reactors: the demonstration of parasitic reactions in the water desalination by capacitive de-ionization. Desalination 2011;268:253–61.
[14] Zhao R, Biesheuvel PM, Van der Wal A. Energy consumption and constant current operation in membrane capacitive deionization. Energy Environ Sci 2012;5:9520–7.
[15] Demirer ON, Naylor RM, Rios Perez CA, Wilkes E, Hidrovo C. Energetic performance optimization of a capacitive deionization system operating with transient cycles and brackish water. Desalination 2013;314:130–8.
[16] Dlugolecki P, van der Wal A. Energy recovery in membrane capacitive deionization. Environ Sci Technol 2013. http://dx.doi.org/10.1021/es305320.
[17] Bouhadana Y, Avraham E, Noked M, Ben-Tzion M, Soffer A, Aurbach D. Capacitive deionization of NaCl solutions at non-steady-state conditions: inversion functionality of the carbon electrodes. J Phys Chem C 2011;115:16567–73.
[18] Suss ME, Baumann TF, Bourcier WL, Spadaccini CM, Rose KA, Santiago JG, et al. Capacitive desalination with flow-through electrodes. Energy Environ Sci 2012;5:9511–9.
[19] Jeon S-I, Park H-R, Yeo J-G, Yang S, Cho CH, Han MH, et al. Desalination via a new membrane capacitive deionization process utilizing flow electrodes. Energy Environ Sci 2013. http://dx.doi.org/10.1039/C3EE24443.
[20] Yang J, Zou L, Song H, Hao Z. Development of novel MnO_2/nanoporous carbon composite electrodes in capacitive deionization technology. Desalination 2011;276:199–206.
[21] Lee JW, Kim HI, Kim HJ, Park SG. Electrosorption behavior of TiO_2/activated carbon composite for capacitive deionization. Appl Chem Eng 2010;21:265–71.
[22] Zou L, Li L, Song H, Morris G. Using mesoporous carbon electrodes for brackish water desalination. Water Res 2008;42:2340–8.
[23] Biesheuvel PM, Fu YQ, Bazant MZ. Diffuse charge and Faradaic reactions in porous electrodes. Phys Rev E: Statist Nonlinear Soft Matter Phys 2011;83:061507.
[24] Biesheuvel PM, Bazant MZ. Nonlinear dynamics of capacitive charging and desalination by porous electrodes. Phys Rev E: Statist Nonlinear Soft Matter Phys 2010;81:031502–12.
[25] Biesheuvel PM, Fu Y, Bazant MZ. Electrochemistry and capacitive charging of porous electrodes in asymmetric multicomponent electrolytes. Russ J Electrochem 2012;48:580–92.
[26] Zhao R, van Soestbergen M, Rijnaarts HHM, van der Wal A, Bazant MZ, Biesheuvel PM. Time-dependent ion selectivity in capacitive charging of porous electrodes. J Colloid Interface Sci 2012;384:38–44.
[27] Rouquerol J, Avnir D, Fairbridge CW, Everett DH, Haynes JM, Pernicone N, et al. Recommendations for the characterization of porous solids (technical report). Pure Appl Chem 1994;66:1739–58.
[28] Blair JW, Murphy GW. Electrochemical demineralization of water with porous electrodes of large surface area. Saline watter conversion. American Chemical Society; 1960. p. 206–23.
[29] Arnold BB, Murphy GW. Studies on electrochemistry of carbon and chemically modified carbon surfaces. J Phys Chem 1961;65:135–8.
[30] Murphy GW, Caudle DD. Mathematical theory of electrochemical demineralization in flowing systems. Electrochim Acta 1967;12:1655–64.
[31] Murphy GW, Cooper JL, Hunter JA. Activated carbon used as electrodes in electrochemical demineralization of saline water. Washington: U.S. Dept. of the Interior; 1969.
[32] Evans S, Hamilton WS. The mechanism of demineralization at carbon electrodes. J Electrochem Soc 1966;113:1314–9.
[33] Evans S, Accomazzo MA, Accomazzo JE. Electrochemically controlled ion exchange. J Electrochem Soc 1969;116:307–9.
[34] Accomazzo MA, Evans S. Electrochemically controlled ion exchange. J Electrochem Soc 1969;116:309–11.
[35] Reid GW, Townsend FM, Stevens AM. Filed operation of a 20 gallons per day pilot plant unit for electrochemical desalination of brackish water. Washington: U.S. Dept. of the Interior; 1968.
[36] Soffer A, Folman M. The electrical double layer of high surface porous carbon electrode. J Electroanal Chem Interfacial Electrochem 1972;38:25–43.
[37] Oren Y, Soffer A. Water desalting by means of electrochemical parametric pumping. I. The equilibrium properties of a batch unit cell. J Appl Electrochem 1983;13:473–87.
[38] Oren Y, Soffer A. Water desalting by means of electrochemical parametric pumping. II. Separation properties of a multistage column. J Appl Electrochem 1983;13:489–505.
[39] Oren Y. Capacitive delonization (CDI) for desalination and water treatment – past, present and future (a review). Desalination 2008;228:10–29.
[40] Avraham E, Noked M, Bouhadana Y, Soffer A, Aurbach D. Limitations of charge efficiency in capacitive deionization. II. On the behavior of cdi cells comprising two activated carbon electrodes. J Electrochem Soc 2009;156:P157–62.
[41] Farmer JC, Fix DV, Mack GV, Pekala RW, Poco JF. The use of capacitive deionization with carbon aerogel electrodes to remove inorganic contaminants from water. In: Low level waste conference, Orlando, 1995.
[42] Farmer JC, Fix DV, Mack GV, Pekala RW, Poco JF. Capacitive deionization of NaCl and $NaNO_3$ solutions with carbon aerogel electrodes. J Electrochem Soc 1996;143:159–69.
[43] Farmer JC, Bahowick SM, Harrar JE, Fix DV, Martinelli RE, Vu AK, et al. Electrosorption of chromium ions on carbon aerogel electrodes as a means of remediating ground water. Energy Fuels 1997;11:337–47.
[44] Yan C, Zou L, Short R. Single-walled carbon nanotubes and polyaniline composites for capacitive deionization. Desalination 2012;290:125–9.

[45] Peng Z, Zhang D, Shi L, Yan T. High performance ordered mesoporous carbon/carbon nanotube composite electrodes for capacitive deionization. J Mater Chem 2012;22:6603–12.
[46] Nie C, Pan L, Liu Y, Li H, Chen T, Lu T, et al. Electrophoretic deposition of carbon nanotubes–polyacrylic acid composite film electrode for capacitive deionization. Electrochim Acta 2012;66:106–9.
[47] Peng Z, Zhang DS, Shi LY, Yan TT, Yuan SA, Li HR, et al. Comparative electroadsorption study of mesoporous carbon electrodes with various pore structures. J Phys Chem C 2011;115:17068–76.
[48] Bard J, Faulkner R. Excess charge and capacitance. In: Harris D, editor. Electrochemical methods: fundamentals and applications. New York: John Wiley & Sons, Inc.; 2001.
[49] Posey FA, Morozumi T. Theory of potentiostatic and galvanostatic charging of the double layer in porous electrodes. J Electrochem Soc 1966;113:176–84.
[50] de Levie R. On porous electrodes in electrolyte solutions: I. Capacitance effects. Electrochim Acta 1963;8:751–80.
[51] Jung-Ae L, Nam-Soo P, Jin-Soo P, Jae-Hwan C. Fabrication and characterization of a porous carbon electrode for desalination of brackish water. Desalination 2009;238:37–42.
[52] Chang LM, Duan XY, Liu W. Preparation and electrosorption desalination performance of activated carbon electrode with titania. Desalination 2011;270:285–90.
[53] Dai K, Shi L, Fang J, Zhang D, Yu B. NaCl adsorption in multi-walled carbon nanotubes. Mater Lett 2005;59:1989–92.
[54] Lee J-B, Park K-K, Yoon S-W, Park P-Y, Park K-I, Lee C-W. Desalination performance of a carbon-based composite electrode. Desalination 2009;237:155–61.
[55] Leonard KC, Genthe JR, Sanfilippo JL, Zeltner WA, Anderson MA. Synthesis and characterization of asymmetric electrochemical capacitive deionization materials using nanoporous silicon dioxide and magnesium doped aluminum oxide. Electrochim Acta 2009;54:5286–91.
[56] Li H, Zou L, Pan L, Sun Z. Novel graphene-like electrodes for capacitive deionization. Environ Sci Technol 2010;44:8692–7.
[57] Park K-K, Lee J-B, Park P-Y, Yoon S-W, Moon J-S, Eum H-M, et al. Development of a carbon sheet electrode for electrosorption desalination. Desalination 2007;206:86–91.
[58] Porada S, Bryjak M, van der Wal A, Biesheuvel PM. Effect of electrode thickness variation on operation of capacitive deionization. Electrochim Acta 2012;75:148–56.
[59] Zhao R, Biesheuvel PM, Miedema H, Bruning H, van der Wal A. Charge efficiency: a functional tool to probe the double-layer structure inside of porous electrodes and application in the modeling of capacitive deionization. J Phys Chem Lett 2010;1:205–10.
[60] Bourcier WL, Aines RD, Haslam JJ, Schaldach CM, O'Brien KC, Cussler E. Deionization and desalination using electrostatic ion pumping. United States (Livermore, CA): Lawrence Livermore National Security, LLC; 2011.
[61] Porada S, Sales BB, Hamelers HVM, Biesheuvel PM. Water desalination with wires. J Phys Chem Lett 2012;3:1613–8.
[62] Porada S, Weinstein L, Dash R, van der Wal A, Bryjak M, Gogotsi Y, et al. Water desalination using capacitive deionization with microporous carbon electrodes. ACS Appl Mater Interfaces 2012;4:1194–9.
[63] Lee J-H, Bae W-S, Choi J-H. Electrode reactions and adsorption/desorption performance related to the applied potential in a capacitive deionization process. Desalination 2010;258:159–63.
[64] Wang M, Huang Z-H, Wang L, Wang M-X, Kang F, Hou H. Electrospun ultrafine carbon fiber webs for electrochemical capacitive desalination. New J Chem 2010;34:1843–5.
[65] Li H, Pan L, Zhang Y, Zou L, Sun C, Zhan Y, et al. Kinetics and thermodynamics study for electrosorption of NaCl onto carbon nanotubes and carbon nanofibers electrodes. Chem Phys Lett 2010;485:161–6.
[66] Huang Z-H, Wang M, Wang L, Kang F. Relation between the charge efficiency of activated carbon fiber and its desalination performance. Langmuir 2012;28:5079–84.
[67] Kim Y-J, Choi J-H. Selective removal of nitrate ion using a novel composite carbon electrode in capacitive deionization. Water Res 2012;46:6033–9.
[68] Li H, Zou L. Ion-exchange membrane capacitive deionization: a new strategy for brackish water desalination. Desalination 2011;275:62–6.
[69] Humplik T, Lee J, O'Hern SC, Fellman BA, Baig MA, Hassan SF, et al. Nanostructured materials for water desalination. Nanotechnology 2011;22:292001–19.
[70] Avraham E, Noked M, Bouhadana Y, Soffer A, Aurbach D. Limitations of charge efficiency in capacitive deionization processes III: the behavior of surface oxidized activated carbon electrodes. Electrochim Acta 2010;56:441–7.
[71] Cohen I, Avraham E, Noked M, Soffer A, Aurbach D. Enhanced charge efficiency in capacitive deionization achieved by surface-treated electrodes and by means of a third electrode. J Phys Chem C 2011;115:19856–63.
[72] Perez CAR, Demirer ON, Clifton RL, Naylor RM, Hidrovo CH. Macro analysis of the electro-adsorption process in low concentration nacl solutions for water desalination applications. J Electrochem Soc 2013;160:E13–21.
[73] Jeon BG, No HC, Lee JI. Development of a two-dimensional coupled-implicit numerical tool for the optimal design of CDI electrodes. Desalination 2011;274:226–36.
[74] Andersen MB, van Soestbergen M, Mani A, Bruus H, Biesheuvel PM, Bazant MZ. Current-induced membrane discharge. Phys Rev Lett 2012;109:108301.
[75] Kamran K, van Soestbergen M, Huinink HP, Pel L. Inhibition of electrokinetic ion transport in porous materials due to potential drops induced by electrolysis. Electrochim Acta 2012;78:229–35.
[76] Mani A, Bazant MZ. Deionization shocks in microstructures. Phys Rev E: Statist Nonlinear Soft Matter Phys 2011;84:061504–13.
[77] Biesheuvel PM. Two-fluid model for the simultaneous flow of colloids and fluids in porous media. J Colloid Interface Sci 2011;355:389–95.
[78] von Helmholtz H. Über einige Gesetze der Vertheilung elektrischer Ströme in körperlichen Leitern mit Anwendung auf die thierisch-elektrischen Versuche. Ann Phys Chem 1853;89:211–33.
[79] Gouy G. Sur la constitution de la charge électrique à la surface d'un électrolyte. J Phys 1910;9:457–68.
[80] Chapman DL. A Contribution to the Theory of Electrocapillarity. Philos Mag. 1913;25:475–81.
[81] Stern O. Zur Theorie der Elektrolytischen Doppelschicht. Z Elektrochem Angew Phys Chem. 1924;30:508–16.

[82] Bazant MZ, Thornton K, Ajdari A. Diffuse-charge dynamics in electrochemical systems. Phys Rev E: Statist Nonlinear Soft Matter Phys 2004;70:021506.
[83] Levi MD, Levy N, Sigalov S, Salitra G, Aurbach D, Maier J. Electrochemical quartz crystal microbalance (EQCM) studies of ions and solvents insertion into highly porous activated carbons. J Am Chem Soc 2010;132:13220–2.
[84] Sigalov S, Levi MD, Salitra G, Aurbach D, Jänes A, Lust E, et al. Selective adsorption of multivalent ions into TiC-derived nanoporous carbon. Carbon 2012;50:3957–60.
[85] Kastening B, Heins M. Electrolyte composition and ionic mobility in micropores. Phys Chem Chem Phys 2001;3:372–3.
[86] Rica RA, Ziano R, Salerno D, Mantegazza F, Brogioli D. Thermodynamic relation between voltage-concentration dependence and salt adsorption in electrochemical cells. Phys Rev Lett 2012;109:156103.
[87] Yang K-L, Ying T-Y, Yiacoumi S, Tsouris C, Vittoratos ES. Electrosorption of ions from aqueous solutions by carbon aerogel: an electrical double-layer model. Langmuir 2001;17:1961–9.
[88] Ying T-Y, Yang K-L, Yiacoumi S, Tsouris C. Electrosorption of ions from aqueous solutions by nanostructured carbon aerogel. J Colloid Interface Sci 2002;250:18–27.
[89] Hou C-H, Liang C, Yiacoumi S, Dai S, Tsouris C. Electrosorption capacitance of nanostructured carbon-based materials. J Colloid Interface Sci 2006;302:54–61.
[90] Yang K-L, Yiacoumi S, Tsouris C. Monte Carlo simulations of electrical double-layer formation in nanopores. J Chem Phys 2002;117:8499.
[91] Huang J, Sumpter BG, Meunier V. A universal model for nanoporous carbon supercapacitors applicable to diverse pore regimes, carbon materials, and electrolytes. Chem Eur J 2008;14:6614–26.
[92] Feng G, Qiao R, Huang J, Sumpter BG, Meunier V. Ion distribution in electrified micropores and its role in the anomalous enhancement of capacitance. ACS Nano 2010;4:2382–90.
[93] Biesheuvel PM, van Limpt B, van der Wal A. Dynamic adsorption/desorption process model for capacitive deionization. J Phys Chem C 2009;113:5636–40.
[94] Kamran K, van Soestbergen M, Pel L. Electrokinetic salt removal from porous building materials using ion exchange membranes. Transport Porous Med 2012;96:221–35.
[95] Kastening B, Heins M. Properties of electrolytes in the micropores of activated carbon. Electrochim Acta 2005;50:2487–98.
[96] Arafat HA, Franz M, Pinto NG. Effect of salt on the mechanism of adsorption of aromatics on activated carbon. Langmuir 1999;15:5997–6003.
[97] Zhao R, Satpradit O, Rijnaarts HHM, Biesheuvel PM, van der Wal A. Optimization of salt adsorption rate in membrane capacitive deionization. Water Res 2013;47:1941–52.
[98] Grahame DC. The electrical double layer and the theory of electrocapillarity. Chem Rev 1947;41:441–501.
[99] Bazant MZ, Chu KT, Bayly BJ. Current–voltage relations for electrochemical thin films. SIAM J Appl Math 2005;65:1463–84.
[100] de Levie R. On porous electrodes in electrolyte solutions—IV. Electrochim Acta 1964;9:1231–45.
[101] Newman JS, Tobias CW. Theoretical analysis of current distribution in porous electrodes. J Electrochem Soc 1962;109:1183–91.
[102] Rica RA, Brogioli D, Ziano R, Salerno D, Mantegazza F. Ions transport and adsorption mechanisms in porous electrodes during capacitive-mixing double layer expansion (CDLE). J Phys Chem C 2012;116:16934–8.
[103] Rica RA, Ziano R, Salerno D, Mantegazza F, Bazant MZ, Brogioli D. Electro-diffusion of ions in porous electrodes for capacitive extraction of renewable energy from salinity differences. Electrochim Acta 2013;92:304–14.
[104] Brogioli D, Zhao R, Biesheuvel PM. A prototype cell for extracting energy from a water salinity difference by means of double layer expansion in nanoporous carbon electrodes. Energy Environ Sci 2011;4:772–7.
[105] Mani A, Zangle TA, Santiago JG. On the propagation of concentration polarization from microchannel–nanochannel interfaces. Part I: analytical model and characteristic analysis. Langmuir 2009;25:3898–908.
[106] Wilson JR. Demineralization by electrodialysis. London: Butterworths; 1960.
[107] Biesheuvel PM. Thermodynamic cycle analysis for capacitive deionization. J Colloid Interface Sci 2009;332:258–64.
[108] Zhang D, Shi L, Fang J, Dai K, Li X. Preparation and desalination performance of multiwall carbon nanotubes. Mater Chem Phys 2006;97:415–9.
[109] Wang G, Pan C, Wang L, Dong Q, Yu C, Zhao Z, et al. Activated carbon nanofiber webs made by electrospinning for capacitive deionization. Electrochim Acta 2012;69:65–70.
[110] Oh HJ, Lee JH, Ahn HJ, Jeong Y, Kim YJ, Chi CS. Nanoporous activated carbon cloth for capacitive deionization of aqueous solution. Thin Solid Films 2006;515:220–5.
[111] Li J, Wang X, Huang Q, Gamboa S, Sebastian PJ. Studies on preparation and performances of carbon aerogel electrodes for the application of supercapacitor. J Power Sour 2006;158:784–8.
[112] Nightingale ER. Phenomenological theory of ion solvation. Effective radii of hydrated ions. J Phys Chem 1959;63:1381–7.
[113] Sing KSW, Everett DH, Haul RAV, Moscou L, Pierotti RA, Rouquerol J, et al. Pure and applied. Chemistry 1984;1985(57):603–19.
[114] Nikitin A, Gogotsi Y. Nanostructured carbide-derived carbon. In: Nalwa HS, editor. Encyclopedia of nanoscience and nanotechnology. CA: American Scientific Publishers; 2004. p. 553–74.
[115] Presser V, Heon M, Gogotsi Y. Carbide-derived carbons – from porous networks to nanotubes and graphene. Adv Funct Mater 2011;21:810–33.
[116] Zhai Y, Dou Y, Zhao D, Fulvio PF, Mayes RT, Dai S. Carbon materials for chemical capacitive energy storage. Adv Mater 2011;23:4828–50.
[117] Korenblit Y, Rose M, Kockrick E, Borchardt L, Kvit A, Kaskel S, et al. High-rate electrochemical capacitors based on ordered mesoporous silicon carbide-derived carbon. Acs Nano 2010;4:1337–44.
[118] Huang J, Sumpter BG, Meunier V, Gogotsi YG, Yushin G, Portet C. Curvature effects in carbon nanomaterials: exohedral versus endohedral supercapacitors. J Mater Res 2010;25:1525–31.
[119] He L, Chathoth SM, Melnichenko YB, Presser V, McDonough J, Gogotsi Y. Small-angle neutron scattering characterization of the structure of nanoporous carbons for energy-related applications. Micropor Mesopor Mater 2012;149:46–54.

[120] Gabelich CJ, Tran TD, Suffet IHM. Electrosorption of inorganic salts from aqueous solution using carbon aerogels. Environ Sci Technol 2002;36:3010–9.
[121] Chmiola J, Largeot C, Taberna PL, Simon P, Gogotsi Y. Monolithic carbide-derived carbon films for micro-supercapacitors. Science 2010;328:480–3.
[122] Hung K, Masarapu C, Ko T, Wei B. Wide-temperature range operation supercapacitors from nanostructured activated carbon fabric. J Power Sour 2009;193:944–9.
[123] Jost K, Perez CR, McDonough JK, Presser V, Heon M, Dion G, et al. Carbon coated textiles for flexible energy storage. Energy Environ Sci 2011;4:5060–7.
[124] Presser V, Zhang L, Niu JJ, McDonough J, Perez C, Fong H, et al. Flexible nano-felts of carbide-derived carbon with ultra-high power handling capability. Adv Energy Mater 2011;1:423–30.
[125] Marsh H. Activated carbon. 1st ed. Boston (MA): Elsevier; 2006.
[126] Wang G, Dong Q, Ling Z, Pan C, Yu C, Qiu J. Hierarchical activated carbon nanofiber webs with tuned structure fabricated by electrospinning for capacitive deionization. J Mater Chem 2012;22:21819–23.
[127] Wang G, Qian B, Dong Q, Yang J, Zhao Z, Qiu J. Highly mesoporous activated carbon electrode for capacitive deionization. Sep Purif Technol 2013;103:216–21.
[128] Zou L, Morris G, Qi D. Using activated carbon electrode in electrosorptive deionisation of brackish water. Desalination 2008;225:329–40.
[129] Ahn H-J, Lee J-H, Jeong Y, Lee J-H, Chi C-S, Oh H-J. Nanostructured carbon cloth electrode for desalination from aqueous solutions. Mater Sci Eng: A 2007;449–451:841–5.
[130] Ryoo MW, Kim JH, Seo G. Role of titania incorporated on activated carbon cloth for capacitive deionization of NaCl solution. J Colloid Interface Sci 2003;264:414–9.
[131] Ryoo MW, Seo G. Improvement in capacitive deionization function of activated carbon cloth by titania modification. Water Res 2003;37:1527–34.
[132] Myint MTZ, Dutta J. Fabrication of zinc oxide nanorods modified activated carbon cloth electrode for desalination of brackish water using capacitive deionization approach. Desalination 2012;305:24–30.
[133] Han L, Karthikeyan KG, Anderson MA, Gregory K, Wouters JJ, Abdel-Wahab A. Mechanistic insights into the use of oxide nanoparticles coated asymmetric electrodes for capacitive deionization. Electrochim Acta 2013;90:573–81.
[134] Kyotani T, Chmiola J, Gogotsi Y. Carbide derived carbon and templated carbons. In: Beguin F, Frackowiak E, editors. Carbon materials for electrochemical energy storage systems. Boca Raton: CRC Press/Taylor and Francis; 2009. p. 77–113.
[135] Li L, Zou L, Song H, Morris G. Ordered mesoporous carbons synthesized by a modified sol–gel process for electrosorptive removal of sodium chloride. Carbon 2009;47:775–81.
[136] Wen X, Zhang D, Shi L, Yan T, Wang H, Zhang J. Three-dimensional hierarchical porous carbon with a bimodal pore arrangement for capacitive deionization. J Mater Chem 2012;22:23835–44.
[137] Pekala RW, Alviso CT, Kong FM, Hulsey SS. Aerogels derived from multifunctional organic monomers. J Non-Cryst Solids 1992;145:90–8.
[138] Yang C-M, Choi W-H, Na B-K, Cho BW, Cho WI. Capacitive deionization of NaCl solution with carbon aerogel–silicagel composite electrodes. Desalination 2005;174:125–33.
[139] Moreno-Castilla C, Maldonado-Hódar FJ. Carbon aerogels for catalysis applications: an overview. Carbon 2005;43:455–65.
[140] Yoshizawa N, Hatori H, Soneda Y, Hanzawa Y, Kaneko K, Dresselhaus MS. Structure and electrochemical properties of carbon aerogels polymerized in the presence of Cu^{2+}. J Non-Cryst Solids 2003;330:99–105.
[141] Landon J, Gao X, Kulengowski B, Neathery JK, Liu K. Impact of pore size characteristics on the electrosorption capacity of carbon xerogel electrodes for capacitive deionization. J Electrochem Soc 2012;159:A1861–6.
[142] Feng G, Qiao R, Huang J, Dai S, Sumpter BG, Meunier V. The importance of ion size and electrode curvature on electrical double layers in ionic liquids. Phys Chem Chem Phys 2011;13:1152–61.
[143] Pech D, Brunet M, Durou H, Huang P, Mochalin V, Gogotsi Y, et al. Ultrahigh-power micrometre-sized supercapacitors based on onion-like carbon. Nat Nanotechnol 2010;5:651–4.
[144] Gabelich CJ, Xu P, Cohen Y. Concentrate treatment for inland desalting, 2010. p. 295–326 [chapter 10].
[145] Farmer JC, Fix DV, Mack GV, Poco JF, Nielsen JK, Pekala RW, et al. Capacitive deionization of seawater. In: Pacific rim environmental conference, San Francisco, 1995.
[146] Wang XZ, Li MG, Chen YW, Cheng RM, Huang SM, Pan LK, et al. Electrosorption of NaCl solutions with carbon nanotubes and nanofibers composite film electrodes. Electrochem Solid-State Lett 2006;9:E23–6.
[147] Dai K, Shi L, Zhang D, Fang J. NaCl adsorption in multi-walled carbon nanotube/active carbon combination electrode. Chem Eng Sci 2006;61:428–33.
[148] Zou L. Developing nano-structured carbon electrodes for capacitive brackish water desalination. In: Ning RY, editor. Expand Issues Desalinat [INTECH2011].
[149] Wang H, Zhang D, Yan T, Wen X, Shi L, Zhang J. Graphene prepared via a novel pyridine-thermal strategy for capacitive deionization. J Mater Chem 2012;22:23745–8.
[150] Zhang D, Wen X, Shi L, Yan T, Zhang J. Enhanced capacitive deionization of graphene/mesoporous carbon composites. Nanoscale 2012;4:5440–6.
[151] Zhang D, Yan T, Shi L, Peng Z, Wen X, Zhang J. Enhanced capacitive deionization performance of graphene/carbon nanotube composites. J Mater Chem 2012;22:14696–704.
[152] Stoeckli F, Guillot A, Slasli AM, Hugi-Cleary D. Microporosity in carbon blacks. Carbon 2002;40:211–5.
[153] Nadakatti S, Tendulkar M, Kadam M. Use of mesoporous conductive carbon black to enhance performance of activated carbon electrodes in capacitive deionization technology. Desalination 2011;268:182–8.
[154] Li HB, Lu T, Pan LK, Zhang YP, Sun Z. Electrosorption behavior of graphene in NaCl solutions. J Mater Chem 2009;19:6773–9.
[155] Kim Y-J, Choi J-H. Enhanced desalination efficiency in capacitive deionization with an ion-selective membrane. Sep Purif Technol 2010;71:70–5.

[156] Li H, Pan L, Lu T, Zhan Y, Nie C, Sun Z. A comparative study on electrosorptive behavior of carbon nanotubes and graphene for capacitive deionization. J Electroanal Chem 2011;653:40–4.
[157] Jia B, Zou L. Wettability and its influence on graphene nansoheets as electrode material for capacitive deionization. Chem Phys Lett 2012;548:23–8.
[158] Li H, Pan L, Nie C, Liu Y, Sun Z. Reduced graphene oxide and activated carbon composites for capacitive deionization. J Mater Chem 2012;22:15556–61.
[159] Wang Z, Dou B, Zheng L, Zhang G, Liu Z, Hao Z. Effective desalination by capacitive deionization with functional graphene nanocomposite as novel electrode material. Desalination 2012;299:96–102.